LENS - European Laboratory for Nonlinear Spectroscopy
Università degli Studi di Firenze

DOTTORATO INTERNAZIONALE IN SPETTROSCOPIA ATOMICA E MOLECOLARE

XXV CYCLE - FIS/03

TRANSPORT PHENOMENA IN DISORDERED TIME-DEPENDENT POTENTIALS

Candidate: MARCO MORATTI

Coordinator: Prof. FRANCESCO PAVONE .....

Supervisor: Ch.mo Prof. MASSIMO INGUSCIO .....

A mia madre
e mio padre

Contents

List of Figures

Introduction

> We are not to tell nature what she's gotta be. ... She's always got better imagination than we have.
>
> Richard P. Feynman

Describing Nature using simple and clean model is, since its first time, one of the main goal of physics. There are many and many examples in which, with the help of the simplest possible toy model, one can not only describe what he observes but also predict new features. The simplification of natural processes is mandatory, otherwise we will end up with plenty of things that we can not manage properly. Classical physics does this but, of course, also quantum physics follows the same path: it solves some problems and then tries to extend results to a class of systems similar to the solvable one by applying the same methods, with little modifications needed by the specific situations. We can divide problems into two macro-classes: one deals with static (equilibrium, stationary, nomenclature depends onto the field of research) properties, the other with dynamics (out of equilibrium, non stationary).

This thesis deals with the second one, with special attention for atomic systems. The interests onto dynamical properties of microscopic (and mesoscopic) systems was born long time ago and, as many of others stuff in physics, this interest grew up with the birth of quantum mechanics: understanding how the small particles behave, interacts, moves and how this can affect the properties at larger scales was, and still is, a great challenge that cover a lot of branches of physical science. Many things are to be taken into account when starting to face these problems: first a proper way to describe underling structures onto which particles moves, then a good model to describe how they interacts one each other and with the surrounding or other systems. Here I consider one dimensional disordered potentials, mean field approximation for interactions

and stochastic time-dependent potential, that mimes some noise present in the system. All problems are studied from theoretical point of view, with numerical techniques and also analytic approximation when possible. Because of this the results I am going to present can be applied to all systems described by the same models (i.e. Hamiltonians and equation of motions), but I will in particular make a comparison with experiments on ultracold atoms, due to the fact that part of this work was developed in collaboration with experimental group at LENS.

I start studying non interacting particles in one dimensional disordered chains, then take into account effects of interactions, noise and both of them. In the first case I review Anderson localization phenomenon, and give a description of wave packet localization complementary to the usual ones. Regarding noise and interactions I study the expansion of a system of particles, giving a characterization for the dynamics by looking to the properties describing the entire system (i.e. the evolution of its spatial width): with just noise spreading follows the classical diffusion equation; interactions give rise to slower dynamics, while the combinations of the two ends up in a set of possible results going from expansion slower then diffusive (also said subdiffusive) to faster then diffusive (super-diffusive). I try to find a model that describes all the common properties and then to give an explanation to the cases in which it can not be applied. Systems in which this aspects disorder noise and interactions are present in different combinations are still subject of a lot of studies: going from atomic physics to biology, passing through chaotic systems, it is possible to find many examples of physical processes that posses at least one of the ingredients I take into account in the thesis.

Influence of disorder is one of the widely studied problems (e.g. [1]) because it is ubiquitous in nature and it strongly affects the behavior of systems: the most famous works on it is the one by P.W. Anderson[1], in which he introduced the concept of strong localization [2]. This opened a new way of looking to the microscopic behavior of insulating and conducting materials: waves scattered by impurities and defects sums together coherently, rather than with an incoherent process as it was thought to be until that times [3]. This coherent process leads to the suppression of diffusion for an initially localized wave packet and to an exponential decay of the disordered system's eigenstates [4]. Plenty of works have been published about localization ever since, also because it is found that is a general behavior of waves in the presence of non regular structures. Today localization of waves has been found for electrons [5], light [6–11], acoustic [12] and ultrasounds waves [13] and also for seismic waves [14]. For the aim of my thesis the most important experiments are the one performed with ultracold atoms. Since the first realizations of Bose-Einstein condensation (BEC) in ultracold dilute atomic gases [15–18] their great usefulness was clear to all the scientific community. The possibility of tuning many of the system's parameters gives to them a special role: in ultracold atoms experiments the Hamiltonian describing the system plays a central role, i.e. an experiment can be

[1] For studies on localization he was awarded the Nobel Prize in Physics in the 1977.

modeled in order to mime a given Hamiltonian. In the case of Anderson localization interactions between electrons and between electron and phonons can not be canceled in real electronic systems, thus the exact Anderson model [2] will never be realized. With ultracold atoms, on the contrary, it is possible to create a disordered potential by the means of lasers beams and put them onto it without having interactions: studies of pure Anderson localization become possible. Its direct observation [19–21] is a proof of how a powerful tool ultracold atoms can be for exploring a number of problems concerning the theory of localization [22–24].

The presence of interactions or other sources of disturbance for the bare disordered potential is a problem if one searches for localizations but, on the other hand, is of extreme importance for transport: everything that could break localization and goes into the direction of making the system, or part of it, move is important. Of course atom-atom and atom-surrounding interactions are the most diffuse origins of delocalization and so they studied with special attention, in particular the case of a surrounding described as a stochastic time-dependent potential.

The latter is studied since Einstein published its famous work on Brownian motion [25], and then the interest onto this kind situations has been grown due to the fact that many time-dependent processes can be modeled as a stochastic bath. In condescend matter physics a typical example is the interactions between electrons and phonons, when these are seen as a thermal bath to describe random lattice vibrations [26–30]. Transport in random time-dependent environment is also discussed in [31–37] and more recently in [38–43] with a particular attention to the chemical transport, similar arguments can be found for virus transport in porous media [44]. Interplay with noise and disorder was also considered for light transport [10], light-harvesting systems [45] or coupled cavities [46].

Interactions between particles are the other delocalizing mechanism we take into account: they fight against Anderson localization and under their influence systems spread slower that diffusive. Extensive studies were done regarding this subdiffusion, especially under the light of chaotic systems [47–60]. In [61] interactions are assimilated to an intrinsic noise: this point of view create a direct connection between the two aspect that up to now are always considered separately. I do not find any other papers in which the contemporary presence of noise and interactions is considered, this in my opinion makes the problems very interesting because a complete understanding of both macroscopic and microscopic behavior is still missing.

Finally I want to say that all of the models and simulations presented in this thesis are developed in the mean field regime. This a good approximations for many physical situations, and also for ultracold atoms experiments, but does not take into account quantum fluctuations at all. Those are very interesting and their effect could influence a lot all the systems. Reconsidering all those results in the light of a fully quantum system, e.g. those described by Bose Hubbard models, will be a very interesting future development of this work.

Outline of the thesis

- **Chapter 1:** here I review fundamental properties of disordered systems, giving the definitions of the important quantities which characterize them. Then I present the three types of disordered potential that are used in all the following chapters: Anderson disorder, optical speckles an quasi-periodic lattices.

- **Chapter 2:** basic theory of Bose-Einstein condensates (BEC). Assuming that systems are at $T = 0$K and that theory of BEC is already known, we derive the basic equations for the dynamics of a weakly interacting condensate, i.e. the Gross-Pitaevkii equation (GPE). At the end of the chapter we consider the case of periodic optical potentials: the spatial discretization they introduce allows us to go from the continuous model of GPE to its discrete counterpart, the Discrete Nonlinear Schrödinger Equation (DNSL).

- **Chapter 3:** new point of view on Anderson localization is presented. The basic idea lies onto the quantum interference of eigenstates of a given disordered potential: it acts in such a way that in the tails of a wave packet macroscopic dynamics disappears, leaving just a Anderson localized profiles with tails that do not show any relevant time dependence. We prove it with the two typical discorded potentials used with cold atoms: quasi-periodic lattices and speckles. Before doing this we show how our idea works in some simple examples involving quantum harmonic oscillators. How a wave packet evolves in time is due to this interference which brings all the informations about time evolution.

- **Chapter 4:** after having considered localization, in this chapter I study what happens when onto disordered systems acts sources of delocalization. I focus my attention onto stochastic time-dependent potentials, which is also called noisy potential, and interactions. About the latter I review some basic results regrading the subdiffusive expansion of the wave packet they generate and the intriguing phenomenon of self-trapping, which comes from the interplay between the bounded energy spectrum of the system (due to the presence of a periodic lattice) and the nonlinearity (due to the interactions). Speaking about noise I introduce a couple of possible way of generating controllable noise, one of those has been implemented in experiments with ultracold atoms, characterizing different types of noise obtained and stressing equivalences and differences. Then I analyze its influence onto disordered systems, finding that it breaks localization and drive the system into a diffusive regime. I compare numerical simulations with experimental results with also a microscopic model for the diffusion coefficient which is in accordance with the data.

  After this I consider combined action of noise and interactions and build up a model for it. I found that within some intervals for interactions strength and noise

amplitude the dynamics of a wave packet follows a simple law described by the linear superposition of the two single effects. Moreover I explore some situations in which this model is not valid but in which systems shows interesting behavior: for sufficient strong interactions the interplay between self-trapping and noise lead to a transient super-diffusive expansion, before normal diffusion is restored.

- **Chapter 5:** in this chapter I will present a possible proposal for the experiment on Anderson localization with cold atoms: disordered is not generated by usual optical potentials but with another condensate. This is not to a new idea, but novelties lie in the method of creating the disorder with atoms. All the proposal I found just deals with trapping some atoms onto different sites of a lattices, sites that are chosen randomly; instead of this we use intrinsic instability of DNLS. Interplay between periodicity of the lattice and interactions could lead to situations in which perturbations onto a uniform condensates grows and destroy its flat density profile, this is analogous to the self-trapping in Chap. 4. I analyze the characteristics of the disorder obtained for different interactions, finding that one can obtain two classes of disorder, both uncorrelated in space but with different distributions. I also discuss the possibility of connecting this different disorders with systems at positive or negative absolute temperature (strictly speaking it is not possible in the usual way being the system microcanonical) which is similar to what was done recently again with ultracold atoms in periodic lattices. Once we characterize the disorder we study the localization properties of another condensate onto it, applying the idea of Chap. 3 which again works as expected.

1

One dimensional disordered systems

In this chapter we will briefly present some basic concepts concerning the theory of disordered systems, in particular we will focus on purely one dimensional system that will be the only one we take into account in this thesis. We start by giving a first definition of disorder and showing some of its fundamental properties, distinguishing strong and weak disorder. Then we will analyze the effects of this disorder, focusing on the eigenstates localization and the general behavior of the spectrum. During this, we will introduce the phenomenon of *Anderson localization* and spend some words about Lifshits tails an localization.

1.1 Disordered systems

The main characteristic that a disordered system has is that it shows an irregular structure. Both "irregular" and "structure" could have a different meaning depending on the system one has to menage, but of course there are some concepts which are common to all of them. First of all, when one speaks about disorder, is assuming that the structure does not change in time, at least on the typical time scale of the evolution of the system; generally one refers to the parameters which define the disorder as the slow degrees of freedom, in contrast to the fast degrees of freedom which are linked to the dynamical variables of the system itself. Another main feature is that disordered system are not uniquely determined: disordered structure changes a lot between two different realization; this implies that we are forced to use stochastic Hamiltonians [62] in which disorder depends onto a set of random parameters which are time independent, but changes from a realization of the system to the other, in accordance with a given probability distribution function. Moreover the average properties of a certain system do not coincide with that of a single realization, so we need to perform averages over all the possible realizations, each weighted with its probability. Because of this one can understand how difficult is to treat those kind of problems, and it is evident that

numerical simulations become not only a powerful, but also a necessary tool.

Finally we want to recall that the disorder could be classified as compositional or topological [1, 62]. The former category is composed by those systems which disorder is due to the random position of the elements onto a underlying structure that is regular (for example we can think about impurities in a lattice); in the case of topological disorder there is no order at all in the geometry of the system, but there could be other kind of regularities. Generally a disordered system shows characteristics of both of them.

1.2 Weak and strong disorder

The theory of disordered system was initially developed in solid state physics, in order to study defects in crystalline structures [2, 63, 64]. Because of this first toy models created in this field dealt mainly with compositional disorder, describing structures which are naturally defined onto a lattice. In [64] the author consider a one dimensional crystal with attractive impurities (i.e. potential wells) randomly distributed along it and, for the first time, introduces the idea of strong and weak disorder, in average. The original definitions was that one observe weak disorder if the concentration of impurities is low, i.e. for every part of the system one consider the distance between two subsequent wells are of several lattice constant; on the contrary a strong disorder was associated to a high concentration of defects, separated one another by few lattice sites. The crucial aspect of the distinction lies on the presence, or absence it depends, of potentials wells that are quite far apart and have a depth which is much larger than $\sigma_R = \sqrt{\langle v_R^2 \rangle}$. This definition, with respect to the other, allow an extension of these concepts to a generic disordered potential (see for example [65]).

1.2.1 Three models for disordered potentials

After having defined disorder we will now present three examples of it which plays an important role in physics both theoretical (Anderson) and experimental (speckles, quasi-periodic lattices). The Anderson model, which was used in [2] to demonstrate the strong eigenstate localization (see next paragraph) that since them has taken his name, is the prototype of all the disordered potential. Then we will describe speckles, which are peculiar light pattern generated when a monochromatic beam, i.e. a laser, passes through a medium in which are present scattering centers at random position, for example a frosted glass [66]. The last disorder we take into account is the quasi-periodic, sometimes called bichromatic, lattice; it was studied in a famous paper by Aubry and André [67] in which they demonstrate that above a certain threshold the eigenstates of that potential are exponentially localized, while under it they are extended as predicted by the Bloch's theorem. This is a very peculiar feature because for purely random system in one dimension all the eigenstates are localized, in general with a localization length which

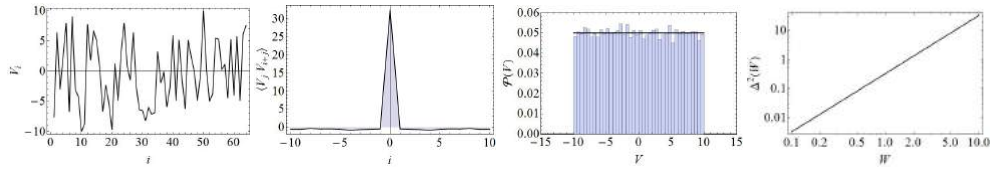

Figure 1.1: An example of Anderson disorder. From left to right: V_i, autocorrelation function and the probability distribution function, for $W = 10$. Last panel shows Δ^2 as function of W.

is a function of energy, for any amount, even small, of disorder. The transition between extended and localized states is a fingerprint of this kind of non periodic system [23, 68]

Anderson model

In his famous paper [2] Anderson uses this type of random potential in order to introduce the concept of exponential localization. Usually Anderson model refers to discrete system, i.e. systems defined on a lattice (we will see how it can be associated to a continuous one), and the disorder V_j has to be specified for all sites $j = 1, 2 \dots M$. V_j is an uncorrelated chain of random numbers, picked up from a uniform distribution:

$$\begin{aligned} V_j &\in [-W, W] \,, \\ \mathcal{P}(V) &= \frac{1}{2W} \left[\Theta(V + W) - \Theta(V - W)\right] \,, \\ \langle V_{j+i} V_j \rangle &= \Delta^2(W) \delta_{ij} \,. \end{aligned} \tag{1.1}$$

Here we have considered a disorder with zero mean, i.e. $\langle V_j \rangle = 0$, and we introduce the quantities W that measures the amplitude of the disorder distribution and Δ to which we refer as the disorder strength. In equations (1.1) we explicit that the Δ is a function of W, a plot of it is in Fig. (1.1) together with all the other quantities in (1.1).

Speckle potential

Optical speckles are unique diffraction pattern that have attracted the attention of scientists long ago [66] and they have been become very useful in atomic physics, in particular in experiments with ultracold atoms, because they can be used as potentials which introduce disorder in atomic systems [69–76].

If we shine a rough surface with a laser beam, as a piece of paper or a wall, and we look at the image reflected onto an other surface, what we can see is a large image with intense with light spot and dark region mixed together without any apparent rule. This is a speckle [62, 66, 76], and the origin of that pattern lies on the fact that the surface which reflects light has random distributed defects on length scale comparable to the wavelength of the laser. Each of those impurities should be assimilated to a

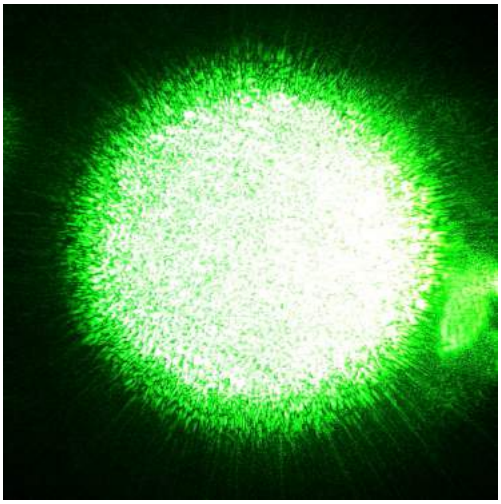

Figure 1.2: An image of the speckle pattern obtained with monochromatic light. Image from `http://en.wikipedia.org/wiki/Speckle_pattern`

scattering center, which are reasonably randomly distributed in space and uncorrelated. The same pattern can be obtained by sending the beam through a frosted glass. Very naively we can explain how the speckle is created by telling that the intensity of the light in each point of the pattern takes into account all the contributions of the scattering center that were been illuminated: because they are randomly distributed so it is for the light intensity. The characteristic granular structure observable in speckles is a finite size effect: we shine light just onto a finite part of the diffusing medium, this fixes an upper bound for the intensity variation between to nearest point of the speckle. We now describe a way to obtain a one dimensional speckle disorder starting from a three dimensional one [62, 77]. Let us consider a perfectly monochromatic, collimated, laser beam, and suppose to put a diffusive plate onto a plane orthogonal to the direction of its propagation. Parallel to the plate, at a distant D is placed the screen onto which we want to create the speckle pattern. In order to simplify, without loosing generality, it is possible to assimilate the laser beam to a plane wave of frequency ω and wavelength λ, moving along the z direction

$$\Psi(\vec{x}, t) = A \exp[-i(\omega t - kz)] \, .$$

Now suppose that the glass has just a region $\mathcal{S}$ that let the light passes through, and for simplicity's sake take $\mathcal{S}$ centered in $x = y = 0$ and the plate lie on the $z = 0$ plane. Because of the structure of the plate, e.g. a frosted glass, every light ray follows an optical path of random length, length that does not have any correlation between two different points. In order to describe what is going on it is possible to associate a complex number $\mathcal{A}(x, y)$ to every point of $\mathcal{S}$, with the prescription that it unimodular,

$|\mathcal{A}| = 1$ with a random phase. Moreover we have to take into account that it is spatially incoherent which allows to write

$$\langle \mathcal{A}(x,y)\mathcal{A}(x+\Delta x, y+\Delta y)\rangle_{\mathcal{S}} \propto \delta(\Delta x)\delta(\Delta y)\,. \tag{1.2}$$

From the basic theory of optics, i.e. the Huygens principle [62, 66], the pattern onto a plane at $z = D$ is proportional to the superposition of each contribution coming from $\mathcal{S}$; because of (1.2) those contributions are uncorrelated and we can make use of the central limit theorem [78, 79], from which follows that $\Psi(x, y, D)$ has a Gaussian distribution. Now we suppose that bot real and imaginary part of $\mathcal{A}$ have a Gaussian distribution and, recalling classical diffraction theory, one get

$$\Psi(x,y,D) \simeq C \int_{\mathcal{S}} dx'dy' \mathcal{A}(x',y') \exp\left[-ik\frac{xx'+yy'}{D}\right]. \tag{1.3}$$

Eq. (1.3) is the light field at $z = D$, the intensity associated to it is the speckle:

$$I(x) = |\Psi(x,y,D)|^2 \propto \left| \int_{-l/2}^{+l/2} dx'\, \Phi(x') \exp\left(-ik\frac{xx'}{D}\right)\right|^2, \tag{1.4}$$

where we consider a segment of length l along x and $\Phi(x')$, which is what result from (1.3) after integrating over y' with y kept fixed, still random Gaussian distributed. This is our first goal: from a complex three dimensional field we get a one dimensional function $I(x)$, which is the potential we are going to study, and it is the one used in the experiments [69–76].

Eq. (1.3) describes a two dimensional field, from which one has to obtain the 1D potential we are searching for. In the experiments this can be done be employing a system of lenses that elongates the speckle in one direction; as we see in the following speckles have a characteristic autocorrelation length ξ in each direction so if one consider a region of the $z = D$ plane of width $y < \xi$, in order to avoid any spatial dependence of I in the y direction, he can suppose to work with a one dimensional disordered potential. The intensity of the speckle expressed trough Eq. (1.4) has the advantage of being easy to implement in numerical simulations, indeed we can think about it as the Fourier transform of the product between $\Phi(x')$ and a step function of width l. Ideally $I(x)$ is defined for all x between $\pm\infty$, while the step function has a finite domain $-l/2 < x < l/2$; numerically we obtain it by generating an array of N of complex random number Gaussian distributed, i.e. we create $\Phi(x)$, then we retain only a certain set of them, lets call this number M, so we now have a vector with N entries, M of which are complex numbers, and all the other are zeros. We then transform this vector using a Fast Fourier Transform algorithm, and take the modulus squared of the result: we have obtained the one dimensional speckle potential, as shown in Fig. (1.3). Once we have created the disorder we have to characterize it and, as described before, this is done by specifying its autocorrelation

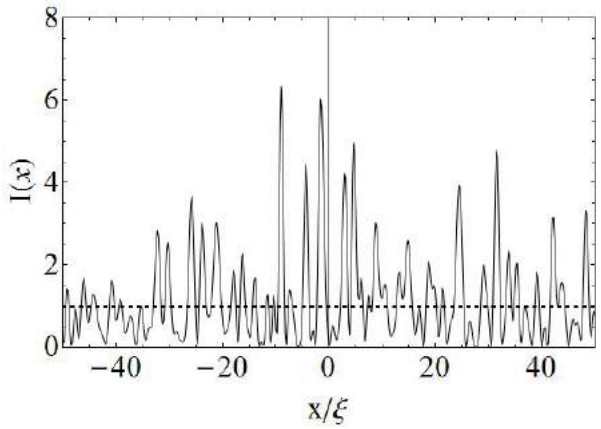

Figure 1.3: An example of a 1D speckle potential, here $I(x)$ recall us that speckles potential are generated by light intensity. Dashed line correspond to the standard deviation σ_R of $I(x)$ which characterize the disorder strength. Correlation length ξ is used as unit for lengths.

function and probability distribution function. This can be done analytically for the speckle potential, and the results will be used as criterion for comparison with numerical simulations. For convenience we define $\psi(x) \equiv \Psi(x, y_0, D)$ where (x, y_0) represent the line along which we define the one dimensional speckle. Before we have mention the central limit theorem [78, 79], due to it we known that for the probability distribution

$$\begin{aligned} \mathcal{P}\left(\Re[\psi], \Im[\psi]\right) &= \frac{1}{\sigma^2 2\pi} \exp\left[-\frac{\Re[\psi]^2 + \Im[\psi]^2}{2\sigma^2}\right], \\ \sigma^2 &= \sigma^2_{\Re[\psi]} = \sigma^2_{\Im[\psi]}, \\ \sigma^2_{\Re[\psi]} &= \langle \Re[\psi]^2 \rangle = \int_{\mathbb{R}} dx\, \Re[\psi]^2; \end{aligned} \tag{1.5}$$

where we assume that both real and imaginary part of the field $\psi(x)$ are Gaussian distributed (central limit theorem [78, 79]) with zero average

$$\langle \Re[\psi] \rangle = \langle \Im[\psi] \rangle = 0. \tag{1.6}$$

Now we introduce a modulus-phase representation of the fields, and this is convenient due to the fact that we are interested into the study of the intensity rather then the field itself:

$$\begin{aligned} (\Re[\psi], \Im[\psi]) &\to (A, \varphi), \\ A &= \sqrt{\Re[\psi]^2 \Im[\psi]^2}, \\ \varphi &= \arctan\left(\frac{\Im[\psi]}{\Re[\psi]}\right); \end{aligned} \tag{1.7}$$

substituting those equations in (1.5) we get

$$\mathcal{P}(A) = \int_0^{2\pi} d\varphi \, \mathcal{P}(A, \varphi) = \frac{A}{\sigma^2} \, e^{-\frac{A^2}{2\sigma^2}} \, , \tag{1.8}$$

where we are allowed to perform the integration over the phase φ which is uniformly distributed in the interval $[0; 2\pi]$. From Eq. (1.5) it is clear that

$$2\sigma^2 = \langle I \rangle \, ,$$

then with the substitution $A \to I = A^2$ Eq. (1.8) becomes

$$\mathcal{P}(I) = \frac{1}{\langle I \rangle} \, \exp\left[-\frac{I}{\langle I \rangle} \right] \, , \tag{1.9}$$

which is the probability distribution function of the speckle potential defined in Eq. (1.4). In Fig. (1.4) we plot an histogram for $\mathcal{P}(i)$ calculated over 100 different potential, and compare it with Eq. (1.9).

At this point we only need to determine the autocorrelation function, derive is not difficult but requires quite long algebra so we report just the result suggesting the reader to look [62, 66, 76] for all the details. Then we have

$$\langle I(y) I(x+y) \rangle = \Gamma_I(y) = 1 + \mathrm{sinc}^2 \left(\frac{x}{\xi} \right) \, , \tag{1.10}$$

in which the *correlation length* ξ is defined ad

$$\xi = \frac{\lambda D}{l} \, , \tag{1.11}$$

that depends on the laser beam trough the wavelength λ and on the geometry of the system because of D, i.e. distance between the scattering plate and the plane where the speckle is collected, and l, the dimension of the scattering plate. Sometimes in literature one can find that the correlation length is defined as the width at half height of $\Gamma_I(x)$, which turns out to be 0.88ξ. In Fig. (1.4) we plot $\Gamma_I(x)$ obtained from numerical simulations and the function defined in Eq. (1.10), that coincide perfectly.

Quasi-periodic potential

Quasi-periodic potential, often called incommensurate, are an interesting family of the non-periodic Hamiltonians [67, 68, 80] that posses two or more periodic structure whose period are incommensurate with each other. Incommensurate means that the ratio between two periods can not be expressed as the ration between to integers number. The typical, and simplest, example of this is a one dimensional potential generated by

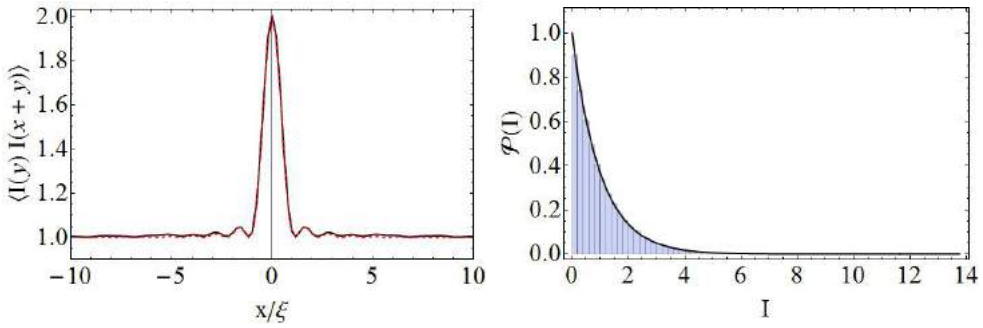

Figure 1.4: Autocorrelation function and intensity distribution (solid line is a fit with $\exp(-I/\langle I\rangle)/\langle I\rangle$). Correlation length ξ is used as unit for lengths.

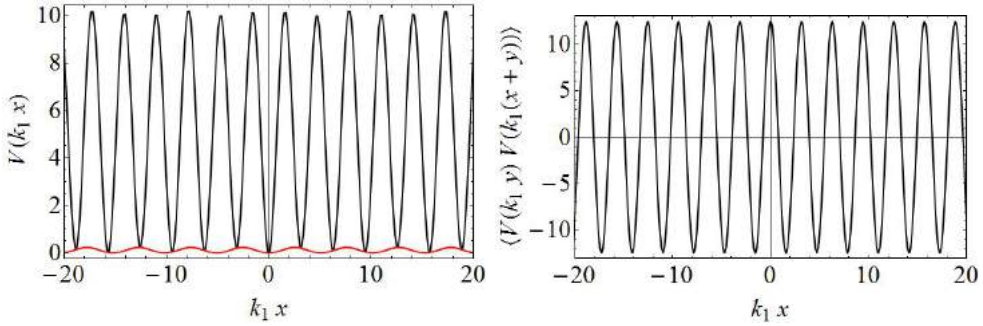

Figure 1.5: **Left panel:** a possible realization of $V(x)$ in Eq. (1.12). Red lines shows the secondary lattice $\propto \cos(k_2 x + \theta)$. Ratio between wavelengths is chosen as $k_2/k_1 = (\sqrt{5}-1)/2$, the inverse of the golden mean.
Right panel: Autocorrelation function. $V(x)$ is perfectly correlated, then we cannot say it is truly random.

the superposition of two lattices of wavelength $\lambda_1 = 2\pi/k_1$ and $\lambda_2 = 2\pi/k_2$:

$$V(x) = V_1 \cos(k_1 x) + V_2 \cos(k_2 x + \theta)\,, \tag{1.12}$$

with $k_1/k_2 \notin \mathbb{Q}$, we report in Fig. (1.5) a possible realization of Eq. (1.12). Incommensurate lattices are quite peculiar because they are neither periodic nor random; of course they are not periodic due the incommensurate ratio between wavelengths, but also they cannot be defined as truly random because from Eq. (1.12) one knows how $V(x)$ exactly behave in each point of the space. More over the lack of pure randomness is evident looking to the autocorrelation function, that is reported in Fig. (1.5). Because of this intermediate behavior it is not strictly possible to apply to incommensurate potentials not only the Bloch's theorem for pure periodic structures, but also the standard results found for completely disordered system, in particular those concerning the exponential localization of eigenstates. We can state naively that quasi-periodic lattices lie between periodic and random potential, so one expects to find both extended and localized states

depending on the parameters that define the potential.

Although the quasi-periodic potentials, and the Schrödinger equation associated to them if thought as external potentials in a quantum system, are interesting by themselves and the studies on their mathematical properties is a subject of many papers (e.g. [67, 81–85]), the discovery of natural quasi-crystals [86]. Moreover these potentials come to the fore in the last years due to the fact that they have been used in experiments with Bose-Einstein condensates in order to study the physics of Anderson localization [19] and related phenomena [87–89]. Even if these lattices are not purely random both theory [55, 67, 68, 80, 90] and experiment [19] have shown that the localization which one observes follows the same mechanism of the Anderson localization for real random disordered arrays.

1.3 Eigenstate localization

In this section we will present the most important aspect of disordered system: localization, with more attention put on Anderson localization. We follow the scheme of [62, 77] which seems to us very simple and clear.

Let us first recall that if the Hamiltonian $\mathcal{H}(x)$ of the system is periodic, i.e. $\mathcal{H}(x) = \mathcal{H}(x + X)$ for some X, also its eigenstates are periodic, as predicted by the Bloch theorem [91], and then they are extended all over the lattice. A disordered potential, with no trace of symmetry under translation, is just the opposite of the perfectly periodic lattice. It then becomes natural to suppose that in this case eigenstates behave in the opposite way with respect to the extended Bloch states. One in general expect a generic eigenfunction to be localized, at least in the lower part of the energy spectrum of the system; by this we mean that it will decay exponentially, or even faster, as we move far away from the point at which the modulus of the wave function has a maximum. This peculiar behavior has different origin in the case of weak disorder, where one usually has Lifshitz localization, or strong disorder, where Anderson localization takes place, and this localization presents in two different ways depending on the phenomenon from which it originates.

1.3.1 Weak disorder: Lifshitz states

In the previous paragraph we show how a high concentration of defects leads to Anderson localization, nevertheless it exists another type of localized states, called Lifshitz states which localize due to just a single fluctuations of the potential when it is far away from other fluctuations similar to it. Strictly speaking if we think to the defects as potential wells one of them is enough to localize state, while if one considers barriers at least two of them are need, and they have to be closer [62].

Let assume to create an one dimensional array of wells such as the separation between

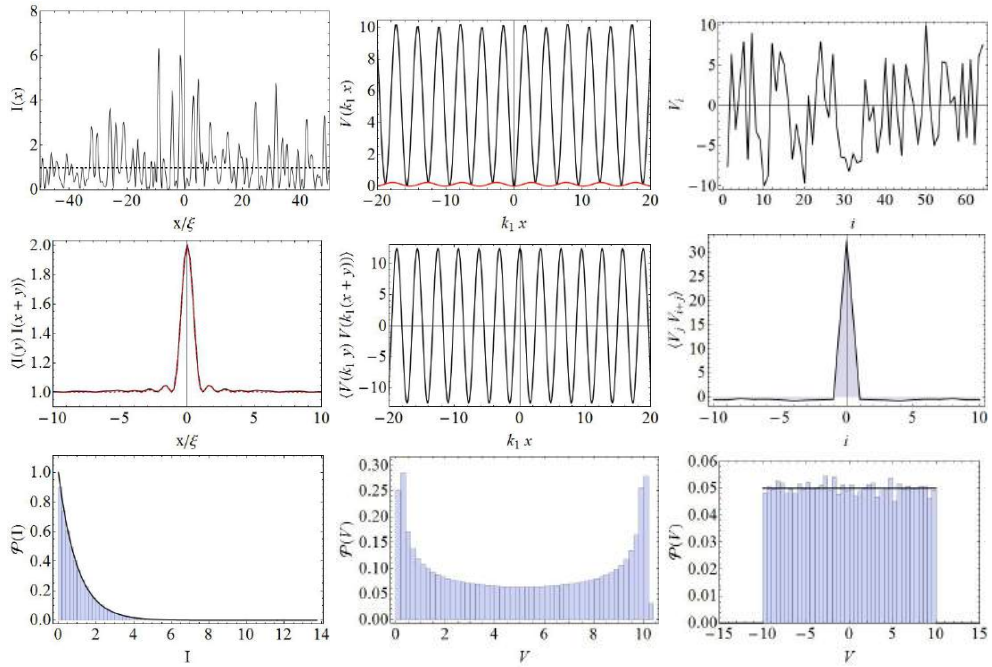

Figure 1.6: Summary of the three types of disorder presented: from left to right we have speckles, quasi-periodic and Anderson model, respectively. First rows shows a typical realization of the disorder, second the autocorrelation function and in the last we put the Probability Density Function. Looking at the autocorrelation function we can see that Anderson model is real random (of course, it is by definition) and speckles could be assimilate to a random one due the fast decay ($\propto \text{sinc}^2(z)$) of its autocorrelation. Finally we note that because of this quasi-periodic potential could not be considered as real random potential, they are perfectly correlated.

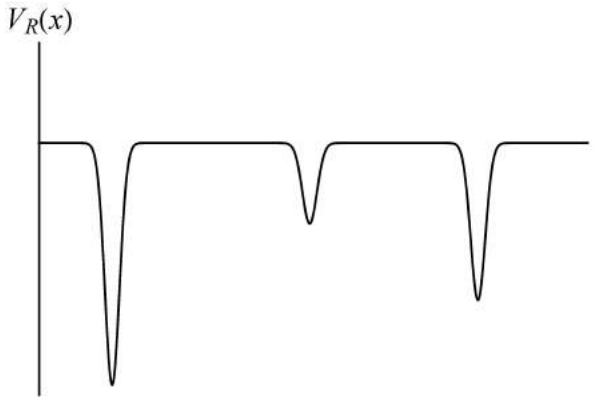

Figure 1.7: Sketch of a possible realization of a weak disordered chain.

two of them is quite large and also the depth are very different among different wells. A possible representation of this could be

$$V_R(x) = \begin{cases} \sum_{i=1}^{N} A_i f(x - x_i) & \text{if } 0 \leq x_i \leq L\,, \\ 0 & \text{otherwise}\,; \end{cases} \tag{1.13}$$

with $f(x)$ being an analytical function always negative defined onto a region centered around 0 of dimension $a \ll L$, with its absolute minimum in $x = 0$.If $L/N \ll a$ we could say that system is in the weak disorder regime; so, not only there is no superposition between wells, but also $\langle |x_i - x_{i-1}| \rangle \gg a$. Now consider the ground state of such a system, that we will denote by $\psi_{gs}(x)$: it is reasonable to think that its maximum will be centered onto the deepest wells $V_k = \max_i\{V_i\}$, centered in $x = x_k$. The hypothesis of analyticity of $f((x)$ ensure that we can expand it up to the second order around its minimum, then we approximate the well with an harmonic potential. Higher term in the expansion of the well, and all the other wells will be treated as stationary perturbation, and so the standard techniques will be applied. Because of this harmonic approximation of V_k we intuitively get to

$$\psi_{gs}(x) \begin{cases} \propto e^{-B(x-x_k)^2} + \phi(x) & x \in \left[x_k - \frac{a}{2}, x_k + \frac{a}{2}\right]\,, \\ \simeq 0 & \text{otherwise}\,, \end{cases} \tag{1.14}$$

where $\phi(x)$ represents corrections to $\psi_{gs}(x)$ coming from higher order in the series of $f(x)$. For sure this approximation becomes better in the limit of small N, i.e. small number of wells, and for $f(x)$ which naturally approaches a parabola. Eigenstates that feel mainly the effect of a single well are called *Lifshitz states* and generally they can not be associated to a localization length because, despite they live just onto a single well, they decay faster then an exponential [1, 64].

The idea of Lifshitz states in the case of an array of barriers is quite more complicated,

and it is not as immediate to define as for the wells. We need at least two barriers quite close one to the other in such a way that the space between them could be considered as a single well, and moreover they have to be quit high in order to ensure that a state can be confined between them.

1.3.2 Strong disorder: Anderson states and localization

An Anderson localized state is characterized by an exponential decay of its modulus, going from the localization center to the boundaries of the potential, over distances larger then the average separation between to fluctuation of the disorder.

The vast field of studies about motion in random 1D potentials was initiated by Anderson [2] and several reviews have been published since then [1,3,4,92,93]. Those systems play a fundamental role for better understanding the physics of disorder and nowadays there is quite a good understanding of the localization phenomenon [1,4,63,94–96]. There are several reasons to justify this importance, the greatest is that in such a low dimension disorder has the strongest effects: avoiding impurities by turning around them is not possible. Moreover one can recover some rigorous results both analytical and numerical. Last but not least those numerical calculation are faster and easier to implement [80]. Mott and Twose in [63] was the first who suggested that eigenstates of random potential will be exponentially localized no matter how strong is the disorder, but they supported their thesis only by qualitative arguments. A couple of years later Borland in [97] gives the first rigorous proof of the statement made by Mott and Twose: even a small amount of disorder give rise to Anderson localization. To give proof of localization in one dimensional system it is very useful to take advantage of techniques involving random matrices about which, in the same years of [97], Borland [97] and Oseledec [98] demonstrate some important theorems; in the following we will give a first idea of their main results.

One first possible way to visualize localization or, alternatively, absence of diffusion (as in the title by Anderson [2]) is to think about the disorder as a sequence of bumps of finite height separated by a flat region and to consider transmission and reflection through the bumps. In the j-th flat region the wave function can be written as

$$\psi_j(x) = A_j e^{ikx} + B_j e^{-ikx} \,. \tag{1.15}$$

Coefficients A_j and B_j obey

$$\begin{pmatrix} A_{j+1} \\ B_{j+1} \end{pmatrix} = T_j \begin{pmatrix} A_j \\ B_j \end{pmatrix} \,, \tag{1.16}$$

where the we introduce the *transfer matrix*

$$T_j = \begin{pmatrix} 1/t_j & -r_j/t_j \\ -r_j^*/t*_j & 1/t_j \end{pmatrix} \tag{1.17}$$

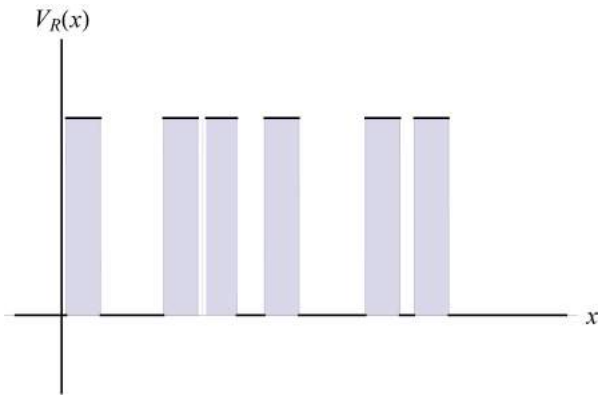

Figure 1.8: Sketch of a possible representation for the Anderson model, as described by Eq. (1.18).

which is a function of the height of each bump. $|r_j|^2$ and $|t_j|^2$ define the reflection and transmission coefficients respectively. We assume that the physics is governed by an Hamiltonian that is symmetric under time-reversal. Since in quantum mechanics probability amplitude rather then amplitude has to been considered, one finds that average transmission coefficients through two bumps is smaller then the product of the transmission coefficients through these bumps. *Transmission through the infinite chain vanishes*. Dealing with periodic chains one get that the conditions for complete transmission through a single barrier its the same for all of them and it exists energies that satisfy those conditions, this is the idea underlying Bloch's theorem [91]. In random chains each bumps gives a different contribution to total transmission: *for infinite chains transmission coefficient vanish with probability one*. One of the most important feature is that this remains true even if the energy of $\psi_j(x)$ is higher than the bump's one. As done in [62, 77] we model an Anderson random chain as a series of steps, all width Δ and height V_0, placed at random position (in Fig. (1.8) we plot an example of this):

$$V_R(x) = \begin{cases} V_0 \sum_{i=1}^{N} [\Theta(x - x_i) - \Theta(x - x_i - \Delta)] & \text{if } 0 \leq x \leq L\,, \\ 0 & \text{otherwise}\,; \end{cases} \tag{1.18}$$

in which $V_0 > 0$ measures the hight of barriers, while x_i are random variables coming from an uniform distribution

$$\mathcal{P}(x_i) = C\,[\Theta(x_i - x_{i-1} - \Delta') - \Theta(x_i - x_{i-1} - \Delta'')]\ , \tag{1.19}$$

with $C \neq 0$ and $\Delta', \Delta'' > \Delta$. Having in mind the potential in Eq. (1.18) one can obtain the behavior of the eigenstates $\psi(x)$ from very simple hypothesis: the only requests are the continuity of $\psi(x)$ and of its logarithmic derivative $d\ln[\psi(x)]/dx$ at each boundary of one barrier. We remind the reader to [62, 77] and references therein for more details,

we here just report results. In what follows we consider, as an example, the case of $E < V_0$.

Let start from the left edge of our array, i.e. $x = 0$. Moving to the opposite edge $x = L$ the eigenfunction passes through a lot of barriers. Solving the Schrödinger equation for just on barrier gives that within the barrier $\psi(x)$ is a superposition of an increasing and one decreasing exponential functions, but it turns out that former dominates. Coming back to the behavior of $\psi(x)$ between to barriers it is reasonable that, in the limit of strong disorder, its shape does not influence the overall envelope of the state. This means that an eigenstate $\psi(x)$, of energy less the the barrier's height V_0, grows exponentially, apart local fluctuations which does not play any important role for our purpose, going from $x = 0$ to $x = L$. For symmetry reasons one can follows the same arguments but starting from $x = L$ and going to $x = 0$. Again $\psi(x)$ will be characterized by an exponential increasing form between $x = L$ and 0.

So, we deal with functions $\psi(x)$ exponentially growing both from the left and right side; this paradox will be overcome by introducing the so-called *localization center* x_0: by definition it is the point at which the eigenstate has its maximum, i.e. $|\psi(x_0)|^2 = \max[|\psi(x)|^2]$, and where the two exponentials join analytically. This does not happen for all the energies: the set of E of the states satisfying those request forms the spectrum of the the disordered potential. In Fig. (1.9) we report a figure from [63] where the author shows a case in which E does not belong to the spectrum; it does not exists any localization center, but the behavior of $\psi(x)$ inside a barrier, i.e. its exponentially behavior is put on evidence. Finally,

$$|\psi(x)|^2 \propto e^{-2\frac{|x-x_0|}{\xi}} + \phi(x)\,, \tag{1.20}$$

$$|\psi(x_0)|^2 = \max\left[|\psi(x)|^2\right]\,, \tag{1.21}$$

where $\phi(x)$ is responsible for local fluctuations resulting from the effects of the potential, and we reasonably assume $\langle\phi(x)\rangle = 0$ and $|\phi(x)|/|\psi(x)| \ll 1$. A state which satisfy Eq. (1.20) is called Anderson state [1, 2, 62, 64, 94, 99], due to the fact that Anderson was the first who introduces this idea in his seminal paper [2].

Very often the problem of localization is studied within the framework of discrete system, i.e. system defined on a lattice, for which the tight-binding approximation work properly. So we have to solve the discrete eigenvalue problem

$$-K\left(\psi_{j+1} + \psi_{j-1}\right) + V_j = E\psi_j\,, \tag{1.22}$$

which physically describes a field ψ_j living on a lattice, the sites of which are labeled by j. The lattice is characterized by a tunneling energy between two neighboring sites K and a potential V_j, while E is the energy of the field. For the Anderson model V_j has the properties showed in Eq. (1.1).

It is possible to rewrite Eq. (1.22) in a very simple matrix form, by the mean of the

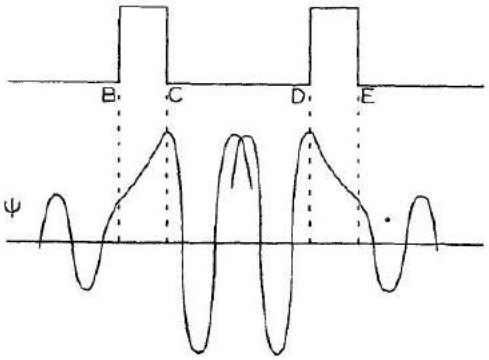

Figure 1.9: An example of a situation in which eigenstates for a certain energy E do not exist: between point C and D there is no match between to exponentials. Figure take from [63].

discrete version of transfer matrix T_j [94]:

$$T_j \begin{pmatrix} \psi_j \\ \psi_{j-1} \end{pmatrix} = \begin{pmatrix} \psi_{j+1} \\ \psi_j \end{pmatrix} , \tag{1.23}$$

with

$$T_j = \begin{pmatrix} V_j - E & -1 \\ 1 & 0 \end{pmatrix} , \tag{1.24}$$

which allows us to determine the value of the wave function at an arbitrary point by repeated application of it starting from an arbitrary point, namely

$$\begin{pmatrix} \psi_{j+1} \\ \psi_j \end{pmatrix} = T_j \cdot T_{j-1} \cdot T_{j-2} \cdot \ldots \cdot T_1 \begin{pmatrix} \psi_1 \\ \psi_0 \end{pmatrix} ,$$

with the appropriate boundary condition ψ_0. It is possible to demonstrate that each matrix T_j belong to $SL(2,\mathbb{R})$, the group formed by the unimodular, i.e. with determinant equal to 1, matrices of order 2; if we define by G_E the smallest subgroup of $SL(2,\mathbb{R})$ for which $\{T_j\}_j \subseteq G_E$, we can apply a theorem by Fustenberg [100] which states that for a subgroup of $SL(m,\mathbb{R})$ satisfying certain hypothesis, verified by G_E [94] one has

$$\lim_{j\to\infty} \frac{1}{j} \log |A_j \ldots A_1 \vec{x}| = \gamma > 0 , \tag{1.25}$$

where $\vec{x} \in \mathbb{R}^m$ is a vector that fixes the initial conditions, in this case (ψ_1, ψ_0) and $\{A_j\}$ is an arbitrary sequence of elements of G_E, so we can limit to $A_j = T_j$. This theorem together another one by Oseledec [98] state that for almost all realizations of the random potential V_j, an initial vector ψ_j will grow o decay exponentially as $e^{\pm\gamma(E)j}$, where $\gamma(E)$ is the same of Eq. (1.25) in which we explicit the dependence on the energy E which comes from the definition of T_j (see Eq. (1.24)); $\gamma(E)$ is known as the Lyapunov

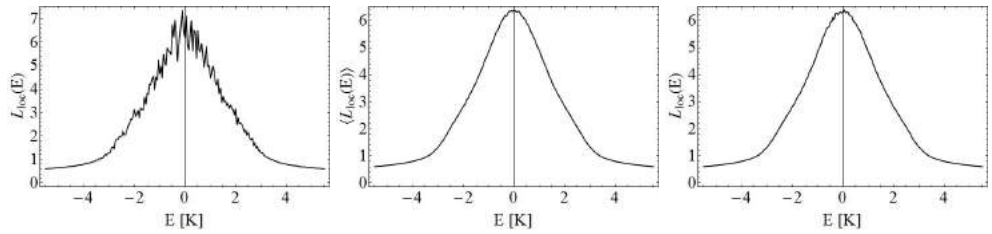

Figure 1.10: From left to right: $L_{loc}(E)$ for a single lattice of $M = 2^{10}$ sites, $\langle L_{loc}(E)\rangle$ averaged over 250 realizations of disorder and $L_{loc}(E)$ for a single lattice of $M = 100 \times 2^{10}$ sites. The proof of self-averaging comes form the comparison between second and third panel: they coincide, so a single realization of large systems describe the properties of an ensemble of smaller systems.

exponent [1, 62, 80, 94]. As we state previously, a solution for a given E belong to the spectrum of V_j only if exist a couple of vectors $\psi_0^{\pm}$ that decay respectively for $j \to \pm\infty$ and coincede at some site (localization center).

The inverse of the Lyapunov exponent is the localization length of the state with energy E:

$$\boxed{L_{loc}(E) = \frac{1}{\gamma(E)}\,.} \tag{1.26}$$

A fundamental property of this quantity is that it is *self-averaging* [1]. This property plays an important role in the case of disordered systems when usually the averaged over many realizations is needed. If a certain physical quantity satisfies certain requirements [1] a single large system is sufficient to represent the whole ensemble: when this happens the quantity under study is said to be self-averaging. It has been demonstrated that both Lyapunov exponent and localization length in Eq. (1.26) are self-averaging. In Fig. (1.10) we show how self-averaging works: we compare $L_{loc}(E)$ computed for a single chain with its average over many disordered realizations $\langle L_{loc}(E)\rangle$, then we plot $L_{loc}(E)$ for a single realization of a chain 100 times larger than the previous. The latter coincides with the disorder-averaged one, this is the proof of self-averaging: one single larger chain is sufficient to describe an ensemble of smaller systems.

1.4 Anderson localization: numerical examples

In previous sections we have described both different types of disorder and the effects a generic disordered potential has onto its eigenstates, remarking that the most important is the appearance of the Anderson localization phenomenon. In 1.3 the idea of exponential localization is presented in relation with a theoretical method which is useful in determining the localization $L_{loc}(E)$. In this section we will give a short summary

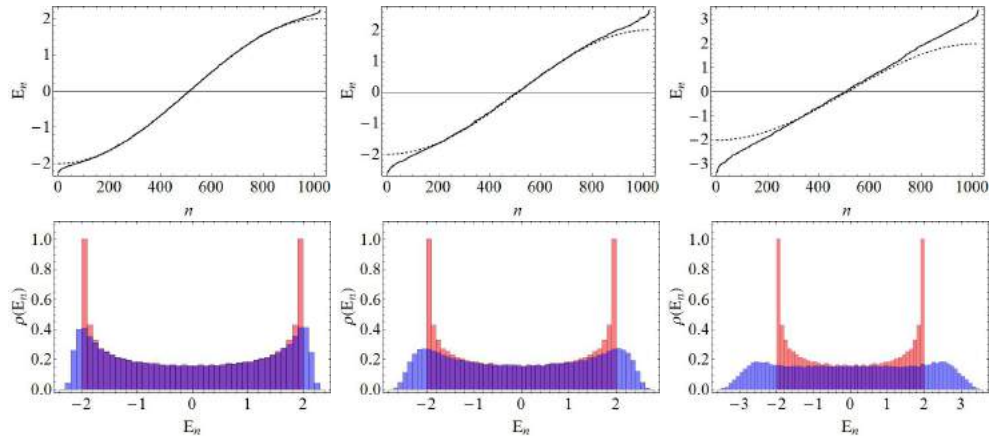

Figure 1.11: **Upper row:** energy spectrum; dashed lines correspond to perfect periodic lattice ($V_j = 0$), solid lines to disordered lattice. **Bottom row:** density of states; red bars correspond to the pure periodic lattice ($V_j = 0$), blue ones to the Anderson disorder. From left to right we consider increasing disorder $W = 0.5$, 1 and 2.

of what said, in particular we report some examples that put in evidence how Anderson localization set in in the case of the Anderson potential while the quasi-periodic lattice will be taken into account in the next chapter.

Let us take into account the disorder defined in Eq. (1.1). We put in Eq. (1.22) and then numerically diagonalize in order to find its spectrum (both eigenenergies and eigenstates). In Fig. (1.11) we report the energy spectra for single realizations of V_j and density of states $\rho(E)$ for different disorder strength. For each case we also plot the correspondent quantity in the case of a pure periodic system, in order to stress the effects of disorder. In [101] Thouless generalizes a formula developed few years before by Herbert and Jones [102] that shows how the spectral properties of disordered one dimensional systems could be put into connection with the localization properties of their eigenstates. The relation between Lyapuonv exponent $\gamma(E)$ and the DOS is expressed by

$$\gamma(E) = \int_{-\infty}^{+\infty} \ln(E - \varepsilon)\, \rho(\varepsilon)\, d\varepsilon\,. \tag{1.27}$$

Eq. (1.27) becomes useful in the case of Anderson disorder, in the limit of small disorder W, together with perturbation theory it gives[1] [80]

$$\gamma(E) = \frac{(W/K)^2}{6[4 - (E/K)^2]}\,. \tag{1.28}$$

When Eq. (1.28) is applied to a state in the center of the spectrum, i.e. $E \approx 0$, we recover that the localization length for those states are $L_{loc}(E \approx 0) = 24(K/W)^2$: the

[1] In literature Anderson model is defined with $V_i \in [-W/2; W/2]$. With this definition in Eq. (1.28) the numerical factor 6 has to be substituted with 24.

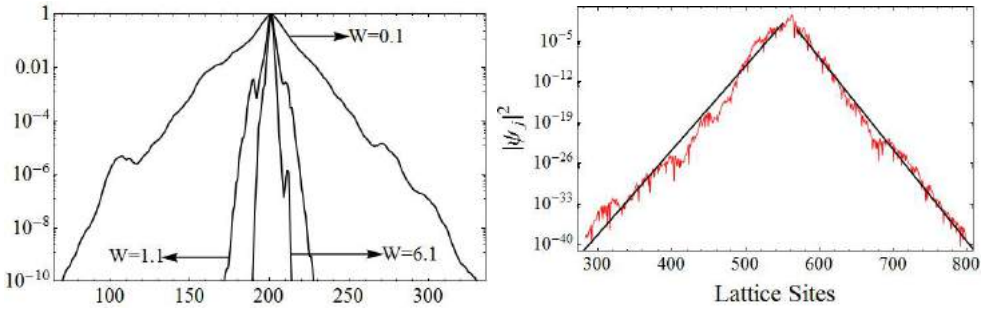

Figure 1.12: **Left panel:** ground states of Anderson disorder for different W (indicated in the figure). It is evident that the higher the disorder, the more localization we have. **Right panel:** eigenstate corresponding to $E \approx 0$ of an Anderson chain with $W = 2$. Dashed line correspond to $\propto \exp\left[-|x - \bar{x}|/L_{loc}(0)\right]$, with $L_{loc}(E = 0)$ as indicated in the text.

important results is that states situated at the center of the band, with $E = 0$, are localized on longer length scales. It also has been found that the behavior of L_{loc} for small W, i.e. the fact that it diverges as W^{-2} is quite general and does not apply only to the Anderson model.

2

Ultracold dilute bosonic gases: from GPE to DNLS

In this thesis we will present a long list of numerical simulations and models, which could be applied to all the system that are describe by equations of motions, or Hamiltonian, similar to those we consider. Although this we will consider in Chap. 4 some specific experiment, the simulations and models were developed for. Those experiments were done in Florence, at LENS, by the ultracold atoms group [87]. The great versatility of ultracold atoms and the possibility of building up experiments in which one could know the Hamiltonian and tune its parameters is the most powerful characteristic of those systems.

Here we will report some basic properties, that are important in the realizations and managing of those atoms, and derive the equations which will be used trough all this thesis. Those results are of course not new and can be find in many textbook and papers about ultracold atoms, we refer in particular to [103–106]; many thesis are also written on this subject and in particular [77, 80] were very useful for us.

2.1 Atomic dilute gases: systems with tunable interactions

The use of atomic dilute gases in BEC experiments turns out to be very useful do to the fact that, because of their low density, they can be conveniently assimilated to quasi ideal systems. This means that interactions between atoms can be considered very low, at least in principle. Quantum theory of scattering tells us that in this regime the only important collisions are the one described by the s-wave approximation. Bose-Einstein condensation is realized in laboratory at temperature that are fractions of one Kelvin, then the energies are very low and we are justified in considering the limit of small momenta. In this case the cross section σ, that a fundamental quantity in scattering,

assumes a very simple form:

$$\lim_{k\to 0} \sigma(k) = 4\pi a_s^2 \,, \tag{2.1}$$

where a_s is the s-wave scattering length and $a_s > 0$ or $a_s < 0$ for attractive and repulsive interactions, respectively.

Eq. (2.1) give us a considerable help, allowing us to substitute the two body interaction potential $V(\mathbf{r}_i, \mathbf{r}_j)$ with a hard-core pseudopotential:

$$V(\mathbf{r}_i, \mathbf{r}_j) \approx \frac{4\pi\hbar^2 a_s}{m}\delta^{(3)}(\mathbf{r}_i - \mathbf{r}_j) \equiv g\delta^{(3)}(\mathbf{r}_i - \mathbf{r}_j)\,, \tag{2.2}$$

which is sometimes called Fermi approximation.

This formula is useful also because it allows to introduce a condition for the density of a (bosonic) gas at low temperature which defines if its dilute or not, an it is

$$n(\mathbf{r})|a_s|^3 \ll 1\,. \tag{2.3}$$

One of the greatest advantage of ultracold atoms is that this scattering length a_s that define interactions among particles can be tuned by the mean of a magnetic field. This is the so-called Fano-Feshbach, usuallu just Feshbach, magnetic resonance. At the beginning Feshbach resonances were studied in nuclear systems [107–109] and years later become a fundamental tool in atomic physics [110–112]. The theory of Feshbach resonance leads to a scattering length a_s which depends onto the applied magnetic field:

$$a_s(B) = a_0\left(1 - \frac{W}{B - B_0}\right)\,, \tag{2.4}$$

where B_0 the center of the resonance and W its width. It is possible by the application of an homogeneous magnetic field to control the atomic interaction from strongly attractive to strongly repulsive. We notice that, although the resonance phenomenon is general as derived from quantum mechanical reasoning, the parameter involved in (2.4) depends on the specif atomic system under study [77].

2.2 Condensates dynamics: Gross Pitaevskii Equation

In this section we will take into account a system of bosons at $T = 0K$ showing that the condensate could be described by a single wave function, which plays the role of the order parameter for the system, and to which we refer as the macroscopic wave function of the condensate. Then we will derive the equation of motion for it, that will be similar to a standard Schrödinger equation, but due to the interactions among particle it has a nonlinear term.

In quantum mechanics a system composed by N particles is described by the following

Hamiltonian:

$$H = \sum_{i=1}^{M} -\frac{\hbar^2}{2m}\nabla_i^2 + U(\mathbf{r}_i) + \frac{1}{2}\sum_{i,j=1}^{N} V(\mathbf{r}_i, \mathbf{r}_j) \equiv \sum_{i=1}^{N} h_i + \frac{1}{2}\sum_{i,j=1}^{N} V(\mathbf{r}_i, \mathbf{r}_j)\,, \tag{2.5}$$

where $U(\mathbf{r}_i)$ is the external potential which confines the atoms, $V(\mathbf{r}_i, \mathbf{r}_j)$ is the interaction potential between atoms and h_i is a single particle Hamiltonian, i.e. an Hamiltonian acting only onto the i-th particle. Notice that the consider just two body interactions. Eq. (2.5) acts onto the total wave function of the N-body system, which we indicate by $\Psi^{(N)}(\mathbf{r}_1, \mathbf{r}_2, \ldots, \mathbf{r}_N)$. The total energy of the system is then expressible as a functional of that wave function:

$$E[\Psi^{(N)}] = \langle \Psi^{(N)} | H | \Psi^{(N)} \rangle\,. \tag{2.6}$$

From now on we will consider the ground state of the system, and we will assume that $\Psi^{(N)}(\mathbf{r}_1, \ldots, \mathbf{r}_N)$ is normalized to 1,

$$\int \overline{\Psi^{(N)}}(\mathbf{r}_1, \ldots, \mathbf{r}_2)\, \Psi^{(N)}(\mathbf{r}_1, \ldots, \mathbf{r}_2)\; d^3\mathbf{r}_1 \ldots d^3\mathbf{r}_N = 1\,, \tag{2.7}$$

with $\overline{\Psi^{(N)}}$ being the complex conjugate of $\Psi^{(N)}$.

To find the ground state energy we will use a variational approach [106] in which we need to take into account that the total number of particle N is fixed. Because of this prescription one has to recall the method of Lagrange multiplier and, supposed to work with a canonic ensemble, it will be N that fixes the chemical potential μ. We therefore obtain the free energy functional

$$E_\mu\left[\Psi^{(N)}\right] = \langle \Psi^{(N)} | H - \mu N | \Psi^{(N)} \rangle\,. \tag{2.8}$$

Now we search for a simple form of $\Psi^{(N)}$. By the means of mean field theories (also known as Hartree method) the N-particle wave function will be factorized into the product of N single particle wave functions that are not necessarily eigenstates of the respective h_i. We are dealing with bosonic system then this product of single particle functions needs to be symmetrized in the proper way; in this case $\Psi^{(N)}$ will be a permanent of them. The fundamental property of bosons is that there is no limitation to the occupation of a single quantum state, so between the N function there could be n_i $(i = 0, 1, Idots, N)$ that are equals and which describe the state φ_i. The total wave function $\Psi^{(N)}$ is therefore the sum of all this possible combinations.

From basic theory of statistical mechanics it is possible to demonstrate that for $T < T_{BEC}$ the ratios $n_{i\neq 0}/N$ tends to zero in the limit of large N. On the other hand if one counts the particles not in the ground state, i.e. $\sum_{i\neq 0} n_i$, he will find a finite that is smalled than N. All the remaining particle occupy the state with minimum energy. In the case of a non interacting gas this behavior will be present also at the absolute zero,

notice that also at that temperature there is a small non condensed fraction of atoms in the system. Taking into account an ideal gas for $T \to 0K$ and $N \to \infty$, not only $n_{i\neq 0}/N$ tends to zero, but also $\sum_{i\neq 0} n_i/N \to 0$, which demonstrate that for an ideal Bose gas at $T = 0K$ all the particles are condensed in the ground state of the system.

The system we will take into account in all this thesis will be composed by weakly interacting atomic gases so, having in mind what we have just find, we are allowed in writing

$$\Psi^{(N)}(\mathbf{r}_1, \ldots, \mathbf{r}_2) = \prod_{i=1}^{N} \varphi_0(\mathbf{r}_i) \,, \tag{2.9}$$

where each of the $\varphi(\mathbf{r}_i)$ is normalized to 1, $\int |\varphi_0(\mathbf{r}_i)|^2 \, d^3\mathbf{r}_i = 1$. Substituting (2.9) in (2.5) we get

$$E = N \int d^3\mathbf{r} \frac{\hbar^2}{2m} |\nabla\varphi(\mathbf{r})|^2 + U(\mathbf{r}) |\varphi(\mathbf{r})|^2 + g\frac{N(N-1)}{2} \int d^3\mathbf{r} \, |\varphi(\mathbf{r})|^4 \,, \tag{2.10}$$

in which we use the Fermi approximation for $V(\mathbf{r}_i, \mathbf{r}_j)$. Because of (2.9), and due to the fact that $N_0/N \to 1$ as $T \to 0$ it is useful to define the system's order parameter:

$$\Phi(\mathbf{r}) = \sqrt{N}\varphi_0(\mathbf{r}) \,, \tag{2.11}$$

which is of course normalized to N and directly linked to the gas density

$$n(\mathbf{r}) = |\Phi(\mathbf{r})|^2 \,. \tag{2.12}$$

Inserting (2.11) in (2.10) the energy functional becomes

$$E[\Phi] = \int d^3\mathbf{r} \left[\frac{\hbar^2}{2m} |\nabla\Phi(\mathbf{r})|^2 + U(\mathbf{r}) |\Phi(\mathbf{r})|^2 + \frac{g}{2} |\Phi(\mathbf{r})|^4 \right] . \tag{2.13}$$

To obtain the optimal form for $\Phi(\mathbf{r})$ we have to minimize the energy (2.13) with respect to independent variations of $\Phi(\mathbf{r})$ and $\overline{\Phi}(\mathbf{r})$, together with the prescription that the total number of particles has to be kept constant. We will then write $\delta E - \mu\delta N = 0$, with arbitrary variations of Φ and Φ^*. Let us impose

$$\frac{\delta E[\Phi]}{\delta\Phi^*} - \mu\frac{\delta N}{\delta\Phi^*} = 0 \,, \tag{2.14}$$

from which readily

$$\left[-\frac{\hbar^2}{2m}\nabla^2 + U(\mathbf{r}) + g |\Phi(\mathbf{r})|^2 \right] \Phi(\mathbf{r}) = \mu\Phi(\mathbf{r}) \,. \tag{2.15}$$

Eq. (2.15) is known as the stationary Gross-Pitaevskii equation, due to the fact that both Gross [113, 114] and Piataevskii [115] had independently introduced it. It is a nonlinear Schrödinger equation in which each atom feels a potential which is the sum of

the external $U(\mathbf{r})$ and of a term $g|\Phi(\mathbf{r})|^2$ which describes the mean field generated by all the other bosons.

We have now stressed that Eq. (2.15) describe the properties of the condensate at the equilibrium. Obviously there are an infinite number of cases in which it is important to study the dynamics of the system, and then follow its evolution during the time. It therefore necessary to find an equation like (2.15) but that will take into account the time dependence of the wave function. A clean and rigorous way to do it is to apply the least action principle

$$\delta S = \delta \int_{t_1}^{t_2} L \, dt = 0 \,, \tag{2.16}$$

to the Dirac's functional [103]

$$S = \int dt \, \langle \Psi^{(N)}(t) | i\hbar \frac{\partial}{\partial t} - H | \Psi^{(N)}(t) \rangle \,, \tag{2.17}$$

where H is the N-particle Hamiltonian in (2.5), and

$$\langle \mathbf{r} | \Psi^{(N)}(t) \rangle = \prod_{i=1}^{N} \varphi(\mathbf{r}_i, t) \,.$$

Inserting this into (2.17) and applying (2.16) we get

$$i\hbar \frac{\partial \Phi(\mathbf{r}, t)}{\partial t} = \left[-\frac{\hbar^2}{2m} \nabla^2 + U(\mathbf{r}) + g \, |\Phi(\mathbf{r}, t)|^2 \right] \Phi(\mathbf{r}, t) \,, \tag{2.18}$$

where again in H we used $V(\mathbf{r}_i, \mathbf{r}_j) = g\delta(|\mathbf{r}_i - \mathbf{r}_j|)$.

2.3 From 3D to 1D systems

The great advantage of using ultracold atoms is not only determined by the possibility of tuning the interactions, but also because there are very precise experimental technique based on lasers and magnetic filed which create a series of different traps for the atoms. Those traps creates not only different shapes and geometry, but the can also generates system of different dimensionality. The idea is very simple: a cloud of atoms is three dimensional, if we separate it in a stack planes which do not interact we have created an ensemble of two dimensional system. Finally if those plans are cut in different slice we get an array of one dimensional tubes.

Another possibility for generating a one dimensional system is to freeze the dynamics of the system along two spatial directions, quantum mechanics demonstrate that this is possible. Let us consider the Eq. (2.18), and define the confining potential $U(\mathbf{r}_i)$ as the

sum of three component:

$$U(\mathbf{r}) = U(x) + U(y) + U(z) = \frac{m\omega^2}{2}\left(y^2 + z^2\right) + V_{1D}(x)\,, \tag{2.19}$$

in principle along the y and z direction one could have different trapping frequencies $\omega_{x,y}$, in that case one could recover expression (2.19) using an appropriate average of the two frequencies, we use the same ω just for simplicity. Having divided the potential into an harmonic part, in the (y, z) plane, and a radial part, along x allows us to factorize the wave function as

$$\Phi(x, y, z, t) = \psi(x, t)\phi(z)\phi(y)\,. \tag{2.20}$$

Strictly speaking this is not possible, because the Hamiltonian is written as the sum of different parts each depending on just one variable, the nonlinear term mixes the three spatial direction. Although it has been demonstrated by an enormous amount of theoretical papers but especially experiments, that for a strong enough harmonic confinement Eq. (2.20) gives the right results. When ω has the proper value system can populate just the ground state of $U(y)$ and $U(z)$ leading to a simple form

$$\Phi(x, y, z) = \frac{1}{a_\perp\sqrt{\pi}} e^{-\frac{y^2+z^2}{2a_\perp^2}}\,\psi(x)\,,$$

where $a_\perp = \sqrt{\hbar/m\omega}$ is called oscillator's length and is the characteristic dimension of the harmonic confinement. Once we get it we just integrate over $dydz$ and, after discarding constant terms resulting from the integration, we come to

$$i\hbar\frac{\partial\psi(x, t)}{\partial t} = \left[-\frac{\hbar^2}{2m}\frac{\partial^2}{\partial x^2} + U(x) + g_{1D}\left|\psi(x, t)\right|^2\right]\psi(x, t)\,, \tag{2.21}$$

where in the nonlinear term appears the rescaled interaction strength

$$g_{1D} = \frac{g}{2\pi a_\perp^2}\,. \tag{2.22}$$

2.4 Optical lattices and tight-binding approximation

Eq. (2.21) describes an infinite number of systems, depending on the specific form of $U(x)$. In this section will take into account one of the most used configurations in experiments with ultracold atoms that is also implemented in experiments presented in [87] which will be the subject of Chapter 4: optical lattices. Their are generated by the superposition of two counter propagating laser beams, the electromagnetic fields of which combine to create a standing wave that is perfectly periodic in space. This is of great importance because the possibility of having periodic structure without any

defects opens many and many new branches of research, in particular it allows to create a link between ultracold atomic systems and condensed matter, in which the presence of systems defined onto lattices is usual (e.g. the common crystal structure in solids). Thus we have

$$U(x) = U_{OL}(x) + V(x)$$

where $V(x)$ is an arbitrary potential and U_{OL} is the lattice potential

$$U_{OL}(x) = s_1 E_{r1} \cos^2(k_1 x)\,, \tag{2.23}$$

where we had introduced the following parameters:

- E_{r1}: recoil energy. It is a quantity with the dimensions of an energy, which gives the right dimensions to all $U_{OL}(x)$: $E_{r1} = \hbar^2 k_1^2/2m$, m being the mass of the atomic species;

- s_1: dimensionless parameter measuring the strength of $U_{OL}(x)$;

- k_1: wave vector of the laser beam generating the potential.

The index 1, which has no significance here, will become useful in the following.

As described in Appendix A, in the presence of such a periodic potential one can implement a formalism based onto the Wannier functions $w_{n,j}(x)$, which we recall are eigenstate of the periodic potential and they are strongly localized around each lattice site. For deep lattice, i.e. large s_1, one can restrict to the first energy band of the system, due to the fact that the gap between lowest and first excited band are so large compared with the energy scale of the problem that transition between them are forbidden. In that case we will drop out the band-index n and just indicate the functions with $w_j(x)$. We recall that the $w_j(x)$'s form a orthonormal and complete set of functions [68,77,80,91], so it is possible to decompose any functions over them

$$\psi(x) = \sum_j \psi_j w_j(x)\,, \tag{2.24}$$

or, with Dirac's notation

$$|\psi\rangle = \sum_j \psi_j |w_j\rangle\,. \tag{2.25}$$

Using the completeness of $|w_j\rangle$ we have for the Hamiltonaian of the system

$$H = \sum_{i,j} |w_i\rangle\langle w_i|H|w_j\rangle\langle w_j|\,. \tag{2.26}$$

Let us now consider in slightly more details the matrix elements $\langle w_i|H|w_j\rangle$, discarding for a while the non linear term in Eq. (2.21). From Eq. (2.26) we have

$$\langle w_i|H|w_j\rangle = \int dx\, w_i^*(x)\left[-\frac{\hbar^2}{2m}\frac{d^2}{dx^2} + U_{OL}(x)\right] w_j(x) + \\ + \int dx\, w_j^*(x) V(x) w_j(x)\ . \tag{2.27}$$

To go further we need to introduce some other hypothesis, which are common in theory and moreover well satisfied in the ultracold atoms experiments important for this work: one is the restriction to the lowest band, also known as tight-binding approximation, the other is considering hopping only between nearest neighboring sites of the lattice. Both of them are fulfilled in sufficiently deep lattice, where barriers between sites are so high that prevent long range tunneling. Within this framework Eq. (2.27) becomes [77]

$$\langle w_j|H|w_j\rangle \approx \varepsilon_0\delta_{ij} - JE_{r1}\delta_{i,j\pm1} + \delta_{ij}\int dx, V(x)|w_i(x)|^2\,. \tag{2.28}$$

Here it appears the **tunneling matrix element between neighboring sites** J[1]. Numerical calculations gives a good estimation of J in terms of s_1 [68, 116]

$$J \simeq 1.43\, s_1^{0.98}\, \exp\left(-2.07\sqrt{s_1}\right)\,, \tag{2.29}$$

when measured in units of E_{r1}. In Eq. (2.28) the last term corresponds to the discrete version of the potential energy and is clearly diagonal in the site index: $V_{ij} = \delta_{ij}V_j$, and it varies between system depending onto the $V(x)$ used.

Combining Eq. (2.26) and Eq. (2.28) we get

$$H = -\sum_j \left(|w_j\rangle\langle w_{j+1}| + |w_{j+1}\rangle\langle w_j|\right) + V_j|w_j\rangle\langle w_j|\,, \tag{2.30}$$

which is the Hamiltonian for the tight-binding model of the standard Schrödinger equation. Using the usual $i\partial_t|\psi\rangle = H|\psi\rangle$ together with Eq. (2.25) and Eq. (2.26) we come to

$$i\frac{\partial\psi_j(t)}{\partial t} = -\left[\psi_{j+1}(t) + \psi_{j-1}(t)\right] + V_j\psi_j(t) \tag{2.31}$$

that is the *Discrete Schrödinger Equation* (DSE).

We now come back to the interaction term in (2.13), $\int (g/2)|\Phi(x,t)|^4 dx$. Introducing in the integral the Wannier decomposition for $\Phi(x,t)$ it readily find that [80]

$$\frac{G}{2}\sum_j |\psi_j|^4\,,$$

[1] Sometimes K is used instead of J (see for example (1.22)). In this thesis we will use both of notation freely, if there will be misunderstanding we will specify the choice of notation at the right moment.

with

$$G = g_{1D} \int |w_j(x)|^4 dx \ .$$

If one consider a function normalized to N instead of 1 (as $\Phi(x,t)$ in (2.21)) and defines

$$U = \frac{NG}{JE_{r1}} \,, \tag{2.32}$$

the linear Hamiltionian in Eq. (2.30)) and Eq. (2.31) become

$$\boxed{H = \sum_j -\left(\psi_j^* \psi_{j+1} + \psi_j \psi_{j+1}^*\right) + V_j \left|\psi_j\right|^2 + \frac{U}{2}\left|\psi_j\right|^4 \ ,} \tag{2.33}$$

and

$$\boxed{i\frac{\partial \psi_j(t)}{\partial t} = -\left(\psi_{j+1}(t) + \psi_{j-1}(t)\right) + V_j \psi_j(t) + U\left|\psi_j(t)\right|^2 \psi_j(t) \,,} \tag{2.34}$$

which is known as *Discrete Nonlinear Schrödinger Equation (DNLS)* [68,77,103,117] and is the prototype equation for the study of ultracold atomic system loaded onto periodic optical lattices in the presence of also a potential $V(x)$.

As we just said Eq. (2.34) describes different systems depending on V_j, here we restrict to just the potential that will be considered in the following, and that we already described in 1.2.1: the quasi-periodic potential and the Anderson model.

The latter is simple, because it is already defined as a discrete model since is first appearance [2]:

$$V_j \in [-W, W] \qquad \text{Anderson Model} \ . \tag{2.35}$$

In the case of the quasi-periodic potential we will derive explicitly the form of V_j. We have shown in 1.2.1 that a qausi-periodic potential is a superposition of a deep lattice $V_1 \cos^2(k_1 x)$, which is the one that defines the spatial discretization and one uses to get Eq. (2.34), and a secondary lattice

$$s_2 E_{r2} \cos^2\left(k_2 x + \theta\right) \ , \tag{2.36}$$

that plays the role of $V(x)$ in Eq. (2.28). Here we have expressed the secondary lattice amplitude V_2 in (1.12) as the product of an dimensionless strength s_2 and a recoil energy $E_{r2} = \hbar k_2^2/2m$. Remembering that $\cos^2(x) = [\cos(2x) + 1]/2$, and neglecting the constant terms in (2.28), one gets [68, 77]

$$V_j = \frac{\Delta}{J} \cos\left(2\pi\beta j + \vartheta\right) \qquad \text{Quasi-periodic model} \,, \tag{2.37}$$

where the term Δ is proportional to the strength of the second lattice, i.e. to the disorder:

$$\Delta = \frac{s_2 E_{r2}}{2E_{r1}} \exp\left(-\frac{\beta^2}{\sqrt{s_1}}\right), \tag{2.38}$$

and in (2.37) we have measured energies in units of JE_{r1}. When inserted in Eq. (2.33) it reads

$$\boxed{H = \sum_j -\left(\psi_j^* \psi_{j+1} + \psi_j \psi_{j+1}^*\right) + \lambda \cos\left(2\pi\beta j + \vartheta\right) |\psi_j|^2 + \frac{U}{2} |\psi_j|^4 ,} \tag{2.39}$$

where we define $\lambda = \Delta/J$ for convenience. Eq. 2.39 is the Hamiltonian describing interacting particles in quasi-periodic potentials, the correspondent linear problem ($U = 0$) is known as Aubry-André model [55, 67, 68, 77, 80, 90].

2.5 Anderson localization in quasi-periodic lattice

In 1.2.1 we have included in the class of disordered potentials also quasi-periodic lattices, although they do not show properties typical of purely random systems (see Fig. (1.6)). The choice of considering them in this way comes from the seminal paper of Aubry and André [67] in which authors define the model we reported in Eq. (2.39) in the case of $U = 0$:

$$-\left(\psi_{j-1} + \psi_{j+1}\right) + \lambda \cos\left(2\pi\beta j + \vartheta\right) \psi_j = E\psi_j . \tag{2.40}$$

In that paper they demonstrate that this kind of potential lead to an exponential localization of its eigenstates, i.e. Anderson localization set in also in quasi-periodic lattices, but with the important remark that it takes place only above a certain value of λ.

In [80] the demonstration given by Aubry and André is reported, and we follow the same scheme just to give some important results that will be frequently used in all the rest of the thesis. The key point is that Eq. (2.40) shows a self-duality, it means that defining a new field φ_l through [80]

$$\begin{aligned} \psi_j &= e^{i\theta j} \sum_{l=-\infty}^{+\infty} \varphi_l \, e^{il(2\pi\alpha j + \vartheta)} , \\ \varphi_l &= e^{-i\vartheta l} \sum_{j=-\infty}^{+\infty} \psi_j \, e^{-il(2\pi\alpha l + \theta)} , \end{aligned} \tag{2.41}$$

one get the equation

$$-\left(\varphi_{l-1} + \varphi_{l+1}\right) + \frac{4}{\lambda} \cos(2\pi\alpha l + \theta)\varphi_l = \frac{2E}{\lambda}\varphi_l . \tag{2.42}$$

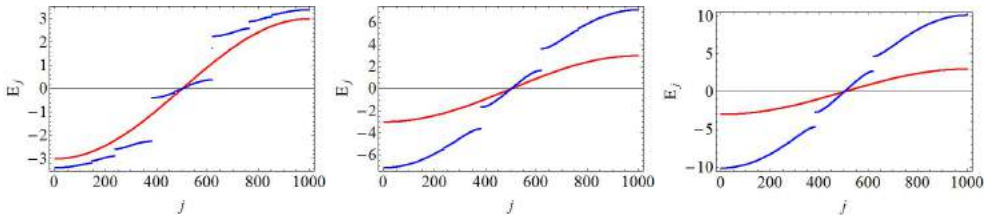

Figure 2.1: Energy spectra for periodic potential (red lines) and quasi-periodic lattices (blue lines). From left to right we consider increasing disorder $\lambda = 3$, 7 and 10.
The peculiarity of quasi-periodic lattices is that each band (here just one because we are in the tight-binding limit) presents an inner structure with bands and gaps as well as the overall spectrum.

Eq. (2.42) clearly has the same form of Eq. (2.40) provided that one makes the right substitutions

$$\frac{4}{\lambda} \to \lambda\,, \quad \varphi_l \to \psi_j\,, \quad \frac{2E}{\lambda} \to E\,, \quad \theta \to \vartheta\,.$$

One important consequence of this self-duality is that *if ψ_l is localized φ_l is extended, and vice versa*. Because we want to investigate localization properties we now recall Thouless formula in Eq. (1.27), which implies that we have also to determine the density of states for the quasi-periodic lattice [101]. The density of states follows from the integrated density of states by applying the usual formula $\rho(E) = \partial\mathcal{N}(E)/\partial E$, where $\rho(E)$ is the density of states and $\mathcal{N}(E)$ the integrated density of states. In [67] authors give a direct derivation of those quantities form which they get the Lyapunov exponent

$$\gamma_{\lambda,\alpha}(E) = \gamma_{\frac{4}{\lambda},\alpha}\left(\frac{2E}{\lambda}\right) + \ln\left(\frac{\lambda}{2}\right)\,. \tag{2.43}$$

In Eq. (2.43) α is assumed to be irrational, and the indexes clearly show the self-duality of the systems, relating γ for a given disorder strength λ and energy E to the same in the case of disorder $4/\lambda$ and energy $2E/\lambda$. In Fig. (2.1) we report some examples of energy spectra and in Fig. (2.2) the correspondent densities of states, for some values of λ. It is important to notice that with quasi-periodic potentials energy spectrum shoes a peculiar behavior: a single band present an inner structure which recalls the one of the overall spectrum, i.e. several allowed energies separated by forbidden gaps. Amplitude and number of those gaps varies with λ. Now, the localization properties for the Aubry-André model can be derived from Eq. (2.43) with the help of some simple assumptions. First of all $\gamma(E)$ is a non-negative number, and it vanishes only in the case of extended states; then we recall the result of few lines above, i.e. the specular behavior of eigenstates for the self-dual systems: if for the disorder λ eigenstates of energy E is localized, the eigenstate relative to $2E/\lambda$ in the disorder $4/\lambda$ is extended. It means that if $\gamma_{\lambda,\alpha}(E)$ has finite value, $\gamma_{4/\lambda,\alpha}(2E/\lambda)$ is zero, and vice versa. We are considering the

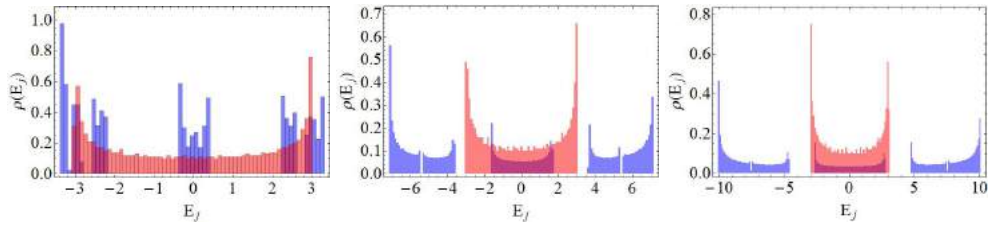

Figure 2.2: Density of states for the same potentials of first row. From left to right we consider increasing disorder $\lambda = 3$, 7 and 10.

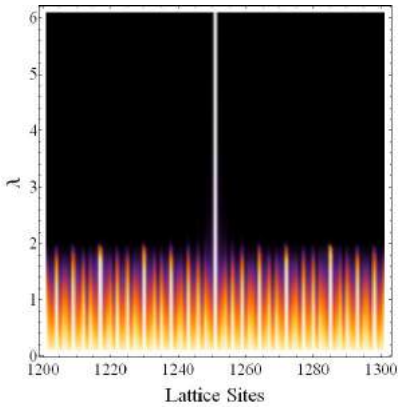

Figure 2.3: Density plot for the ground state of Eq. (2.40). It is clear the transition between extended states for $\lambda < 2$ and localized states for $\lambda > 2$.

disorder defined by λ, thus we have to assume $\gamma_{4/\lambda,\alpha}(2E/\lambda) = 0$, from which

$$\gamma_{\lambda,\alpha}(E) = \ln\left(\frac{\lambda}{2}\right) ,$$

and the positivity of the Lyapunov exponent require $\lambda > 2$. On the contrary, for $\gamma_{\lambda,\alpha} = 0$ we get

$$\gamma_{\frac{4}{\lambda}}\left(\frac{2E}{\lambda}\right) = \ln\left(\frac{2}{\lambda}\right) ,$$

which implies $\lambda < 2$. Following the idea in [68, 77, 80] we report in Fig. (2.3) a density plot of the ground state of Eq. 2.40 for increasing λ. From there it is clear that $\lambda = 2$ is a threshold dividing extended states, below it, from localized states, above it. These two results are fundamental for treating quasi-periodic systems. They state that *the Aubry-André model undergoes a transition from extended to localized eigenstates at* $\lambda = 2$. *All eigenstates are extended for* $\lambda < 2$ *and exponentially localized for* $\lambda > 2$. Moreover it is evident that, once localized, eigenstates posses all the same localization length, which does not depend onto the energy and that is

$$L_{loc} = \frac{1}{\gamma} = \frac{1}{\ln(\lambda/2)} . \tag{2.44}$$

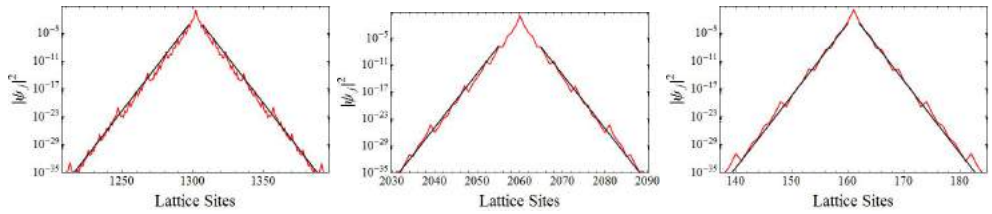

Figure 2.4: Ground state of Eq. (2.40) for increasing disroder. From left to right $\lambda = 3$, 7 and 10. Black lines correspond to fit with $\rho_j \propto \exp[-2|j - j_0|/L_{loc}]$ with L_{loc} defined in (2.44).

In Fig. (2.4) we plot the ground state of Eq. (2.40) for some different λ, together with a fit of its tails showing that they are proportional to $\exp[-|j - j_0|/L_{loc}]$, with L_{loc} defined in Eq. 2.44.

2.6 Experimental observations of Anderson localization

We have explained in the Introduction that direct observation Anderson localization is quite a difficult problems, due to the fact that in real systems many aspects play a role in contrasting it or simply there are some other effects that can not be avoided and so the bare localization is not visible. Despite this localization with classical waves was observed in many different physical systems: from ultrasound waves to light. Two of the main problems are the control of the disorder, which is generally not simple to engineer, and (regarding solid state physics) interactions among particles, that can not be avoided and can play important roles. In this chapter we have shown how ultracold atomic systems are very useful exactly because both external potentials and interactions between atoms are controllable with an high level of confidence. So they became favorite candidates in searching for Anderson localization, and the researches had lead to successful results. Anderson localization was finally observed with matter waves by two different groups in 2008, almost at the same time: the group of Alain Aspect, in Paris, working with speckles [20] and the group of Massimo Inguscio in Florence, working with quasi-periodic lattices [19]. Both the experiments creates one dimensional systems in which the atoms are initially trapped by an harmonic potential; then it is switched-off thus they can expand in the presence of the disordered potential. The crucial point is that during the expansion interactions between atoms are driven as close as possible to zero. The appearance of Anderson localization was searched by looking at the whole expanding clouds: first of all to its spatial width, which stops its increasing when localization set in, and then to the density profile of the wave packet. The exponential decay of the tails is the fingerprint of Anderson localization mechanism. In Fig. (2.5), (2.6) and Fig. (2.7) we report some figures taken from original articles [19,20] in which experimental results give a clear proof of Anderson localization.

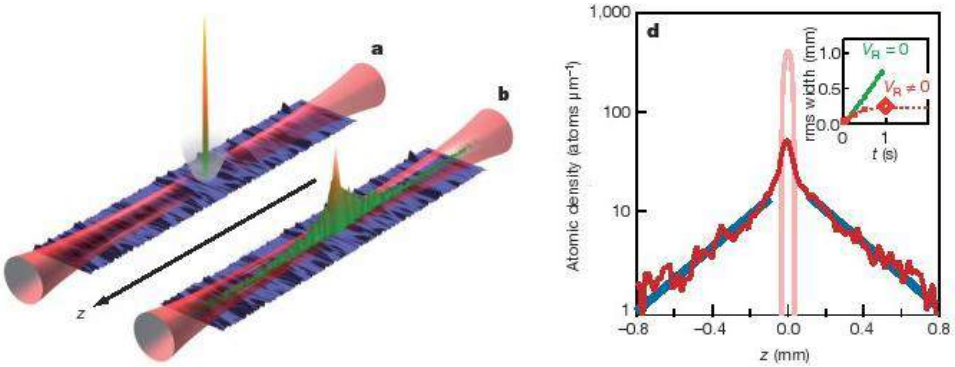

Figure 2.5: **Left panel:** sketches of the experiments on ultracold atoms in the presence of speckle potentials. An initially harmonic-trapped condensate (a) is let free to expand along the z direction after a sudden shut-down of the trapping (b). **Right panel:** semi-log plot of the atomic cloud density profile. The exponential localization is clear. In the inset author plot the spatial width of the atomic distribution, the show that in the presence of the disorder ($V_R \neq 0$) the width stops its increasing and remains constant, meaning that the whole cloud it is not expanding any more.
Figures taken from [20].

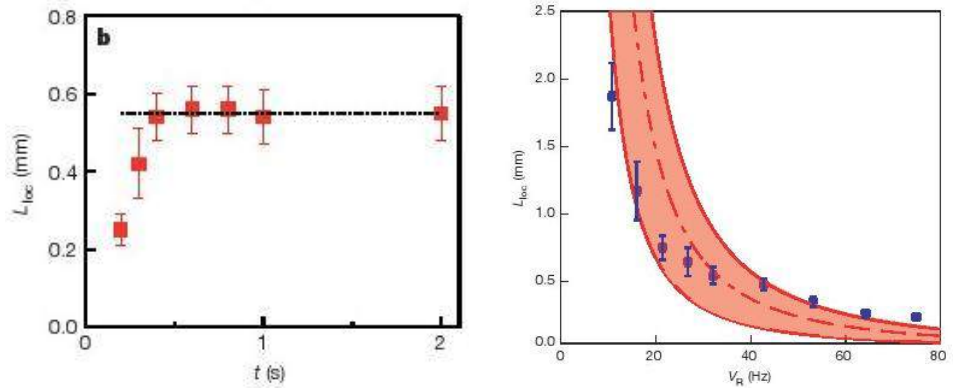

Figure 2.6: **Left panel:** measured localization length for the expanding atomic distribution in the presence of a speckle potential. The fact the it becomes stationary is a signature of Anderson localization. **Right panel:** comparison between measured L_{loc} and its theoretical predictions for increasing disorder. The agreement between experimental data and theoretical model are good.
Figures taken from [20].

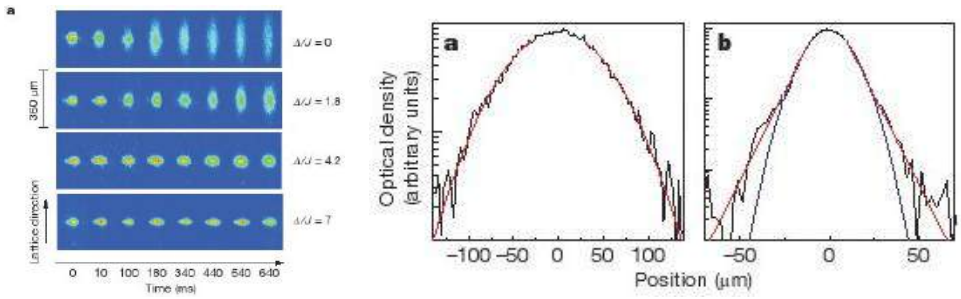

Figure 2.7: **Left panel:** experimental observation of the expansion of an ultracold atomic cloud in the presence of a quasi-periodic lattice. Each rows correspond to a different disorder strength, increasing for top to bottom. **Right panel:** density profile fitting for two different values of disorder. $\Delta = J$ in the left figure, $\Delta = 15J$ in the right. Again, the linear behavior in this semi-log scale is the fingerprint of Anderson localization. Figure taken from [19].

3

Anderson localization: eigenstates interference picture

Quantum mechanics is sometimes also called wave-mechanics, stressing the fact that matter could show behaviors that are peculiar of classical waves. One the most important phenomena is the interference, which also play a fundamental role in the superposition principle (one of the axioms of quantum mechanics): it has a very deep influence in the dynamics of a quantum system, even if one thinks about a single particle.

This will be the subject of this chapter: we put our attention onto one dimensional systems, showing how much the quantum interference between eigenstates of a system is important in the evolution of a wave packet. In particular we are interested in the role it plays in the case of disordered systems, where the phenomenon of Anderson localization (AL) takes place.

3.1 Generalities

Our approach is based on the standard rules of linear quantum mechanics (QM), which can be easily find in any textbook (e.g. [118, 119]).

Let us consider a quantum system, the dynamics of which is described by the Hamiltonian operator $\hat{\mathcal{H}}$, and suppose the we are able to diagonalized it (analytically or numerically it does not matter):

$$\hat{\mathcal{H}}\phi_n(x) = E_n\phi_n(x) \tag{3.1}$$

or, with the Dirac notation,

$$\hat{\mathcal{H}}|n\rangle = E_n|n\rangle\,. \tag{3.2}$$

Now consider a wave packet described by the wave function $|\psi(t)\rangle$ ($\psi(x,t)$ in the coordinate representation): we know that it can be always decompose onto a set of states

which forms an orthonormal basis for its Hilbert space, in particular the eigenstates of $\hat{\mathcal{H}}$ form such a basis. Then at a generic time t we have

$$|\psi(t)\rangle = \sum_n c_n(t)|n\rangle\,; \tag{3.3}$$

notice that all the time dependence is contained in the coefficients

$$c_n(t) = \langle n|\psi(t)\rangle = \int_{-\infty}^{+\infty} \phi_n^*(x)\psi(x,t)\,dx\,.$$

To find how those evolves in time one needs to use the Schrödinger equation

$$i\hbar\frac{d}{dt}|\psi(t)\rangle = \hat{\mathcal{H}}|\psi(t)\rangle\,. \tag{3.4}$$

Inserting Eq. (3.3) into Eq. (3.4) one obtains

$$i\hbar\sum_n \dot{c}_n(t)|n\rangle = \sum_n c_n(t)E_n|n\rangle\,,$$

where we use Eq. (3.1), remembering that $\hat{\mathcal{H}}$ is a linear operator and acts only on $|n\rangle$, while $c_n(t)$ are c-numbers; dot stands for time derivative. Multiplying both sides of the previous equation by $\langle m|$ one get $i\hbar\dot{c}_m(t) = E_m c_m(t)$, the solution of which turns out to be

$$c_m(t) = c_m(0)e^{-\frac{i}{\hbar}E_m t}\,. \tag{3.5}$$

The initial condition $c_m(0)$ is found from Eq. (3.4) setting $t = 0$

$$c_m(0) = \langle m|\psi(0)\rangle\,. \tag{3.6}$$

For our purpose it is convenient to write those coefficient in the modulus-phase representation

$$c_m(t) = |c_m(t)|e^{i\varphi_m(t)}\,;$$

looking at Eq. (3.5) it becomes

$$c_m(t) = |c_m(0)|e^{i\varphi_m(0)}e^{-iE_m t/\hbar} = |c_m(0)|e^{i\varphi_m(t)}\,.$$

In the last equation we set

$$\varphi_m(t) = \varphi_m(0) - \frac{E_m}{\hbar}t\,. \tag{3.7}$$

Here we get a first important result: the phase of each eigenstate evolves in a deterministic way, growing linearly with respect to the time, and each eigenstate evolves independently from the others, i.e. they are not coupled.

Putting together all these results

$$|\psi(t)\rangle = \sum_n |c_n(0)| e^{i\varphi_n(t)} |n\rangle \,. \tag{3.8}$$

Eq. (3.5) gives us the wave function, which brings all the physical information about the particle, but in real world (e.g. in the experiments) one cannot have direct access to it, usually one look to something related to it. In our case we will consider the density distribution

$$n(x,t) = |\psi(x,t)|^2 = |\langle x|\psi(t)\rangle|^2 \,.$$

By the use of Eq. (3.5) we directly calculate

$$\begin{aligned} n(x,t) &= \sum_{n,m} |c_n(0)||c_m(0)| e^{i\Delta\varphi_{nm}(t)} \phi_m^*(x)\phi_n(x) \\ &= \sum_n |c_n(0)|^2 |\phi_n(x)|^2 + 2\sum_{m<n} |c_n(0)||c_m(0)| \phi_m^*(x)\phi_n(x) \cos\left(\Delta\varphi_{nm}(t)\right) \\ &\equiv n_D(x) + n_{off}(x,t) \,, \end{aligned} \tag{3.9}$$

we have defined

$$\Delta\varphi_{nm}(t) = \varphi_n(t) - \varphi_m(t) \,. \tag{3.10}$$

In the last rows we retain only the real part of $\exp[i\Delta\varphi_{nm}(t)]$ because so it is $n(x,t)$.

Eq. (3.9) is the second fundamental result we obtain. The density could be divided into two parts: one (i.e. $n_D(x)$) which is stationary, and that we call *diagonal* due to fact the the sum defining it goes over all the eigenstates without mixing them; and one that we call "off-diagonal", because there is the mixing of different eigenstates in it and which brings all the informations about the difference in phases between eigenstates.

We thus decompose the density into a part which does not evolve in time. i.e. keep its shape constant, and a one which evolves due the interference between eigenstates and so which is responsible of all the changes observed in the density profile.

3.2 Gaussian wave packets in harmonic potential

We here apply our approach to a couple of problems the solutions of which is already known, trying to make the meaning of Eq. (3.9) clearer for the reader. We will study the dynamics of a Gaussian wave packet in the presence of an harmonic potential, in particular we will focus onto dipole oscillations and breathing dynamics. Thus Eq. (3.9) becomes

$$n(x,t) = \sum_n |c_n(0)|^2 |\phi_n(x)|^2 + 2\sum_{m<n} c_m^*(0)c_n(0)\phi_m^*(x)\phi_n(x) \cos\left(\frac{E_n - E_m}{\hbar}\, t\right) ;$$

where it is pointed out that the time dependence depends onto the energy difference between eigenstates. Recalling that $\hat{\mathcal{H}}$ is a linear Hermitian operator, its eigenstates ϕ_n and eigenvalues E_n can always chosen to be real; moreover we assume that the initial wave packet is described by a real wave function: because of this all the $c_n(0)$'s are real, then

$$n(x,t) = \sum_{n=0}^{+\infty} c_n^2(0)\phi_n^2(x) + \sum_{n=0}^{+\infty}\sum_{\substack{m=0\\m<n}}^{+\infty} \mathcal{A}_{nm}(x)\cos(\omega_{n,m}t)\,,$$

where we have introduced the frequencies $\omega_{n,m} = (E_n - E_m)/\hbar$ and

$$\mathcal{A}_{nm}(x) = 2c_n(0)c_m(0)\phi_n(x)\phi_m(x)\,. \tag{3.11}$$

Because $n > m$ we can write

$$E_n - E_m = E_n - E_{n-1} + E_{n-1} + \ldots + E_{n-(n-1)+m} - E_m\,,$$

then, dividing by $\hbar$,

$$\omega_{nm} = \sum_{i=m}^{n-1} \omega_{i+1,i}\,. \tag{3.12}$$

At the end we have:

$$n(x,t) = \sum_{n=0}^{\infty} c_n^2(0)\phi_n^2(x) + \sum_{n=1}^{\infty}\sum_{\substack{m=0\\m<n}}^{\infty} \mathcal{A}_{nm}(x)\cos\left[\left(\sum_{i=m}^{n-1}\omega_{i+1,i}\right)t\right]. \tag{3.13}$$

3.2.1 Harmonic oscillator spectrum

Here we briefly summarize some results about the spectrum of a 1D harmonic oscillator, giving all the useful formulae we need. The Hamiltonian is

$$\hat{\mathcal{H}} = \frac{\hbar^2}{2m}\frac{d^2}{dx^2} + \frac{m\Omega^2}{2}x^2\,, \tag{3.14}$$

which can be rescaeld by measuring energy in units of $\hbar\Omega$ and lengths in unit of $\sqrt{\hbar/m\Omega}$, so Eq. (3.14) becomes

$$\hat{\mathcal{H}} = -\frac{1}{2}\frac{d^2}{dx^2} + \frac{x^2}{2}\,. \tag{3.15}$$

The spectrum of Eq. (3.15) is known exactly, the eigenfunctions are

$$\phi_n(x) = \sqrt{\frac{1}{2^n n!}}\frac{1}{\pi^{1/4}}H_n(x)e^{-x^2/2}\,, \tag{3.16}$$

and the corresponding eigenenergy

$$E_n = n + \frac{1}{2}\,, \tag{3.17}$$

with $n \geq 0$ and $H_n(x)$ being the Hermite's polynomials.

3.2.2 Formal structure

As first we set $1/\Omega$ as the unit of measurement for the time, and define $\tau = t\Omega$.

We want to study how much the quantum interference is important for the dynamics of $n(x,\tau)$ by the means of Eq. (3.13), in which we insert Eq. (3.16), while from Eq. (3.17) we have

$$\omega_{nm} = n - m\,. \tag{3.18}$$

This shows immediately that, in that specific case, there are a lot of frequencies that are equal.

Defining $q = n - m > 0$ ($n > m$), we obtain

$$n(x,\tau) = \sum_{n=0}^{\infty} |c_n(0)|^2 |\phi_n(x)|^2 + \sum_{\substack{n,q=1 \\ n\geq q}}^{\infty} \mathcal{A}_{nq}(x)\cos(q\tau)\,; \tag{3.19}$$

with

$$\mathcal{A}_{nq}(x) = 2c_n(0)c_{n-q}(0)\phi_n(x)\phi_{n-q}(x)\,, \tag{3.20}$$

and n start from 1 because q must be greater then 0 and for $n = 0$ this condition cannot be satisfied. If one expand the second summation in (3.19) finds

$$\mathcal{A}_{11}\cos(\tau) + \mathcal{A}_{22}\cos(2\tau) + \mathcal{A}_{21}\cos(\tau) + \mathcal{A}_{33}\cos(3\tau) + \mathcal{A}_{32}\cos(2\tau) + \mathcal{A}_{31}\cos(\tau) + \ldots$$

so Eq. (3.19) could be rearranged in

$$n(x,\tau) = \sum_{n=0}^{\infty} |c_n(0)|^2 |\phi_n(x)|^2 + \sum_{q=1}^{\infty} \left(\sum_{n=q}^{\infty} \mathcal{A}_{nq}(x) \right) \cos(q\tau)\,.$$

Again, we define

$$\mathcal{C}_q(x) = \sum_{n=q}^{\infty} \mathcal{A}_{nq}(x)\,, \tag{3.21}$$

and finally:

$$n(x,\tau) = \sum_{n=0}^{\infty} |c_n(0)|^2 |\phi_n(x)|^2 + \sum_{q=1}^{\infty} \mathcal{C}_q(x)\cos(q\tau)\,. \tag{3.22}$$

We stress that, with this convention, $\mathcal{C}_q(x)$'s ensure that at $\tau = 0$ the density is properly $n(x,0) = |\psi(x,0)|^2$.

3.2.3 Dynamics of the mean values

We have just found a general recipe to determine the density at any time $\tau > 0$. Now it is useful to calculate how some quantities evolve in time, in particular we look to the mean position of the wave packet and to its width. It will be easier to work with the formalism of creation and destruction operators:

$$a|n\rangle = \sqrt{n}|n-1\rangle\,, \qquad a^+|n\rangle = \sqrt{n+1}|n+1\rangle\,, \tag{3.23}$$

and they obey the standard bosonic commutation rule

$$[a, a^+] = 1\,. \tag{3.24}$$

Thus Eq. (3.15) becomes

$$\hat{\mathcal{H}} = \hat{n} + \frac{1}{2}\,, \tag{3.25}$$

where $a^+a|n\rangle \equiv \hat{n}|n\rangle = n|n\rangle$ is the number operator. The Schrödinger equation turns out to be

$$\hat{\mathcal{H}}|n\rangle = E_n|n\rangle = \left(n + \frac{1}{2}\right)|n\rangle\,;$$

also other operators can be written in function of a and a^+, in particular the position operator x:

$$x = \frac{a + a^+}{\sqrt{2}}\,. \tag{3.26}$$

With a little of algebra we will now determine the mean values of $x(\tau)$ and $x^2(\tau)$, and then we turn to the width $\sigma(\tau) = \sqrt{\langle x^2(\tau)\rangle - \langle x(\tau)\rangle^2}$.

Starting from x one has

$$\langle x(\tau)\rangle = \langle\psi(\tau)|x|\psi(\tau)\rangle = \sum_{m,n=0}^{\infty} c_m(0)c_n(0)\, e^{-i(n-m)\tau}\, \langle m|\frac{a + a^+}{\sqrt{2}}|n\rangle\,. \tag{3.27}$$

The mean value in the last expression are readily found by the means of Eq. (3.23), together with the orthogonality property of $|n\rangle$:

$$\langle m|a|n\rangle = \sqrt{n}\langle m|n-1\rangle\sqrt{n}\delta_{m,n-1}\,, \quad \langle m|a^+|n\rangle = \sqrt{n+1}\langle m|n+1\rangle\sqrt{n}\delta_{m,n+1}\,.$$

Inserting these expression in (3.27) we find:

$$\langle x(\tau)\rangle = \sum_{n=0}^{\infty} \frac{c_{n-1}c_n}{\sqrt{2}}\sqrt{n}\, e^{-i\tau} + \frac{c_{n+1}c_n}{\sqrt{2}}\sqrt{n+1}\, e^{i\tau}\,.$$

At this point we retain only the real part of the previous expression because we are dealing

with a real quantity:

$$\langle x(\tau)\rangle = \left[\sum_{n=0}^{\infty}\left(\frac{c_{n-1}c_n}{\sqrt{2}}\sqrt{n}+\frac{c_{n+1}c_n}{\sqrt{2}}\sqrt{n+1}\right)\right]\cos\tau\,.$$

Because $n \geq 0$ the first term of the summation takes sense only for $n \geq 1$, while setting $n+1=m$ the second series runs from $m=1$ to $m=\infty$, i.e.

$$\sum_{n=1}^{\infty}\frac{c_{n-1}c_n}{\sqrt{2}}\sqrt{n}+\sum_{m=1}^{\infty}\frac{c_m c_{m-1}}{\sqrt{2}}\sqrt{m}\,,$$

thus, finally

$$\langle x(\tau)\rangle = \left(\sum_{n=1}^{\infty}\sqrt{2n}c_{n-1}(0)c_n(0)\right)\cos\tau \equiv \langle x(0)\rangle\cos\tau\,. \tag{3.28}$$

Eq. (3.28) give us a first important result: in a harmonic potential the average of the position oscillates harmonically in time with amplitude fixed by the initial condition.

Similar arguments help us to estimate the mean value of $x^2(\tau)$. We have to consider

$$x^2 = \left(\frac{a+a^+}{\sqrt{2}}\right)^2 = \frac{a^2+(a^+)^2+aa^++a^+a}{2} = \frac{a^2+(a^+)^2+2a^+a+1}{2}\,,$$

where use Eq. (3.24). Thus

$$\langle x^2(\tau)\rangle = \sum_{n,m=0}^{\infty}\frac{c_m(0)c_n(0)}{2}\,e^{-i(n-m)\tau}\langle m|a^2+(a^+)^2+2a^+a+1|n\rangle\,, \tag{3.29}$$

applying the properties of a and a^+ we obtain

$$\langle x^2(\tau)\rangle = \sum_{n=0}^{\infty}\frac{c_{n-2}c_n}{2}\sqrt{n}\sqrt{n-1}\,e^{-2i\tau}+\frac{c_{n+2}c_n}{2}\sqrt{n+1}\sqrt{n+2}\,e^{2i\tau}+\frac{|c_n|^2}{2}(2n+1)\,.$$

Taking the real part of it and rearranging the second series in the r.h.s. by using the same arguments that leads to Eq. (3.28), it becomes

$$\langle x^2(\tau)\rangle = \sum_{n=0}^{\infty}|c_n(0)|^2\left(n+\frac{1}{2}\right)+\left(\sum_{n=2}^{\infty}c_{n-2}(0)c_n(0)\sqrt{n(n-1)}\right)\cos(2\tau) \tag{3.30}$$

3.2.4 Dipole oscillations

Here we study the dynamics of an initial Gaussian wave packet, centered in $\alpha \neq 0$. Under these conditions the system shows the so-called dipole oscillations: the density profile just oscillates harmonically keeping its shape unchanged.

Initial wave-function

For simplicity, but without loosing generality, we choose as initial function $\psi(x,0)$ the ground state of Eq. (3.15), which is a Gaussian, shifted by $\alpha \neq 0$:

$$\psi(x,0) = \frac{1}{\pi^{1/4}} \exp\left[-\frac{(x-\alpha)^2}{2}\right] . \tag{3.31}$$

Projection

Now we put Eq. (3.31) and Eq. (3.16) in Eq. (3.5), which returns out

$$\begin{aligned} c_n(0) &= \int_{-\infty}^{\infty} \phi_n^*(x)\psi(x,0)dx \\ &= \sqrt{\frac{1}{2^n n!}}\frac{e^{-\alpha^2/4}}{\sqrt{\pi}} \int_{-\infty}^{\infty} e^{-x^2} \exp\left[2\left(\frac{\alpha}{2}\right)x - \left(\frac{\alpha}{2}\right)^2\right] H_n(x)dx\,. \end{aligned}$$

Using the generating function

$$e^{2tx-t^2} = \sum_{n=0}^{\infty} \frac{H_n(x)t^n}{n!}$$

together with the previous formulae we come to

$$c_n(0) = \sqrt{\frac{1}{2^n n!}}\frac{e^{-\alpha^2/4}}{\sqrt{\pi}} \sum_{m=0}^{\infty} \frac{1}{m!}\left(\frac{\alpha}{2}\right)^m \int_{-\infty}^{\infty} e^{-x^2} H_n(x)H_m(x)\,,$$

and the integral could be solved recalling Hermite's polynomials obey a generalized orthogonality relation:

$$\int_{-\infty}^{\infty} e^{-x^2} H_n(x)H_m(x) = 2^m m!\sqrt{\pi}\delta_{mn}\,.$$

At the end one obtains:

$$c_n(0) = \sqrt{\frac{1}{2^n n!}}\frac{e^{-\alpha^2/4}}{\sqrt{\pi}} \sum_{m=0} \frac{\alpha^m}{2^m m!} 2^m m!\sqrt{\pi}\delta_{mn} = \frac{\alpha^n}{\sqrt{2^n n!}}\, e^{-\frac{\alpha^2}{4}}\,. \tag{3.32}$$

Constructing $\psi(x,\tau)$ at any time

Now we are able to determine the wave-function at any time $\tau > 0$. Inserting Eq. (3.16), Eq. (3.17) and Eq. (3.32) in the series which defines $\psi(x,\tau)$ one obtains

$$\psi(x,\tau) = \frac{1}{\pi^{1/4}}\, e^{-\frac{\alpha^2}{4}} e^{-\frac{x^2}{2}} e^{-i\frac{\tau}{2}} \sum_{n=0}^{\infty} \frac{H_n(x)(\alpha/2)^n}{n!}\, e^{-in\tau}\,.$$

The sum of the last series is quite hard to find, so we evaluate it with the help of mathematical software which gives

$$\sum_{n=0}^{\infty} \frac{H_n(x) y^n}{n!} e^{-in\tau} = \exp\left[e^{-2i\tau}(2e^{i\tau}x - y)y\right] ,$$

that is just our case with $y = \alpha/2$. Thus we come to

$$\psi(x,\tau) = \frac{1}{\pi^{1/4}} \exp\left\{-\frac{1}{2}\left[i\tau + x^2 + \frac{\alpha^2}{2}\left(1 + e^{-2i\tau}\right) - 2e^{-i\tau}\alpha x\right]\right\} ,$$

which, after some simple calculations, takes the following form:

$$\psi(x,\tau) = \frac{1}{\pi^{1/4}} \exp\left[-\frac{(x - \alpha\cos\tau)^2}{2}\right] e^{i\left[\tau - (\alpha^2\cos\tau - 2\alpha x)\sin\tau\right]} , \tag{3.33}$$

where we separate the modulus and the phase of the complex wave function.

Because we are interested in the dynamics of the density we have to consider the squared modulus of Eq. (3.33)

$$n(x,\tau) = |\psi(x,\tau)|^2 = \frac{1}{\sqrt{\pi}} e^{-(x-\alpha\cos\tau)^2} , \tag{3.34}$$

and then, comparing Eq. (3.34) with the initial density

$$n(x,0) = |\psi(x,0)|^2 = \frac{1}{\sqrt{\pi}} e^{-(x-\alpha)^2} , \tag{3.35}$$

it seems evident that $n(x,\tau)$ oscillates back and forth periodically around α, due to the factor $\alpha\cos\tau$, conserving its Gaussian shape. This behavior it just that one of a classical body subjected to an harmonic force, with initial condition $x(\tau = 0) = \alpha$ and $\dot{x}(\tau = 0) = 0$. Its motion is exactly the harmonic oscillations we found in (3.34). All this results are reported in Fig. (3.2).

We want to discuss these result also under the light of Eq. (3.28), to demonstrate that all our approaches are equivalent. First we evaluate

$$\langle x(0)\rangle = \sum_{n=1}^{\infty} \sqrt{2n}\, c_{n-1}(0) c_n(0) ,$$

by the means of Eq. (3.32):

$$\begin{aligned}
\langle x(0)\rangle &= \sum_{n=1}^{\infty} \sqrt{2n}\, \frac{\alpha^{n-1}}{\sqrt{2^{n-1}(n-1)!}} e^{-\frac{\alpha^2}{4}} \frac{\alpha^n}{\sqrt{2^n n!}} e^{-\frac{\alpha^2}{4}} \\
&= \alpha\, e^{-\frac{\alpha^2}{2}} \sum_{m=0}^{\infty} \frac{(\alpha^2/2)^m}{m!} \\
&= \alpha .
\end{aligned}$$

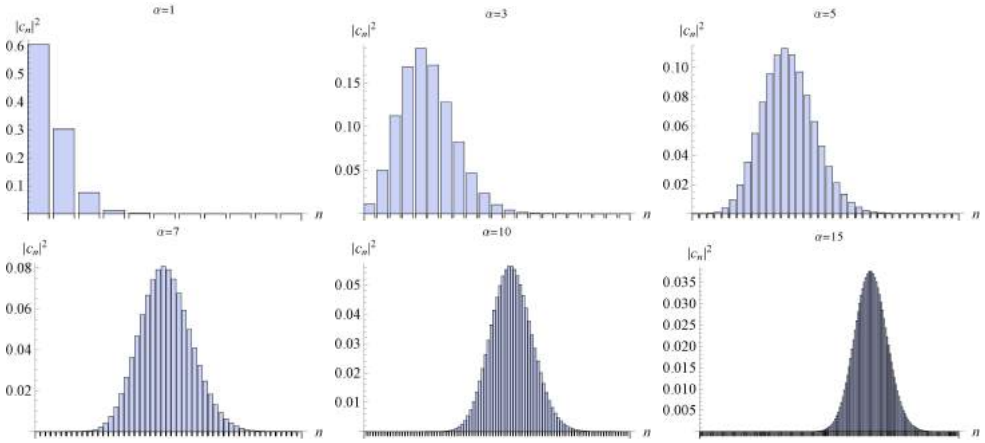

Figure 3.1: $|c_n(0)|^2$ vs. n for different values of α from Eq. (3.32). While α increases, meaning that ta central peak of $n(x,0)$ is moved away from the minimum of harmonic potential (here at $x=0$), more and more eigenstates have to be taken into account in the decomposition of $|\psi(0)\rangle$. The number of eigenstates involved is in principle infinite, but in practical term it is determined by the normalization $\langle\psi(0)|\psi(0)\rangle = \sum_n |c_n(0)|^2 = 1$. We truncate the summation at a certain n_{max} when the normalization is approximately 1.

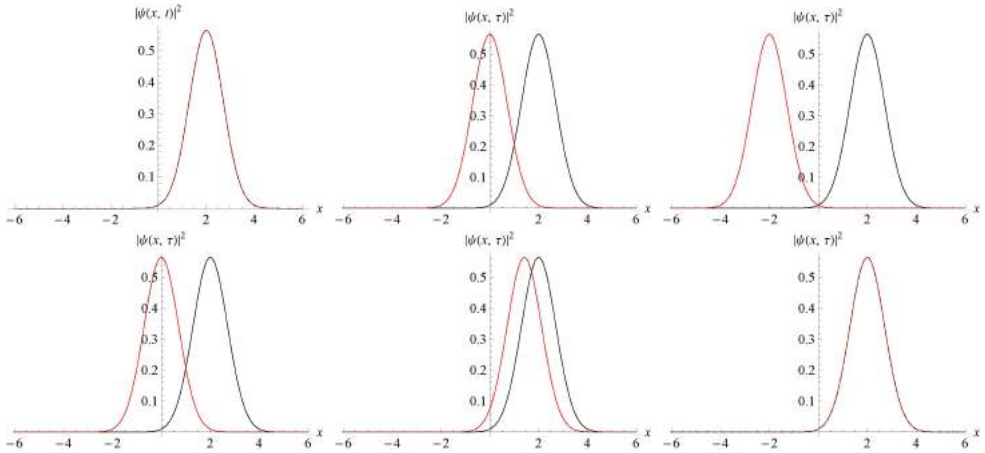

Figure 3.2: Black line correspond to the initial state (3.35) with $\alpha = 2$. Red lines represent (3.34) at different times.

At the end Eq. (3.28) becomes

$$\langle x(\tau)\rangle = \alpha\cos\tau\,, \tag{3.36}$$

that is exactly what we found before. The same result can be derived from (3.34) by

$$\langle\psi(\tau)|x|\psi(\tau)\rangle = \int_{-\infty}^{\infty} x\,|\psi(x,\tau)|^2\,dx = \alpha\cos\tau\,,$$

which coincides with (3.36).

Moreover we want to demonstrate that, while the density oscillates, its profile is kept constant. This can be done by calculating the width of the wave packet and checking that it is constant in time. From Eq. (3.30) we have:

$$\begin{aligned}\langle x^2(\tau)\rangle &= \sum_{n=0}^{\infty}\frac{\alpha^{2n}}{2^n n!}\,e^{-\frac{\alpha^2}{2}}\left(n+\frac{1}{2}\right)+\sum_{n=2}^{\infty}\left[\frac{\alpha^{n-2}\alpha^n e^{-\frac{\alpha^2}{2}}\sqrt{n(n-1)}}{\sqrt{2^{n-2}(n-2)!}\sqrt{2^n n!}}\right]\cos(2\tau)\\ &= \sum_{n=0}^{\infty}\frac{\alpha^{2n}}{2^n n!}\,e^{-\frac{\alpha^2}{2}}\left(n+\frac{1}{2}\right)++e^{-\frac{\alpha^2}{2}}\cos(2\tau)\sum_{n=2}^{\infty}\left[\frac{(\alpha^2/2)^{n-1}}{(n-2)!}\right].\end{aligned}$$

The time independent part leads to

$$\begin{aligned}\sum_{n=0}^{\infty}\frac{\alpha^{2n}}{2^n n!}\,e^{-\frac{\alpha^2}{2}}\left(n+\frac{1}{2}\right) &= e^{-\frac{\alpha^2}{2}}\sum_{n=0}^{\infty}\frac{1}{(n-1)!}\left(\frac{\alpha^2}{2}\right)^n+\frac{e^{-\frac{\alpha^2}{2}}}{2}\sum_{n=0}^{\infty}\frac{1}{n!}\left(\frac{\alpha^2}{2}\right)^n\\ &= \frac{\alpha^2}{2}+\frac{1}{2}\,;\end{aligned}$$

while the second summation gives

$$\begin{aligned}e^{-\frac{\alpha^2}{2}}\cos(2\tau)\sum_{n=2}^{\infty}\left[\frac{(\alpha^2/2)^{n-1}}{(n-2)!}\right] &= e^{-\frac{\alpha^2}{2}}\cos(2\tau)\frac{\alpha^2}{2}\sum_{m=0}^{\infty}\left[\frac{(\alpha^2/2)^m}{m!}\right]\\ &= \alpha^2\cos^2\tau-\frac{\alpha^2}{2}\,.\end{aligned}$$

All together, these two results lead to

$$\langle x^2(\tau)\rangle = \frac{\alpha^2}{2}+\frac{1}{2}+\alpha^2\cos^2\tau-\frac{\alpha^2}{2} = \frac{1}{2}+\alpha^2\cos^2\tau\,.$$

As before, we can also find this result by the use of Eq. (3.34):

$$\langle\psi(\tau)|x^2|\psi(\tau)\rangle = \int_{-\infty}^{\infty} x^2\,|\psi(x,\tau)|^2\,dx = \frac{1}{2}+\alpha^2\cos^2\tau\,.$$

Once we have an exact expressions for both $\langle x(\tau)\rangle$ and $\langle x^2(\tau)\rangle$ is easy to obtain

$$\sigma(\tau) = \sqrt{\langle x^2(\tau)\rangle-\langle x(\tau)\rangle^2} = \sqrt{\frac{1}{2}+\alpha^2\cos^2\tau-(\alpha\cos\tau)^2} = \frac{\sqrt{2}}{2}\,, \tag{3.37}$$

that is constant and equal to the initial width of the Gaussian density shape.

Focusing on interference

We now want to obtain the previous results using the formalism of (3.22). Inserting (3.16) and (3.32) in (3.19) we obtain:

$$\mathcal{A}_{nq}(x) = 2\frac{e^{-\left(x^2+\frac{\alpha^2}{2}\right)}}{\sqrt{\pi}}\left(\frac{\alpha}{2}\right)^{2n-q}\frac{H_n(x)H_{n-q}(x)}{n!(n-q)!}\,. \tag{3.38}$$

And using (3.38) in (3.21) we found for (3.22)

$$n(x,t) = \sum_{n=0}^{\infty}\frac{e^{-\left(x^2+\frac{\alpha^2}{2}\right)}}{\sqrt{\pi}}\left(\frac{\alpha^n}{2^n n!}\right)^2[H_n(x)]^2 + \sum_{q=1}^{\infty}\mathcal{C}_q(x)\cos(q\tau)\,; \tag{3.39}$$

We determine numerically each term, and report the results in Fig. (3.3). In that figure we can directly see what happens to the density while it evolves in time: the diagonal part $n_D(x)$ is fixed and does not evolve with time; on the other hand the off-diagonal part changes and if look at a specific point x it takes both positive or negative values, meaning that the interference between eigenstates could be either constructive or destructive. The superposition of these two parts leads at the end to a density profile $n(x,\tau)$ which is exactly the one we derived in Eq. (3.34).

3.2.5 Breathing modes

Here we study how a generic Gaussian wave packet of initial width σ and centered around $x = 0$ will evolve once it's put on an harmonic potential.

3.2.6 Initial wave function

For our proposal we choose the following wave function:

$$\psi(x,0) = \frac{1}{\sqrt{\sigma\sqrt{2\pi}}}\exp\left[-\left(\frac{x}{2\sigma}\right)^2\right]\,, \tag{3.40}$$

which leads to the initial density profile

$$n(x,0) = \frac{1}{\sigma\sqrt{2\pi}}\exp\left(-\frac{x^2}{2\sigma^2}\right)\,, \tag{3.41}$$

that is normalized to 1.

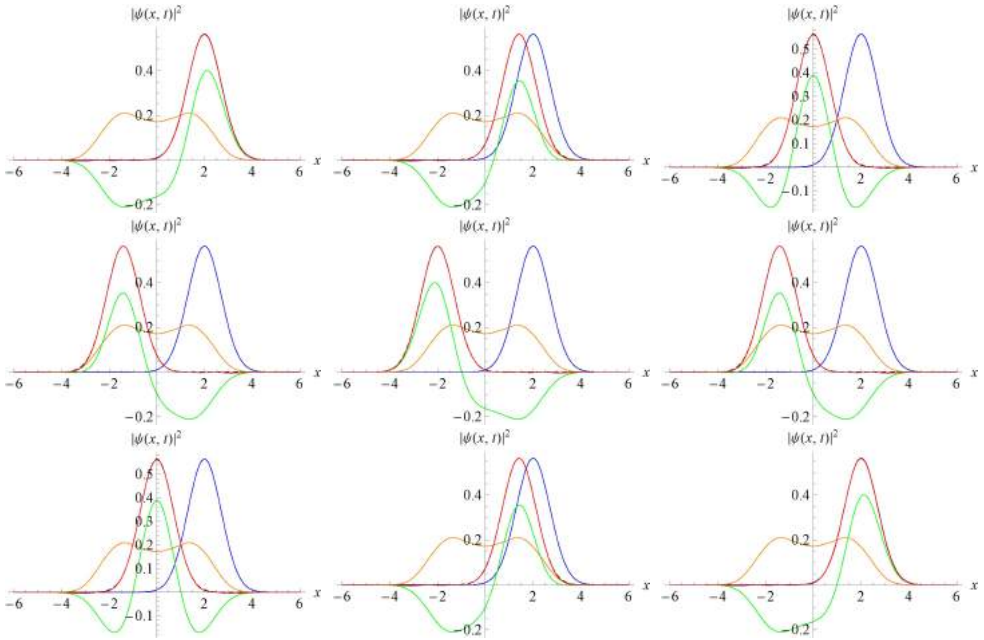

Figure 3.3: Blue line: initial density in Eq. (3.35). Black line: $n(x,\tau)$ from Eq. (3.34). Red line: $n(x,\tau)$ from Eq. (3.39). Orange line: diagonal part of the density, $n_D(x)$. Green line: off-diagonal (interference) part of (3.39). Notice that black and red lines are always superimposed, confirming that it is the interference term that determine the density profile at each steps. From the top left panel: $\tau = 0,\ \frac{\pi}{4},\ \frac{\pi}{2},\ \frac{3\pi}{4},\ \pi,\ \frac{5\pi}{4},\ \frac{3\pi}{2},\ \frac{7\pi}{4},\ 2\pi$. In each panel we have $\alpha = 2$.

3.2.7 Finding initial coefficients

As before we start by calculating

$$c_n(0) = \int_{-\infty}^{\infty} \phi_n(x)\psi(x,0)\,dx = \frac{1}{2^{\frac{1}{4}}\sqrt{\sigma\pi}}\sqrt{\frac{1}{2^n n!}}\int_{-\infty}^{\infty} e^{-\alpha^2x^2}H_n(x)\,dx\,, \qquad (3.42)$$

where we set $\alpha^2 = (1 + 1/2\sigma^2)/2$. To solve the integral we expand the Hermite's polynomial in series of x, by using

$$H_n(x) = n!\sum_{m=0}^{\lfloor \frac{n}{2} \rfloor} \frac{(-1)^m}{m!(n-2m)!}(2x)^{n-2m}\,,$$

where $\lfloor \frac{n}{2} \rfloor$ means $n/2$ for n even and $(n-1)/2$ for n odd. Eq. (3.42) becomes

$$c_n(0) = \frac{1}{2^{\frac{1}{4}}\sqrt{\sigma\pi}}\sqrt{\frac{1}{2^n n!}}\,n!\sum_{m=0}^{\lfloor \frac{n}{2} \rfloor} \frac{(-1)^m}{m!(n-2m)!}\int_{-\infty}^{\infty} e^{-\alpha^2x^2}(2x)^{n-2m}\,dx$$

Because the Gaussian is an even function and the parity of the Hermite's polynomials is $(-1)^n$ the integral in Eq. (3.42) is nonzero only for n even. Therefore we are allowed to consider $n = 2k$ with $k \in \mathbb{N}$ and in the previous summation m goes from 0 to $n/2$. The expression for $c_n(0)$ turns out to be

$$c_{2k} = \frac{1}{2^{\frac{1}{4}}\sqrt{\sigma\pi}}\sqrt{\frac{1}{2^{2k}(2k)!}}\,(2k)!\sum_{m=0}^{k} \frac{(-1)^m}{m![2(k-m)]!}\int_{-\infty}^{\infty} e^{-\alpha^2x^2}(2x)^{2(k-m)}\,dx\,,$$

Setting $q = k - m = 0, 1, 2, \ldots, k$, due the fact that $m = 0, 1, 2, \ldots, k$, and defining $t = \alpha x$, Eq. (3.42) is rewritten as

$$c_{2k} = \frac{1}{2^{\frac{1}{4}}\sqrt{\sigma\pi}}\sqrt{\frac{1}{2^{2k}(2k)!}}\,(2k)!\sum_{q=0}^{k} \frac{(-1)^{k-q}}{(k-q)!(2q)!}\,\frac{1}{\alpha}\left(\frac{2}{\alpha}\right)^{2q}\int_{-\infty}^{\infty} e^{-t^2}t^{2q}\,dt\,. \qquad (3.43)$$

Let us focus just on

$$\int_{-\infty}^{\infty} e^{-t^2}t^{2q}\,dt = 2\int_{0}^{\infty} e^{-t^2}t^{2q}\,dt = \int_{0}^{\infty} e^{-u}u^{q-\frac{1}{2}}\,du\,,$$

where $t^2 = u$. Moreover it is convenient to set $q + 1/2 = l - 1$, from which

$$\int_{0}^{\infty} e^{-u}u^{l-1}\,du = \Gamma(l) \equiv \Gamma\left(q + \frac{1}{2}\right)\,.$$

This result has to be put in Eq. (3.43) which now becomes

$$c_{2k} = \frac{1}{2^{\frac{1}{4}}\sqrt{\sigma\pi}} \frac{\sqrt{(2k)!}}{2^2 k} \sum_{q=0}^{k} \frac{(-1)^{k-q}}{(k-q)!(2q)!} \frac{1}{\alpha} \left(\frac{2}{\alpha}\right)^{2q} \Gamma\left(q+\frac{1}{2}\right).$$

Again, we compute the summation over q with the help of a software, and substituting the result in the expression for c_{2k} we have

$$c_{2k} = \frac{1}{2^{\frac{1}{4}}\sqrt{\sigma\pi}} \frac{\sqrt{(2k)!}}{2^k} \frac{\sqrt{\pi}}{k!\alpha} \left(\frac{1-\alpha^2}{\alpha^2}\right)^k = \frac{1}{2^{\frac{1}{4}}\sqrt{\sigma}} \frac{\sqrt{(2k)!}}{2^k k!} \frac{(1-\alpha^2)^k}{\alpha^{2k+1}}.$$

By definition we have that

$$\alpha = \sqrt{\frac{1}{2}\left(1+\frac{1}{2\sigma^2}\right)};$$

from which $1-\alpha^2 = (1-1/2\sigma^2)/2$ and

$$\frac{(1-\alpha^2)^k}{\alpha^{2k+1}} = \frac{2\sigma}{\sqrt{2\sigma^2+1}} \left(\frac{2\sigma^2-1}{2\sigma^2+1}\right)^k.$$

Finally we put this in the c_{2k}, and we obtain the exact expression we're searching for:

$$c_{2k} = 2^{\frac{3}{4}} \sqrt{\frac{\sigma}{2\sigma^2+1}} \frac{\sqrt{(2k)!}}{2^k k!} \left(\frac{2\sigma^2-1}{2\sigma^2+1}\right)^k. \tag{3.44}$$

3.2.8 Density profile at any time

In the previous paragraphs we have found the exact expression for the coefficients in Eq. (3.19), now we are able to determine $n(x,\tau)$ at any time τ by combining (3.44) and (3.16):

$$\begin{aligned} n(x,\tau) &= \sum_{n=0}^{\infty} \sqrt{\frac{8}{\pi}} \frac{\sigma}{2\sigma^2+1} \frac{1}{(2^{2n}n!)^2} \left(\frac{2\sigma^2-1}{2\sigma^2+1}\right)^{2n} [H_{2n}(x)]^2 e^{-x^2} + \\ &\quad + \sum_{\substack{n,q=1 \\ n\geq q}}^{\infty} \mathcal{A}_{nq}(x)\cos(2q\tau); \end{aligned} \tag{3.45}$$

$$\mathcal{A}_{nq} = \sqrt{\frac{8}{\pi}} \frac{\sigma}{2\sigma^2+1} \frac{1}{2^{2(2n-q)}n!(n-q)!} \left(\frac{2\sigma^2-1}{2\sigma^2+1}\right)^{2n-q} H_{2n}(x)H_{2(n-q)}(x)\, e^{-x^2}$$

We ere unable to find an analytical form for Eq. (3.45), so we limit ourselves to reconstruct numerically the density by performing the summation in Eq. (3.45). From a complete analytical point of view we can determine, as we have done before, the mean position and the width by the use of Eq. (3.28), Eq. (3.30) and Eq. (3.44).

We start from $\langle x(\tau)\rangle$. We can find it by looking at Eq. (3.28): in that formula the products of the projection's coefficients appears: $c_{n-1}(0)c_n(0)$. In the case of a Gaussian wave packet centered in $x = 0$ we have shown that only the coefficient with even index, i.e. c_{2k} with $k \in \mathbb{N}$, are non zero; so if n is even $n-1$ are odd, and vice versa: both $c_{n-1}(0)c_n(0)$ is identically 0 for any n. Consequently:

$$\langle x(\tau)\rangle = 0\,.$$

Now we want to determine the width $\sigma(\tau)$.

We first take into account the time independent part of Eq. (3.30) together to the fact that only $n = 2k$ are considered:

$$\sum_{k=0}^{\infty} |c_{2k}|^2 \left(2k+\frac{1}{2}\right) = \sum_{k=0}^{\infty} 2^{\frac{3}{2}}\,\frac{\sigma}{2\sigma^2+1}\,\frac{(2k)!}{(2^k k!)^2}\,\left(\frac{2\sigma^2-1}{2\sigma^2+1}\right)^{2k}\,\left(2k+\frac{1}{2}\right).$$

Defining

$$\beta \equiv \frac{\sigma}{2\sigma^2+1}\,, \qquad \gamma \equiv \frac{2\sigma^2-1}{2\sigma^2+1}\,,$$

from the previous formulæwe have

$$2^{\frac{5}{2}}\beta \sum_{k=0}^{\infty} \frac{(2k)!}{(2^k k!)^2}\,k\gamma^{2k} + 2^{\frac{1}{2}}\beta \sum_{k=0}^{\infty} \frac{(2k)!}{(2^k k!)^2}\,\gamma^{2k} = \frac{\sqrt{2}\beta(1+\gamma^2)}{(1-\gamma^2)^{3/2}}\,. \tag{3.46}$$

Now, for the time dependent part of Eq. (3.30) we obtain:

$$\begin{aligned}\sum_{k=0}^{\infty} \frac{c_{2(k-1)}c_{2k}}{2}\sqrt{2k}\,\sqrt{2k-1} &= \sum_{k=0}^{\infty} \frac{\sqrt{2k}\,\sqrt{2k-1}}{2}\,2^{\frac{3}{2}}\beta\gamma^{2k-1}\frac{\sqrt{(2k)!}\,\sqrt{(2k-2)!}}{2^{2k-1}k!(k-1)!} \\ &= 2^{\frac{3}{2}}\beta\,\frac{\gamma}{2(1-\gamma^2)^{3/2}}\,,\end{aligned} \tag{3.47}$$

and, similarly,

$$\sum_{k=0}^{\infty} \frac{c_{2(k+1)}c_{2k}}{2}\sqrt{2k+1}\sqrt{2(k+1)} = 2^{\frac{3}{2}}\beta\,\frac{\gamma}{2(1-\gamma^2)^{3/2}}\,. \tag{3.48}$$

Summing Eq. (3.46), Eq. (3.47) and Eq. (3.48) we obtain for Eq. (3.30):

$$\langle x^2(\tau)\rangle = \frac{\sqrt{2}\beta\,(1-\gamma)^2}{(1-\gamma^2)^{3/2}} + \frac{2^{\frac{5}{2}}\beta\gamma}{(1-\gamma^2)^{3/2}}\,\cos^2\tau\,.$$

Now we want to have just the dependence on σ: from previous definitions we obtain

$$\frac{\sqrt{2}\beta\,(1-\gamma)^2}{(1-\gamma^2)^{3/2}} = \frac{1}{(2\sigma)^2}\,; \qquad \frac{2^{\frac{5}{2}}\beta\gamma}{(1-\gamma^2)^{3/2}} = \frac{4\sigma^4-1}{(2\sigma)^2}\,,$$

and finally

$$\langle x^2(\tau)\rangle = \frac{1}{(2\sigma)^2}\left[1 + (4\sigma^4 - 1)\cos^2\tau\right] .$$

At the end we get the explicit expression for the width:

$$\sigma(\tau) = \sqrt{\langle x^2(\tau)\rangle - \langle x(\tau)\rangle^2} = \frac{1}{2\sigma}\sqrt{1 + (4\sigma^4 - 1)\cos^2\tau}\,. \tag{3.49}$$

If one is interested in studying the short time dynamics, $\cos^2\tau$ in Eq. (3.49) should be expanded up to the second order in τ, i.e. $\cos^2\tau \approx 1 - \tau^2$:

$$\sigma(\tau) \approx \frac{1}{2\sigma}\sqrt{1 + (4\sigma^4 - 1) - (4\sigma^4 - 1)\tau^2} \approx \sigma\sqrt{1 - \left(1 - \frac{1}{4\sigma^4}\right)\tau^2}\,. \tag{3.50}$$

This expression for the width can be generalized remembering that σ is nothing but the initial width, i.e. $\sigma(0)$,

$$\sigma(\tau) \approx \sigma(0)\sqrt{1 - \left(1 - \frac{1}{4\sigma^4(0)}\right)\tau^2}\,. \tag{3.51}$$

3.3 Quantum interference and Anderson Localization

Before entering in the details of this section, let us recall the most important results of the previous.

- The density distribution $n(x, t)$ could be always divided into a diagonal, static, and a off-diagonal time-dependent part, i.e.

$$n(x, t) = n_D(x) + n_{off}(x, t)\,.$$

- $n_D(x)$ is determined only by the initial condition, i.e. $\psi(x, 0)$ (the wave function at $t = 0$), and by the spectrum of eigenstates $\phi_n(x)$ of the Hamiltonian $\hat{\mathcal{H}}$ which describes the system we are considering.

- The time dependence of $n_{off}(x, t)$ is due to the quantum interference between different eigenstates.

These sentences show that this approach is quite powerful: once we have an initial wave function $\psi(x, 0)$ and an Hamiltonian $\hat{\mathcal{H}}$ which we can diagonalized (either analytically or numerically it does not matter) we can determine the same wave function, and then all the mean values of physical observables, at any time $t > 0$ without solving the complete Schrödinger equation.

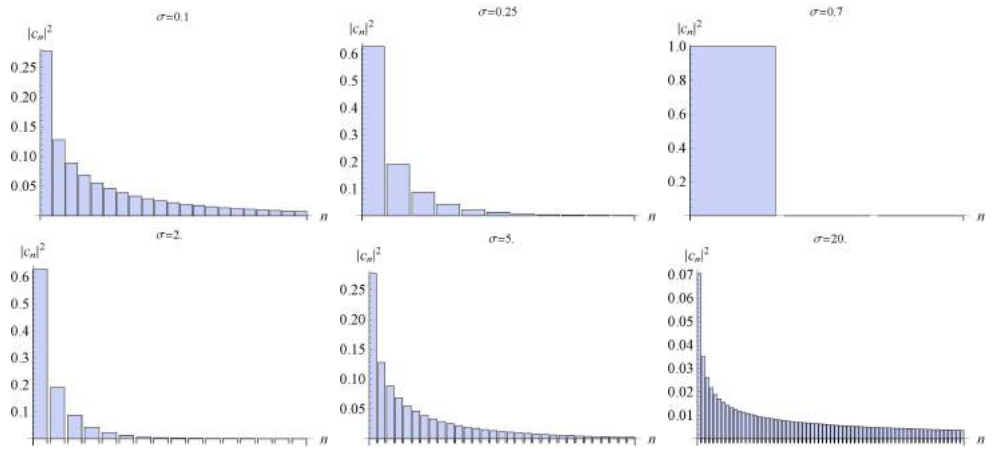

Figure 3.4: Values of $|c_n(0)|^2$ vs. n for different values of σ calculate from Eq. (3.44). Corresponding value of σ are reported in each panel. Clearly for σ approaching $1/\sqrt{2}$, i.e. the width of the harmonic oscillator's ground state, the number of eigenstate over which we project the initial state decreases and $|c_0|^2$ tends to 1.

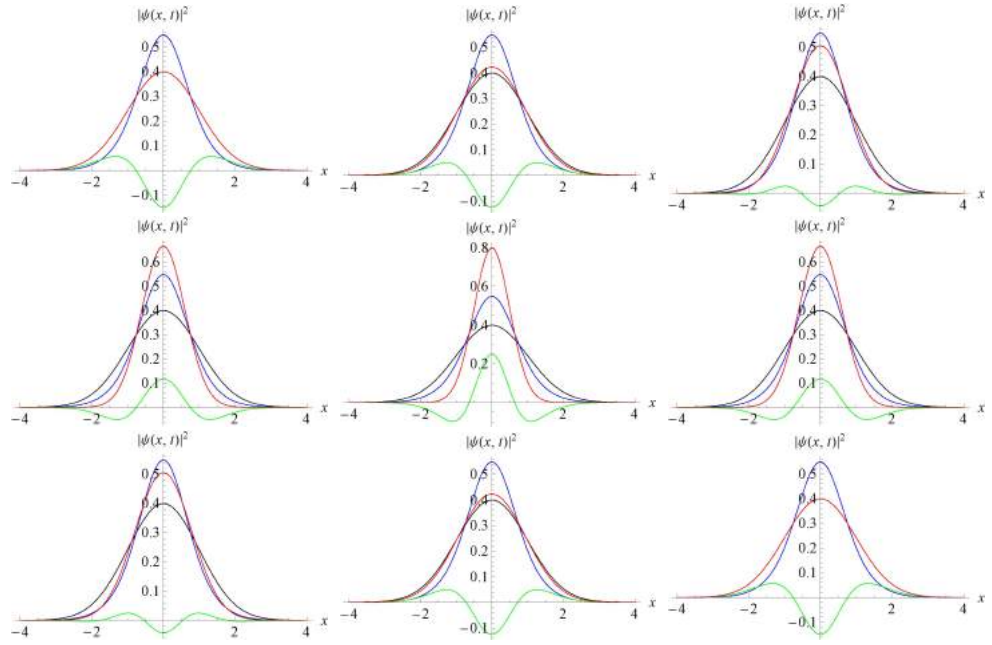

Figure 3.5: Black line: initial density (3.41). Red line: density from (3.45). Blue line: time independent part of (3.45) (first summation). Green line: time-dependent (interference) part of (3.45) (second summation). We can see that, as predicted, $n(x, \tau)$ remains centered around $x = 0$ and its width oscillates harmonically, as described in (3.49). From top to bottom and from left to right: $\tau = 0$, $\frac{\pi}{8}$, $\frac{\pi}{4}$, $\frac{3\pi}{8}$, $\frac{\pi}{2}$, $\frac{5\pi}{8}$, $\frac{3\pi}{4}$, $\frac{7\pi}{8}$, π. We have set the initial width to $\sigma = 1$.

Moreover we notice here that all the calculation we have done up to now refer to systems with a discrete spectrum, this is evident because in all the formulae we have always used the sum over eigenstates and not the integral over some variables. The fact that we are dealing with system with discrete spectrum has a great importance on the dynamics of the particle described by $\psi(x,t)$: it is known from literature that if a system presents a point spectrum any initial wave function will not spread indefinitely, but its motion is limited in a close region of the space [118]. On the other hand we have that if the system posses a continuous spectrum then the initial state will spread all over the space.

We underline this because the one dimensional disordered systems described in Chap possesses a discrete energy spectrum. In those systems we had shown taht not only a state will not spread to infinite but also it will present Anderson localization (AL), the signature of which is the exponential decay which can be observed in the tails of the eigenstates, exponential decay which is then present also in the tails of a generic density distribution $n(x,t)$ of a particle prepared in some initial state $|\psi(0)\rangle$. In this chapter we focus our attention onto two different type of disordered potential of 1.2.1: speckles and quasi periodic potential.

The application of this approach to disordered system will be complementary to the usual description of localization in terms of the localization of single momentum components (plane waves), as result of multiple scattering from the random potential. The plane waves are not good state to consider for the system, because they are not eigenstates and during the evolution waves that carry different momentum will be coupled due to the presence of the disorder. On the other hand considering the evolution on the eigenstate basis has the advantage that each evolves independently from the other, as said before.

3.3.1 Asymptotic regime

We are interested in understanding the role played by $n_D(x)$ and $n_{off}(x,t)$ in the AL mechanism. We know that a given state $|\psi(0)\rangle$ will not suddenly localize, when put into a disorder potential, but there is an initial interval of time after which one can look for the signature of AL. Then we will look to the density profile at large times, i.e. to $\lim_{t\to\infty} n(x,t)$.

When AL occurs we expect the density profile to be stationary, thus we suppose that

$$\lim_{t\to\infty} n(x,t) \equiv n_\infty(x)\,, \tag{3.52}$$

where the right member is defined without any time dependence.

Looking at Eq. (3.9) it is clear that the only way for the density to become stationary is that only the diagonal part $n_D(x)$ plays a role, while the off-diagonal part loose its importance more and more while t grows. We just say that the main signature of AL

is an exponential decay of the tails of eigenstates and density distribution, therefore we pay attention to them and we argue that

$$n_{\infty}^{tails}(x) \approx \sum_{n} |c_n(0)|^2 |\phi_n(x)|^2 \,, \tag{3.53}$$

in which we specify that we are speaking about the tails, and not the bulk, of the distribution. The approximate equivalence refers to local fluctuations related to the specific disorder realization. We perform several numerical simulations in order to study this behavior and at the end we can claim that the off-diagonal term of the density, which brings the time dependence of the entire distribution, contributes just with fluctuations around the profile of Eq. (3.53).

We thus have to find a way to explain this, and we come to a "phase randomization ansatz". To better understand this statement we have to consider again Eq. (3.9), which we report here for simplicity:

$$n(x,t) = \sum_{n} |c_n(0)|^2 |\phi_n(x)|^2 + 2 \sum_{n>m} |c_n(0)||c_m(0)| \phi_m^*(x)\phi_n(x) \cos\Delta\left(\varphi_{nm}(t)\right) \,;$$

Because $c_n(0)$'s are fixed by the choice of initial state $\psi(x,0)$ and $\phi_n(x)$ are determined once we choose a potential then the only way to drop out $n_{off}(x,t)$ is to play with the phases $\phi_n(t)$. Because we want to create a situation in which $n_{off}(x,t) \approx 0$ we substitute each $\psi_n(t)$ by a random number within the interval $[0, 2\pi]$. By this choice also the $\Delta\varphi_{nm}$ (we here drop out the time dependence because they are now just fixed numbers) become random and this of course lead to an interference which is almost totally destructive.

To summarize what just said we introduce a quantity which measure the relaxation of the total density onto the diagonal part while the system evolves:

$$R(t) = \frac{1}{L} \int_{L} \frac{|\ln\left(n_D(x)\right)|}{|\ln\left(n(x,t)\right)|} \,, \tag{3.54}$$

that measure the average relative weight of the diagonal term. The use of a logarithmic scale turns out to be useful especially when the density is exponentially localized, as in the case of AL. We expect that $R(t)$ in Eq. (3.54) approaches 1 and has small fluctuations around that values if $n_D(x)$ is a good approximation for $n(x,t)$.

3.3.2 Quasi-periodic potential

Let us apply all what we learned up to now to a specific and interesting case: the quasi-periodic potential. As discussed in 1.2.1 this kind of potential is generated by the superposition of two periodic potentials, the ratio between their wavelengths being an

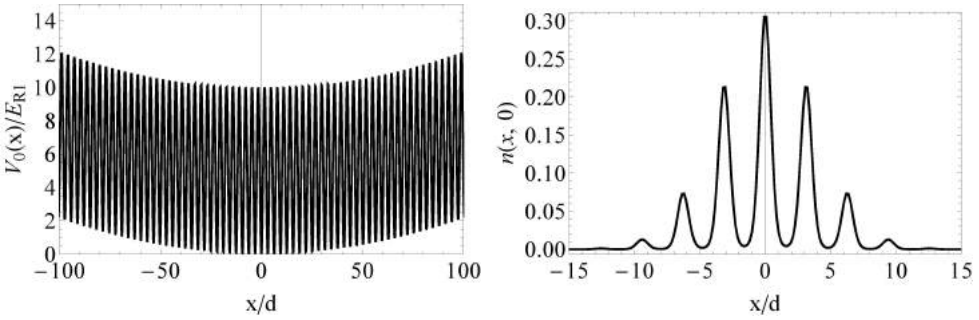

Figure 3.6: Left panel: initial potential, superposition of an harmonic trap and a periodic lattice. Right panel: density distribution for the ground state of the potential $V_0(x)$ on the left.

irrational number (i.e. it can not be expressed as the ratio between two integers):

$$V(x) = V_1 \sin^2(k_1 x) + V_2 \sin^2(k_2 x + \theta)\,, \tag{3.55}$$

in which we set $V_1 \gg V_2$, i.e. one of the two lattice (that we will call primary) is much more deep then the other that just weakly modulate the first one. θ is an arbitrary phase which define each realization of the disorder. The main point is that when $\beta = k_2/k_1$ is incommensurate the system shows a phase transition between a superfluid and an insulator phase: it exists a threshold $\Delta = 2J$ under which the system has eigenstate that are extended (exactly the same of an ordinary periodic lattice obeying Bloch's theorem), but when $\Delta > 2J$ eigenstates become Anderson localized. They are characterized by a profile which has tails going as $\exp(-|x|/l_{AA})$ where $l_{AA} = d/\log(\Delta/2J)$ is the localization length for the Aubry-André model ($d = \pi/k_1$ is the primary lattice spacing).

That regime is the one we are interested in, and so we will analyze a potential with $\Delta/J = 7$ that gives $l_{AA} \approx 0.8d$

Initial State

As $|\psi(0)\rangle$ we choose the ground state of a potential which results form the superposition of the primary lattice and an harmonic confinement, i.e. $V_0(x) = V_1 \sin^2(k_1 x) + m\omega_{ho}^2 x^2/2 = V_1(x) + V_{ho}(x)$. This is a situation that is usually present in experiment involving ultracold atoms, which are both trapped by a magnetic trap (generating the harmonic potential) and loaded into a optical lattice. It results in a density profile that is a Gaussian modulated by the periodic lattice, as shown in Fig. (3.6). The presence of the extra harmonic trap guarantees that the state $|\psi(0)\rangle$ has mainly components in first Bloch band of the primary lattice, which is a choice that put this system closer to the discrete one in which, by definition, one deals with just a single band with a number of state equal to the lattice sites. Once we have found this state then it is implemented into the bichromatic lattice, without any additional confinement. This corresponds more

or less to the real case of an experiment in which the atomic cloud is initially in the harmonic trap which is suddenly turned off, in order to make the atoms free to expand in the remaining potential (i.e. the quasiperiodic lattice).

Because the wave packet expand in the presence of only the quasiperiodic lattice, following our method, we have to diagonalize the Hamiltonian corresponding to Eq. (3.55). The structure of its energy spectrum is known and consists in a series of bands (as the usual periodic potential) and each of them it is again divided into sub-bands. While we were describing $|\psi(0)\rangle$, we have said that the presence of $V_{ho}(x)$ drives to a state the energy component of which mainly occupy in the first Bloch band of $V_1(x)$ which means that also when the second lattice is turned on they will remain in the first band of the resulting potential. This allows us to consider two different situations:

- **Full band problem:** although the state lays principally in the lowest band it has also some components in higher energy bands, which have to be taken into account for a complete description of the system. So in performing the projection of Eq. (3.6) we consider as many eigenstates $|n\rangle$ as we need to reconstruct $|\psi(0)\rangle$, and to be sure of this we look to $\langle\psi(0)|\psi(0)\rangle = \sum_n |c_n(0)|^2$ which must be 1 because we fix the normalization of the state to unity.

- **Single band problem:** on the other hand we can consider the tight binding regime, reached for deep lattices. If one works under those condition could consider the discrete model, described by Eq. (2.39) with $U = 0$, which is intrinsically single band. In the case of continuous model this is not always true, i.e. a general wave packet could have energy components in the higher bands of the quasiperiodic potential even though it was prepared in the lowest band of the primary lattice.

We will start to discuss this problem form the latter.

Single band problem

We consider here the case in which the initial wave packet is menaged in such a way that it will have only components in the first band of the bichromatic lattice. In general, because we are considering a continuous system and our initial state is not and eigenstate of the quasiperiodic Hamiltonian, one has to consider all the bands

$$|\psi(0)\rangle = \sum_{n,j} c_{nj}(0)|n\rangle_j \,,$$

where n is the index labeling the state within the $j-$th band and the sum is performed over all the bands. Moreover we have prepared $\psi(x,0)$ in such a way that most of all its components are in the first band of the primary lattice; due to this also when the second lattice is present (and the spectrum is of course modified by the appearance of the minibands) the initial state lye mainly on the lowest energy band. Then the normalization

turns out to be

$$1 = \sum_n |c_{n1}(0)|^2 + \sum_{\substack{n,j \\ j\geq 2}} |c_{nj}(0)|^2 \,, \tag{3.56}$$

in which $\sum_n |c_{n1}(0)|^2 = \mathcal{N} \approx 1$. The approach we use here leads to a wave packet which is written as

$$|\bar{\psi}(0)\rangle = \sum_{n,1} \tilde{c}_n |n\rangle \,, \tag{3.57}$$

where we have defined

$$\tilde{c}_n = \frac{c_{n1}}{\sqrt{\mathcal{N}}} \,, \tag{3.58}$$

from which we have

$$\langle \bar{\psi}(0)|\bar{\psi}(0)\rangle = 1 \,.$$

The choice of cutting the initial state, which was been already selected in the way we described, could sound strange, but it will be clarified in the following.

Once we have the initial condition we were searching for, we just have to determine the density profile. First we look at the density $n(x,t)$ coming from Eq. (3.57) at $t = 0$, and then at a time t so large that it can be considered asymptotic in the sense we described in the previous section. Both of them are obtained from Eq. (3.8), with the constraint of summing only over state within the first band, setting $t = 0$ and $t = t^* \gg 1$, i.e.

$$n(x,t) = \left| \sum_{n,1} \tilde{c}_n(0)\phi_n(x) e^{i\frac{E_n}{\hbar}t} \right|^2 \,;$$

after this we determine the diagonal part of the density $n_D(x)$

$$n_D(x) = \sum_{n,1} |\tilde{c}_n(0)|^2 |\phi_n(x)|^2 \,.$$

Once we have those density profiles we construct the one based on our phase randomization ansatz, i.e. we take Eq. (3.8) and substitute each $\varphi_n(t)$ with a random number $r_n \in [0, 2\pi]$:

$$n_{rand}(x) = \left| \sum_{n,1} \tilde{c}_n(0)\phi_n(x) e^{ir_n} \right|^2 \,. \tag{3.59}$$

From Eq. (3.59) one get an expression similar to Eq. (3.8), which is

$$n_{rand} = n_D(x) + 2 \sum_{n>m} \phi_n(x)\phi_m(x) \cos(r_n - r_m) \,.$$

Because of the presence of the second term in the summation on the right hand side we have that $n_{rand}(x) \approx n_\infty(x) \approx n_D(x)$ and $R(t) \approx 1$, without being exactly 1.

Moreover all of this formulae are valid for a single realization of the potential $V_{bc}(x)$, i.e. for a fixed phase difference θ between the two lattices in Eq. (3.55). Dealing with

disordered system it is usual to average over different realization of the disorder.

A summary of the results we have obtained in reported in Fig. (3.7). There we show $n(x,0)$ (obtained from Eq. (3.57)), $n(x,t^*)$, $n_D(x)$ and $n_{rand}(x)$ averaged over 100 realizations of $V(x)$. With this averaging the contribution of local fluctuations due to the off-diagonal part $n_{off}(x,t)$ that are important for a single realization drops out, and we remain with just those density distribution that are clearly similar one to the other. This is confirmed also by looking to the (averaged over realization) $R(t)$: it starts at $t=0$ from a value far form 1, this because $n_D(x)$ is not sufficient to reconstruct the whole initial density profile and the role of off-diagonal part is fundamental; while the time goes on $n(x)$ approaches $n_D(x)$ and then $R(t)$ tends to 1.

We also compare the tails of the densities with and exponential decaying function $\propto \exp[-2|x|/l_{loc}]$, fitting them by this function keeping l_{loc} as free parameter. What we find is that $l_{loc} \approx l_{AA}$, i.e. the localization length of the density is the one predicted by the discrete Aubry-André model, and this tells us that the shape of the asymptotic density resemble the one of the eigenstates This could be supposed looking at the expression in Eq. (3.53): it tells us that $n_D(x)$ is obtained from a weighted sum of the density distribution of eigenstates, and because each of them has the same localization length l_{AA} we were expecting that $n_\infty(x)$ will show the same behavior.

After this we perform the same calculation for the pure one-band system, the Aubry André model, i.e. the linear part of Eq. (2.39), and again we find the same results. The only difference is that, because the diagonalization of such a model is faster then the continuous one, we perform an average over 500 realization of the disordered potential. We report the comparison of density distributions in Fig. (3.8)

Full bands problem

After analyzing the situation of a single band problem, i.e. a deep tight binding regime, we come back to the original idea taking into account the continuous model with all the bands. This is a situations quite close to experiments in which there is the possibility that hypothesis for tight-binding regime are not totally satisfied and the atomic cloud, although it is prepared in the presence of an external harmonic trapping, should have components that belong to excited energy band.

To analyze such a situation we perform the same simulations of Fig. (3.7) but with a different initial state, i.e. we do not project $|\psi(0)\rangle$ only onto the states of the lowest band but we also consider higher energy bands. The number of bands we have to use is found by checking the normalization condition expressed in Eq. (3.56): we perform the projection with increasing number of bands and we stop when we see that the normalization does not change any more. In the specific we take into account up to 10 bands, as we show in Fig. (3.9) From Fig. (3.9) it is evident the role played by the states in the higher bands: those are no more localized but extended; if just one of those states is present in the decomposition of $|\psi(0)\rangle$ it will introduce a cut-off in the

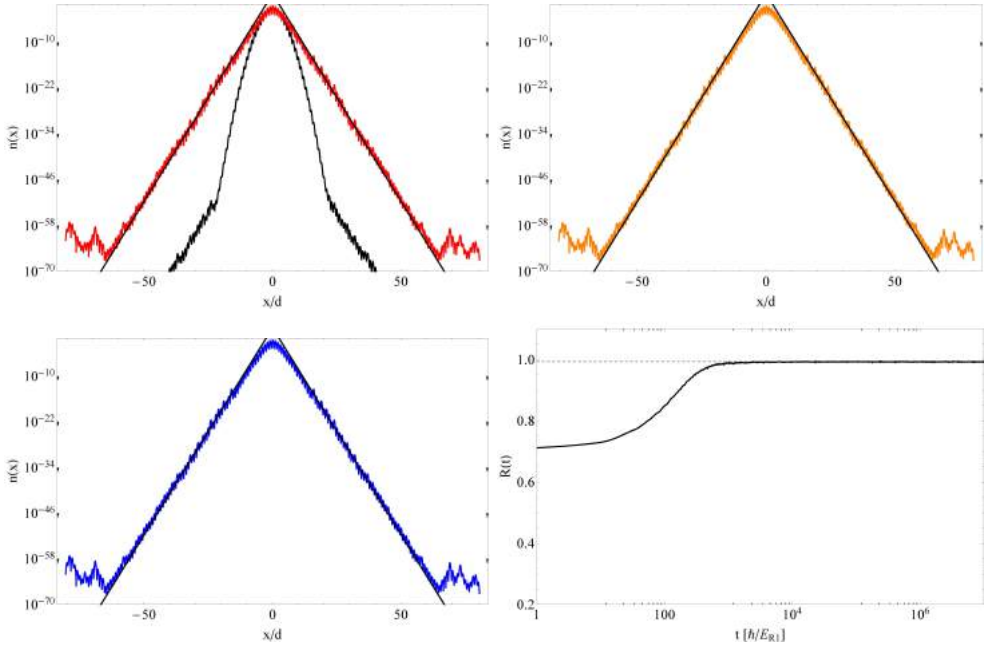

Figure 3.7: Asymptotic density distribution in the quasiperiodic potential, in the localized regime. Top left panel: the full expression in Eq. (3.9) (red line) calculated for $t = 10^7 E_{R1}/\hbar$ is plotted together with the density $n(x, 0)$ found form Eq. (3.57). Top right panel: diagonal part $n_D(x)$, see Eq. (3.53), of the density. Bottom left panel: density profile constructed from Eq. (3.9) but with a random choice for the phases φ_n. In each panel we also put Finally in the bottom right panel we report the time evolution of $R(t)$ as defined in Eq. (3.54) , it is compared with the value of the same quantity computed for the case of random phases (dashed line).

exponentially decaying tails of the distribution. The presence of this intrinsic background should represent a limitation in the experimental research for AL, because if it is too high it is no possible to perform a fit of the tails form which one can demonstrate their exponential decreasing, which we recall is the main signature of AL.

Despite this background the lower-right panel of Fig. (3.9) shows that our assumptions of the relaxation of the whole distribution onto its diagonal part works also in this case. $R(t)$ starts again from a value far form 1, and this is because $n(x, 0)$ and $n_D(x)$ are very different due to the extended background, and then it reaches values closer to unity.

3.3.3 Speckle potential

After the discussion about quasiperiodic potential we now turn to the second type pf disordered potential which is used in the experiments concerning ultracold atoms, the optical speckle potential. As described in 1.2.1 those correlated potentials are characterized by a negative-exponential distribution of the intensity (here indicated by V_0 instead

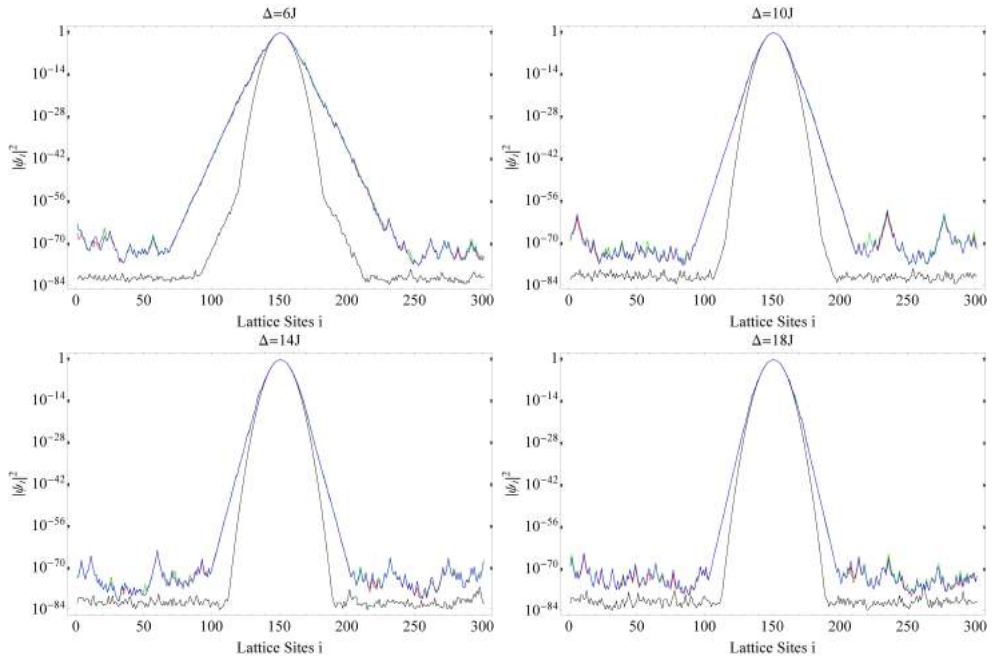

Figure 3.8: Comparison between different density profiles obtained for various Δ/J. We compare $n(x,t)$ with both Eq. (3.53) and Eq. (3.59). They perfectly coincide, giving a strong support for our suppositions.

of I, because we consider speckles as potentials rather then light patterns):

$$P(V_0) = \frac{e^{-V/\langle V_0\rangle}}{\langle V_0\rangle} \tag{3.60}$$

and by thier spatial (auto)correlation function

$$\Gamma(x) = 1 + \mathrm{sinc}^2\left(\frac{0.88x}{\xi}\right), \tag{3.61}$$

where ξ is the correlation length. Once we know this two fundamental aspects of the potential it can be write as

$$V(x) = V_0 v(x)$$

with the distribution of intensities $v(x)$ normalized in such a way that it has a unit standard deviation.

The eigenstate of $V(x)$ are not all Anderson localized, because the speckles are characterized by the presence of an effective mobility edge: i.e. it exists an energy threshold which separates the localized states (below it) from the extended one (over it).

We had seen that the characteristic length of this potential is ξ, so it is natural to express all the other lengths wit ξ as unit of measurement, moreover by it we can define

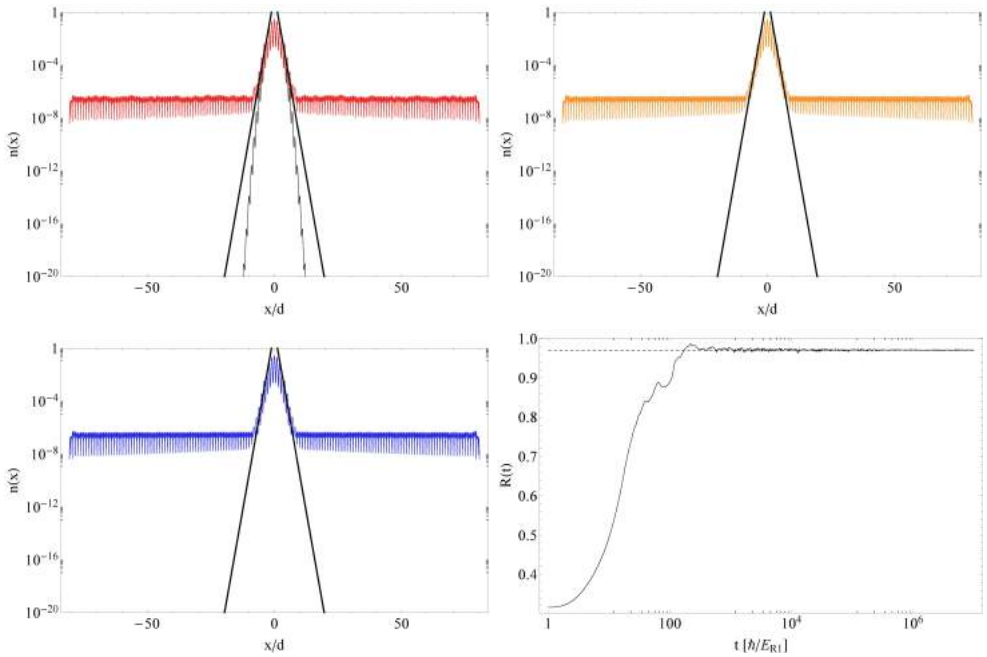

Figure 3.9: Asymptotic density distribution in the quasi-periodic potential, in the localized regime, when the exited bands are taken into account. Top left panel: the full expression in Eq. (3.9) (red line) calculated for $t = 10^7 E_{R1}/\hbar$ is plotted together with the initial density $n(x, 0)$. Top right panel: diagonal part $n_D(x)$, see Eq. (3.53), of the density. Bottom left panel: density profile constructed from Eq. (3.9) but with a random choice for the phases φ_n. In each panel we also put Finally in the bottom right panel we report the time evolution of $R(t)$ as defined in Eq. (3.54) , it is compared with the value, $R \simeq 0.971$, of the same quantity computed for the case of random phases (dashed line).

the energy unit for the system, i.e. $E_\xi = \hbar^2/2m\xi^2$ where m is the mass of the particle loaded into $V(x)$.

Initial state

At this point of the discussion we need to choose what $|\psi(0)\rangle$ is better to use for our purpose. We choose to numerically reproduce what is, at least in principle, done in experiments (in [73] and reference therein it is possible to find the same ideas we present in what follows). We consider an interacting cloud at $T = 0K$; let us forget for a while the time dependence of the wave function and focus on just the spatial coordinate. Under this conditions we have demonstrated in Chap. 2 that the dynamics of $\psi(x)$ is driven by the Gross-Pitaevskii Equation (GPE), i.e. the one dimensional version of Eq. (2.15):

$$\left[-\frac{\hbar^2}{2m}\frac{\partial^2}{\partial x^2} + V(x) + g|\psi(x)|^2\right]\psi(x) = \mu\psi(x)\,,$$

where μ is the chemical potential which fixes the number of atoms.If the cloud is large enough it is possible to neglect the kinetic energy term obtaining an accurate expression for the ground state of the condensate: this is called Thomas-Fermi (TF) approximation. Concerning the case of ultracold atoms we have that for cloud with large number of particles and repulsive interaction the ration between kinetic to potential (or interaction) energy is small, and this justify us to throw away the kinetic part of GPE. Thus one finds

$$\left[V(x) + g|\psi(x)|^2\right]\psi(x) = \mu\psi(x)\,,$$

the solution of which directly gives us the density profile

$$n(x) = |\psi(x)|^2 = \frac{\mu - V(x)}{g}\,.$$

Usually $V(x)$ represent the external trapping which often is an harmonic potential $V(x) = m\omega^2x^2/2$, and because $n(x)$ is the density of atoms it can not be negative. Substituting the expression for $V(x)$ and imposing that $n(x) > 0$ one finds

$$n_{TF}(x) = \frac{m\omega^2}{2g}\left(R_{TF}^2 - x^2\right)\Theta(R_{TF} - |x|)\,, \tag{3.62}$$

where we introduce the Thomas-Fermi radius

$$R_{TF} = \sqrt{\frac{2\mu}{m\omega^2}}\,, \tag{3.63}$$

that is defined by $n(x) = 0$, and $\Theta(x)$ is the Heaviside step function. Eq. (3.62) shows us that in the case of an harmonic trapping the density distribution of the ground state in the TF regime is an inverted parabola.

The presence of g remind us that at this stage the interactions among atoms still plays a crucial role. However we are interested in study the appearance of AL, which is a single-particle phenomena, we thus need to drive the system from nonlinear (GPE) to linear (ordinary Schrödinger) quantum mechanics. What we simulate here is simple: because the energy interaction is written $g\int n^2(x)dx$ (the density being normalized to 1) we let expand the cloud describe by Eq. (3.62) freely, i.e. we turn off $V(x)$. The atoms then start to move and the cloud enlarges becoming more and more dilute, and consequently the interaction energy become less important and form a certain point we can totally avoid it and consider the condensate as a cloud of non interacting atoms. Following scaling arguments one finds that after a time t_{free} during which the cloud expand, it still has an inverted-parabola density profile but looking to the wave function, and not only to the density, one could show that during this interval $\psi(x, t_{free})$ has acquired an additional phase factor with respect to $\psi(x, 0)$. Once we know this phase factor, we just have to proceed in the same way developed in previous paragraphs, projecting it onto the base of energy eigenstates and then finding its time evolution at any $t \geq t_{free}$.

In the case of speckles potential we have to stress an important difference with the case of the quasi-periodic lattice. Here the system does not posses any band structure, so we cannot truncate the system up to a certain energy level. In principle we can do something similar, because the Thomas-Fermi function (which we recall is an approximation, although it is very good) has sharp edges ad $x = R_{TF}$ and this introduce a cut-off in the momentum distribution, i.e. in the energy of the system. So it should be possible to truncate the basis up to eigenstates of the speckle potential which posses energy less then the cut-off.

Numerical results

As first we need to create various speckle potential, and in order to do this we employ method described in [120, 121]. Here we consider the non-interacting evolution of an initial Thomas-Fermi (TF) wave packet with momentum components below the effective mobility edge, and with a dynamical phase resulting from a pre-expansion as discussed in [20, 73, 122–124]. We choose $V_0 = 0.19 E_\xi$ and an initial TF radius $R_{TF} = 340\xi$, that corresponds to an in-trap radius $R_{TF} = 7.96\xi$. During the pre-expansion stage most of the interaction energy is transformed into kinetic energy, so that it can be safely neglected during the subsequent expansion [20, 73, 122].

The average asymptotic density distribution and the evolution of the quantity $R(t)$ are shown in Figure Fig. (3.10). Again, we plot the asymptotic density as obtained from the full expression in Eq. (3.9), that has to be compared with the expression in Eq. (3.53) containing just the diagonal terms (top right panel in figure), and with the expression in Eq. (3.9) but with a random choice of the phases, shown in the left bottom panel. We find that the tails of the density distribution can be nicely fitted with the function $n_0(x) \propto |x|^{-\alpha} \exp(-2\gamma|x|,)$ as discussed in [20, 73, 122] (here we find $\alpha \simeq 2, \gamma \simeq 4\times10^{-4}$). The same fitting lines are reported in all the three, for comparison. These figures confirm that the phase randomization anstaz holds also for the case of the speckle potential, and that the asymptotic density distribution can be reproduced by the diagonal term in Eq. (3.53). Correspondingly, also the evolution of $R(t)$ in the last (right bottom) panel of Fig. (3.10) shows a behavior similar to the quasi-periodic case. Finally, we notice that a similar behavior holds also in case of a single speckle realization, but with larger local density fluctuations with respect to the average case. In fact, the relation in Eq. (3.9) becomes more and more accurate as we average over over an increasing number of disorder realizations.

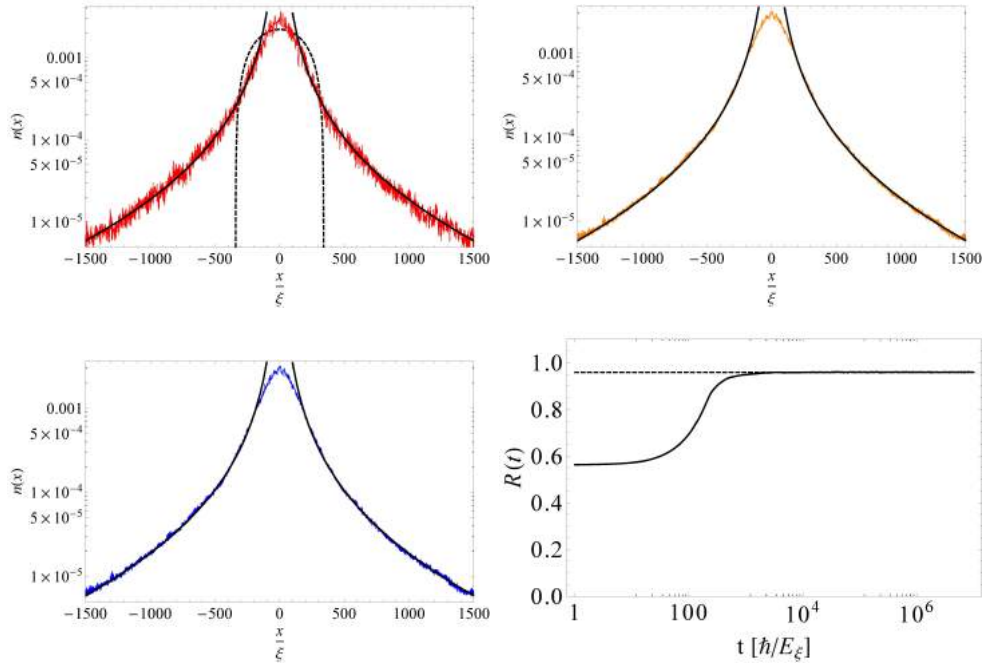

Figure 3.10: Localization in the speckle potential. Top Left: Initial wave packet (black dashed line) and asymptotic density distribution obtained from the full expression in equation Eq. (3.9) (red line), with the tails fitted as $\propto |x|^{\alpha} \exp(-2\gamma|x|)$ (black line); the same lines are plotted also in the other panels for comparison. Top Right: contribution of the diagonal terms, see equation Eq. (3.53) (orange). Bottom Left: Eq. (3.9) with a random choice of the phases φ_n (blue line). Bottom Right: evolution of the quantity $R(t)$ in Eq. (3.54), compared with the case of Eq. (3.9) for a random choice of the phases φ_n (black dotted line), $R \simeq 0.959$.

4

Dynamics of interacting wave packets in disordered time-dependent potentials: destruction of Anderson localization

In the previous chapter we had studied the behavior of a one dimensional eave packet in the presence of a static disordered potential; in particular we focused our attention onto the Anderson localization phenomenon, which is peculiar of these systems and leads to a wide range of macroscopic properties of matter, the most evident being the transition between conducting and insulating phases due to the suppression of the diffusion of the wave packet. One dimensional systems are very useful because they are easier to study than other in higher dimensions but, on the other hand, they could be considered a little bit trivial in the sense that any amount of disorder introduced in the system results in Anderson localized wave function. In the following we want to go a step further, studying what happens if, in addiction to static disorder, one introduces sources of possible delocalization, i.e. mechanism that could restore the expansion of the wave packet; in particular we will consider potentials which are random both in space and time, interactions among particles (i.e., nonlinear systems) and the interplay between them.

The motivation of this study lies on the fact that although disorder plays by itself a fundamental role in nature, as demonstrated by the large amount of papers concerning it, there are situations in which other ingredients, such as variations in time of the potential and interactions, could not be avoided.

We already said that since the pioneering work of Anderson [2] numerous studies of the properties of disordered system have been performed. Most pf these studies have dealt with model systems, generally one dimensional, consisting of static diagonal disorder and focused their attention on single-particle properties like the behavior of the single-particle density of states, the nature of single-particle states, etc. Some year after the publication of Anderson's paper the field of quantum transport in disordered potentials starts to attract the interest of researcher more and more, with particular

attention to the microscopic description of it. An aspect of those systems which has received comparatively little attention [26, 28, 29] is the behavior of particles motion under the influence of dynamic, i.e. time dependent, disorder. In the following we report our result for the motion of a particle in a system with just site *diagonal* disorder. In most of the papers dealing with those systems we found that authors frequently use both V_l (i.e. diagonal disorder) and K[1] (i.e. nearest neighborhood tunneling) are time dependent, in particular this models has been employed to described the effect of an uncorrelated dynamic, thermally induced, disorder, i.e. phonons. In [27] and references therein, in particular [29], effect of this phonon bath is presented in details and exact solutions for site diagonal disorder is reported. Moreover in [30] exact solution for just time varying tunneling $K(t)$, with static potential V_l, is presented.

We know that the Hamiltonian of the system is the linear part of Eq. (2.34), i.e.

$$H = -\sum_{l=1}^{M} \left[\phi_l(t)\phi^*_{l+1}(t) + \phi^*_l(t)\phi_{l+1}(t)\right] + V_l(t)|\phi_l(t)|^2 \,, \tag{4.1}$$

where, as in 2.4, energies are measured in units of KE_{r1}. The correspondent equation of motion for the field $\phi_l(t)$ is found by applying $i\dot{\phi}_l(t) = \partial H/\partial\phi^*_l(t)$ (see Eq. (2.34) with $U = 0$):

$$i\dot{\phi}_l(t) = -\left(\phi_{l-1}(t) + \phi_{l+1}(t)\right) + V_l(t)\phi_l(t) \,, \tag{4.2}$$

in which time is measured in units of $\hbar/KE_{r1}$.

We need to find a possible model for $V_l(t)$, in particular we want to create a function which is not only random in time but also that possesses a controllable degree of randomness. In the following we present two possibilities of doing that, and then we study their effects onto the evolution of an initially localized, i.e. Gaussian with sufficiently small width, wave packet.

4.1 Creation and control of the noise

Our goal is create a potential $V_l(t)$ that shows a behavior in time that is random, or noisy, but we also search for a situation in which this randomness is quite controllable, in order to directly study the influence of this noise.

First of all we suppose to perturb the static potential modulating its amplitude as

$$V_l(t) = V_l[1 + Af(t)] \,, \tag{4.3}$$

where of course V_l is the static disordered potential, A is the amplitude of the modulation and $f(t)$ is the function which brings all the informations about the noise. This specific choice for the perturbing disordered potential is due mainly to the fact that it could be

[1] As mentioned in Chap. 2, here we will use K instead of J for the tunneling energy.

implemented in an experiment, as recently done in [87], and also because for sufficiently small A the noisy part $f(t)$ could in principle being treated with standard time dependent perturbation techniques. Although the latter sounds very interesting, we do not follow that way, because we found (as we will show later) that for large enough time the result of our studies do not depend on A.

We then consider two type of $f(t)$:

$$f(t) = \begin{cases} \sin\left[\omega(t)t + \phi(t)\right] & \text{Frequency noise,} \\ \sin\left[\omega_0 t + \phi(t)\right] & \text{Phase noise.} \end{cases} \tag{4.4}$$

We immediately notice that, in both cases, the noisy nature of this function is not explicit but is carried by the phase $\phi(t)$, or the frequency $\omega(t)$ respectively. Moreover in the case of frequency noise we also make the phase $\phi(t)$ to be time dependent, for a reason that will be explained later, but we will show that the noisy feature is still determined by ω. We stress here that we have to deal with just one parameter in order to change the degree of noisiness of $f(t)$, which makes the system quite simple to treat. In the following we will treat directly the case in which the parameters vary in time in such a way that they lead to a random potential. On the other hand one can mange $\phi(t)$ or $\omega(t)$ in order to have sufficient slow variation and try to describe what happens in those cases by the mean of standard perturbation theory, applying the well known Fermi Golden rule, or, for much slower variation, within adiabatic approximation.

4.1.1 Phase Noise

Let us start considering the *phase noise*, where the name recalls the fact that the noise is all inside the phase of the sinusoidal function in Eq. (4.4). The easiest way we found to generate a random potential is to abruptly change ϕ every fixed time step, which from now on we call *dephasing time* and it will be denoted by T_d. We will show that its value, compared to other fundamental time scale of the system, defines completely all the noise properties in particular correlation function (in time) and power spectrum.

As just said, how much $f(t)$ is random or not depends non only on T_d but also on other time intervals, in particular with the total time of the simulation, or experiment, T_{max} and the period of periodic function $T_0 = 2\pi/\omega_0$. The reason of this is simple: suppose to have $T_d > T_{max}$, this means that the first change of phase takes place after the end of our experiment (we use this term for both numerical and real experiments), i.e. no change of phase are performed. For $T_d \geq T_{max}$ we have no random potential. Due to this we take into account only $T_d < T_{max}$, even $T_d \ll T_{max}$, which means that during the experiment we have $n_\phi = T_{max}/T_d$ changes of phase:

$$\phi(t) = \sum_{j=1}^{n_\phi} \phi_i \left[\Theta(t - (j-1)T_d) - \Theta(t - jT_d)\right] , \tag{4.5}$$

In Eq. (4.5) ϕ_j is a randomly chosen within the interval $[-\pi, +\pi]$, with uniform probability; $\Theta(t)$ is the Heaviside step function, and the term in square parentheses ensure that the phase is kept constant between tho subsequent change. In Fig. (4.4) some examples of the application of Eq. (4.5) are reported, showing both $\phi(t)$ and $f(t)$ for different T_d. We now have the ingredients that have to be used in order to modify the degree of noisiness of $f(t)$: we have to compare T_d with both T_{max} and T_0. First of all, let us look to the time correlations of $f(t)$ for different values of dephasing, while we keep T_{max} and ω_0 fixed, with the prescription that $T_{max} \gg T_d$. In Fig. (4.4) we plot some examples of $g(\tau) = \langle f(t)f(t+\tau)\rangle$, where angular brackets $\langle\cdots\rangle$ stand for average over realizations. From these graphs it is evident that T_d set the correlations time for the disorder, i.e. we can write

$$\begin{aligned}\langle f(t)f(t+\tau)\rangle &= \frac{1}{T_{max}}\int_0^{T_{max}} \left(f(t) - \overline{f(t)}\right)\left(f(t+\tau) - \overline{f(t+\tau)}\right)\, dt \\ &= g(\tau)\Theta\left(t - T_d\right)\ ,\end{aligned}$$

in which $\bar{f}$ means the average in time, i.e. $\overline{f(t)} = \int_0^{T_{max}} f(t)dt/T_{max}$. The motivation for the previous result is quite simple, and is a direct consequence of the time dependence of $\phi(t)$: inside an interval of width T_d the function $f(t)$ is perfectly coherent due to the fact that it is a normal periodic function; for $\tau > T_d$ the shifted function $f(t+\tau)$ is no more in phase with $f(t)$ and then coherence drops to values around zero. This suppression of coherence is then enhanced when averaged over realization, due the random choice of different phases. We thus have

$$g(\tau) = \begin{cases} \sum_{j=1}^{n_\phi} \frac{1}{T_d}\int_0^{T_d}\left[f_j(t) - \overline{f_j(t)}\right]\left[f_j(t+\tau) - \overline{f_j(t)}\right]\, dt & \text{if } t \le T_d, \\ 0 & \text{if } t > T_d, \end{cases}$$

where $f_j(t) = \sin(\omega_0 t + \phi_j)$. A good estimation give $T_d = T_0/4$ as the dephasing under which we can say that any possible correlation is canceled (see first column in Fig. (4.4)), in the sense that $g(\tau) > 0$ for $t < T_d$ and zero otherwise. This behavior is also evident if one looks to the the power spectrum of $f(t)$, defined as the squared modulus of its Fourier transform, i.e. $|\mathcal{F}[f(t)]|^2 \equiv |\tilde{f}(\omega)|^2$. Let us start by analyzing the simplest situation, a single step of $f(t)$; this is the main constituent of the whole noise and, as we will show shortly, its behavior influences the overall spectrum. So, consider the function within a generic interval $t \in [jT_d, (j+1)T_d]$, where ϕ_j is kept constant:

$$f_j(t) = \sin(\omega_0 t + \phi_j)\left[\Theta(t - jT_d) - \Theta(t - (j+1)T_d)\right]\ ,$$

in which we do not specify any prescription on T_d. This is clearly written as the product of two function, i.e. $f(t) = g(t)\dot{h}(t)$, and its Fourier transform correspond to the

convolution of the Fourier transform of each member:

$$\tilde{f}_j(\omega) = \left(\tilde{g}_j * \tilde{h}_j\right)(\omega) = \int_{-\infty}^{+\infty} \tilde{g}_j(\omega-\nu)\tilde{h}_j(\nu)\, d\nu\,. \tag{4.6}$$

Identifying $g_j(t)$ with $\sin(\omega_0 t + \phi_j)$ returns immediately

$$\begin{aligned} \tilde{g}_j(\omega) &= \frac{1}{\sqrt{2\pi}} \int_{-\infty}^{+\infty} \sin(\omega_0 t + \phi_j)\, e^{i\omega t}\, dt \\ &= i\sqrt{\frac{\pi}{2}} \left[e^{-i\phi_j}\delta(\omega-\omega_0) - e^{i\phi_j}\delta(\omega+\omega_0)\right]\,, \end{aligned} \tag{4.7}$$

while for $h(t)$ we have

$$\begin{aligned} \tilde{h}_j(\omega) &= \frac{1}{\sqrt{2\pi}} \int_{-\infty}^{+\infty} \left[\Theta(t+jT_d) - \Theta(t-(j+1)T_d)\right]\, e^{i\omega t}\, dt \\ &= -\frac{i}{\sqrt{2\pi}}\, e^{i\left(j+\frac{1}{2}\right)\omega T_d}\, \frac{e^{i\omega T_d/2} - e^{-i\omega T_d/2}}{\omega} \\ &= \frac{T_d}{\sqrt{2\pi}} e^{i\left(j+\frac{1}{2}\right)\omega T_d}\, \mathrm{sinc}\left(\frac{\omega T_d}{2}\right)\,, \end{aligned} \tag{4.8}$$

where we define the function $\mathrm{sinc}(x) = \sin(x)/x$. Eq. (4.8) gives us an important feature of the system, in effect if one works in the limit of $T_d \ll T_0$ it is allowed to consider $T_d\omega \ll 1$; due to this the spectrum of the step function becomes

$$\left|\tilde{h}_j(\omega)\right|^2 \propto T_d^2 \quad \text{if} \quad T_d \ll T_0\,, \tag{4.9}$$

which clearly is a flat spectrum, i.e. we deal with a function which has white noise characteristics, this is nicely shown in Fig. (4.5)

Now, inserting equations (4.7) and (4.8) in (4.6) one get

$$\begin{aligned} \tilde{f}_j(\omega) = \frac{iT_d}{2} e^{i\left(j+\frac{1}{2}\right)\omega T_d} \Bigg\{ & e^{-i\left[\left(j+\frac{1}{2}\right)\omega_0 T_d + \phi_j\right]}\, \mathrm{sinc}\left[\frac{(\omega-\omega_0)T_d}{2}\right] + \\ & - e^{i\left[\left(j+\frac{1}{2}\right)\omega_0 T_d + \phi_j\right]}\, \mathrm{sinc}\left[\frac{(\omega+\omega_0)T_d}{2}\right] \Bigg\}\,, \end{aligned} \tag{4.10}$$

from which the power spectrum $\mathrm{Sp}(\omega) = |\tilde{f}(\omega)|^2$ is immediately found

$$\begin{aligned} |\tilde{f}_j(\omega)|^2 = \frac{T_d^2}{4} \Bigg\{ & \mathrm{sinc}^2\left[\frac{(\omega-\omega_0)T_d}{2}\right] + \mathrm{sinc}^2\left[\frac{(\omega+\omega_0)T_d}{2}\right] + \\ & - 2\cos\left[(2j+1)\omega_0 T_d + 2\phi_j\right] \mathrm{sinc}\left[\frac{(\omega-\omega_0)T_d}{2}\right] \mathrm{sinc}\left[\frac{(\omega+\omega_0)T_d}{2}\right] \Bigg\}\,. \end{aligned} \tag{4.11}$$

In Fig. (4.1) we report the function expressed in Eq. (4.11) for different values of the dephasing time, keeping all the other parameters fixed. From that figure it is evident how the spectrum changes as T_d is lowered: for $T_d \gg T_0$, there are few changes of ϕ

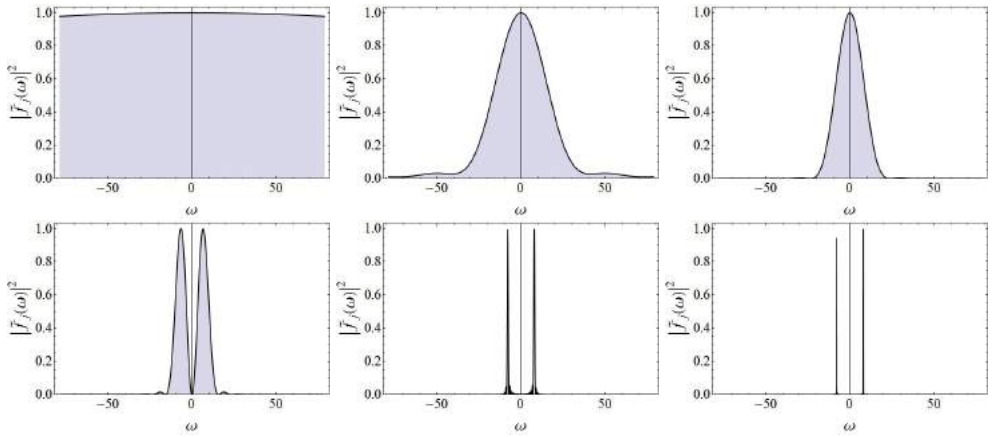

Figure 4.1: Power spectrum defined in Eq. (4.11) (in arbitrary units), normalized in such a way that maximum value is always 1. We emphasize that with this kind of random potential we can obtain a power spectrum which goes from white noise (flat spectrum), for $T_d \ll T_0$, to the pure periodic signal (two delta peaks) for $T_d \gg T_0$. Here we consider $T_d = 0.01T_0$, $0.25T_0$, $0.5T_0$, T_0, $10T_0$ and $100T_0$, with $T_0 = 4/5$, and use the same ϕ for all graphs (e.g. $\phi = 0$).

and so spectrum resemble the one of a periodic function $\sin(\omega_0 t)$ (see Eq. (4.7); as T_d is decreased the peaks at $\pm\omega_0$ becomes broader and broader and the modulation due to the sinc function play a significant role. Going ahead for $T_d = T_0/$ the two separated peaks join together and from that moment the spectrum will be dominated by the Fourier transform (4.8). Finally, for $T_d \ll T_0$ the spectrum could be considered flat over a wide region of ω, so we enter the white noise regime. In Fig. (4.1) we have considered different T_d with all the other parameters being constant, but in Eq. (4.11) we can find that there is also a dependence onto the phase ϕ_j in a specific interval. How the spectrum changes with the phase is reported in Fig. (4.2), where we observe that for different ϕ_j one can get totally different spectra.

Up to now we have considered just the case of a single step but, as described before, the real $f(t)$ is the sum of many steps, namely

$$f(t) = \sum_{j=1}^{n_\phi} f_j(t)\,,$$

that gives

$$\tilde{f}(\omega) = \sum_{j=1}^{n_\phi} \tilde{f}_j(\omega)\,,$$

due the linearity of the Fourier transform. The summations over many time steps modifies the spectrum of $f(t)$ in the sense that there are several interference terms like the last one in Eq. (4.11) between both the same and different steps. In Fig.(4.3) we compare

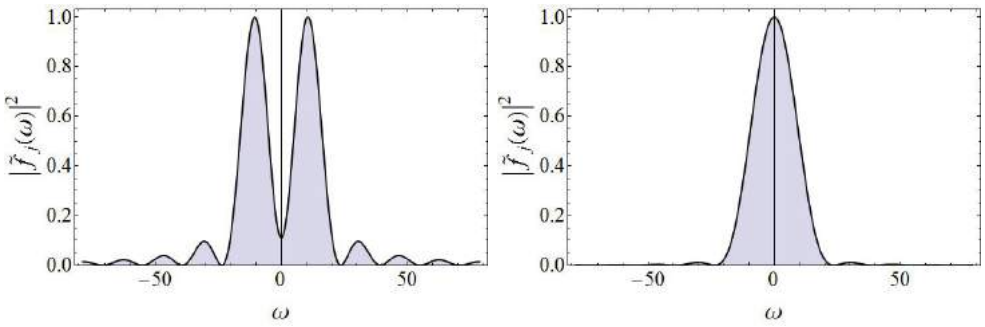

Figure 4.2: Power spectrum defined in Eq. (4.11) (in arbitrary units), normalized in such a way that maximum value is always 1. Here we set $T_0 = 4/5$ and $T_d = T_0/4$ and consider two different values of ϕ. It is clear that a single phase can modify the shape of the spectrum in a very strong way.

$|\tilde{f}(\omega)|^2$ obtained both numerically and by the mean of Eq. (4.10) once inserted in the previous one. Finally, in Fig. (4.4) we report a summary of what we explained up to now for the phase noise, showing all the main quantities, i.e. $\phi(t)$, $f(t)$, $g(\tau)$ and $\langle|\tilde{f}(\omega)|^2\rangle$ for three different values of T_d, from low to high noise.

4.1.2 Frequency Noise

Another possibility to create a random function of time is to change the frequency ω of $f(t)$ with a scheme that is similar to the one described before. Every time step T_d we change ω by picking up a random value from a certain interval centered around a main frequency ω_0:

$$\begin{aligned} \omega(t) &= \sum_{j=1}^{n_\phi} \omega_j \left[\Theta(t-(j-1)T_d) - \Theta(t-jT_d)\right] , \\ \omega_j &\in [\omega_0 - \Delta\omega, \omega_0 + \Delta\omega] ; \end{aligned} \tag{4.12}$$

moreover we want to generate $f(t)$ which does not has any sudden jump; those discontinuity in $f(t)$ are the main feature of the phase noise, and in that case they can not be avoided. If we now change the frequency randomly, instead of the phase, we can make $f(t)$ continuous by adjusting the phase in the proper way: if at T_d frequency changes from ω_1 to ω_2, then asking for continuity results simply in $\sin(\omega_1 T + \phi_1) = \sin(\omega_2 T + \phi_2)$, which gives $\phi_2 = \phi_1 + (\omega_1 - \omega_2)T$. So, in order to preserve the continuity of the signal we have to add to Eq. (4.12) the prescription

$$\phi_j = \phi_{j-1} + [\omega_j - \omega_{j+1}]\, jT_d , \tag{4.13}$$

where ω_j and ϕ_j stand for $\omega(jT_d)$ and $\phi(jT_d)$, respectively. Requiring the continuity of $f(t)$ strongly affects its behavior, in particular we will show in a few that we can not

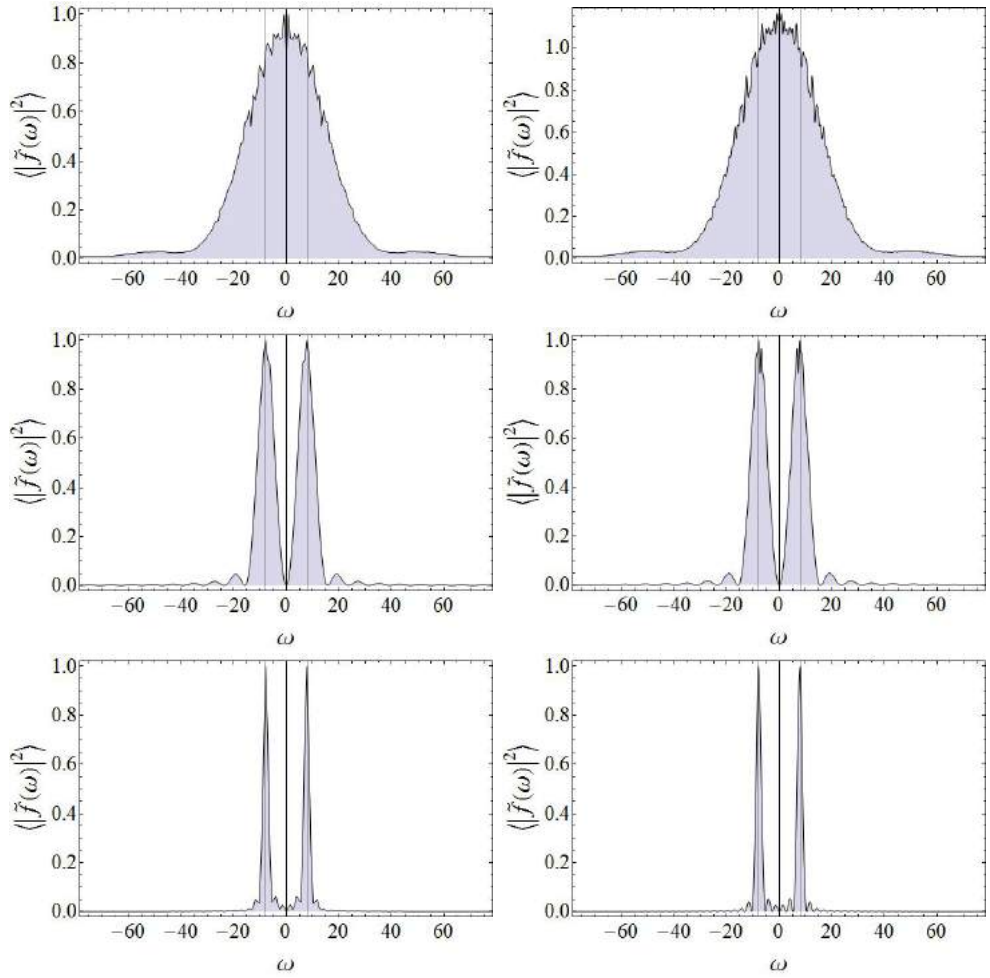

Figure 4.3: Power spectrum $\langle|\tilde{f}(\omega)|^2\rangle$. From top to bottom $T_d = T_0/4$, T_0 and $T_d = 3T_0$. Each plot is obtained by averageing over 500 realizations. Right column shows $\langle|\tilde{f}(\omega)|^2\rangle$ numerically, while left column represent $|\sum_j \tilde{f}_j(\omega)|^2$ with $\tilde{f}_j(\omega)$ expressed in Eq. (4.10). In both cases the spectra obtained with the two technique coincide.

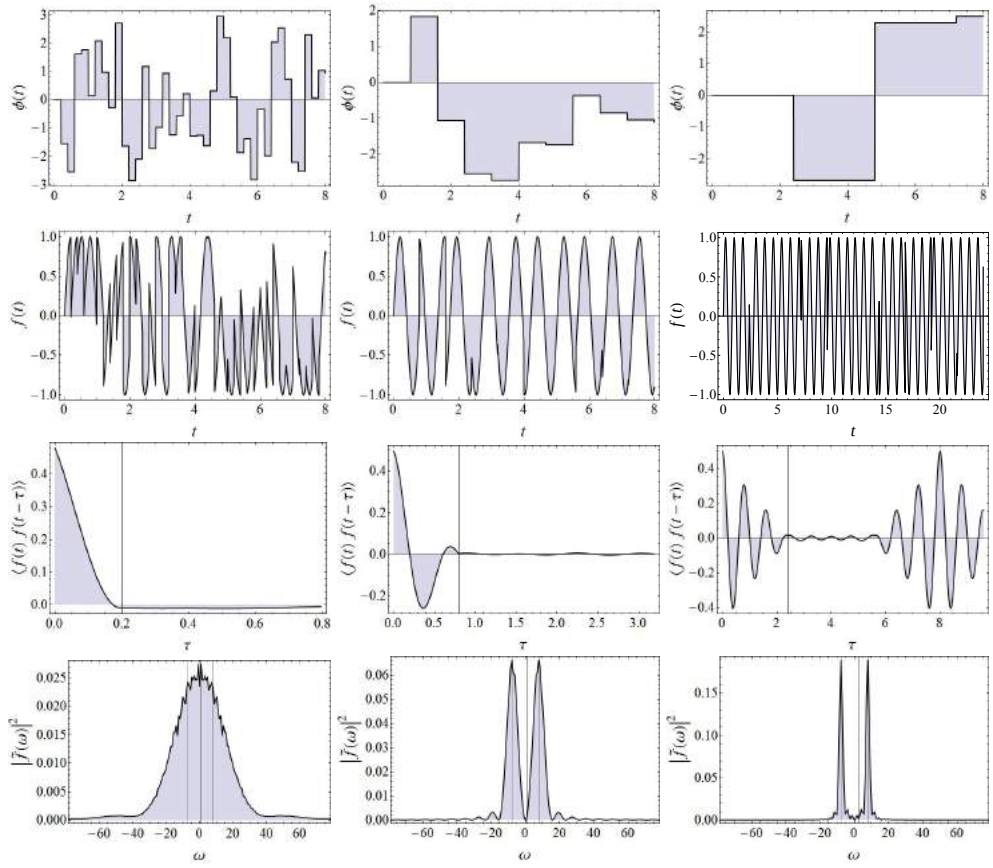

Figure 4.4: Some characteristic features of the time dependent function $f(t)$ in the case of the phase noise. In the first row we report the phase $\phi(t)$, while in the second row we plot the whole $f(t)$. Notice the jumps of $f(t)$ in correspondence to the changes of ϕ. Last two rows show the correlation function $g(\tau)$ and the power spectrum of $f(t)$, respectively. As described in the text $f(t)$ shows coherence only for $t \leq T_d$, because in an interval T_d the phase is constant. This influence $\tilde{f}(\omega)$, which is the convolution of the two delta peaks, coming from the $\sin(\omega_0 t + \phi)$, and the sinc function which is the Fourier transform of a step function. As T_d is lowered, the width of the sinc increases and we approach the white noise limit, which we report in Fig. (4.5). Here we set: $T_0 = 4/5$, so $\omega = 2\pi \times 5/4$, and $T_{max} = 10T_0$. From left to right we consider $T_d = T_0/4$, T_0 and $3T_0$.

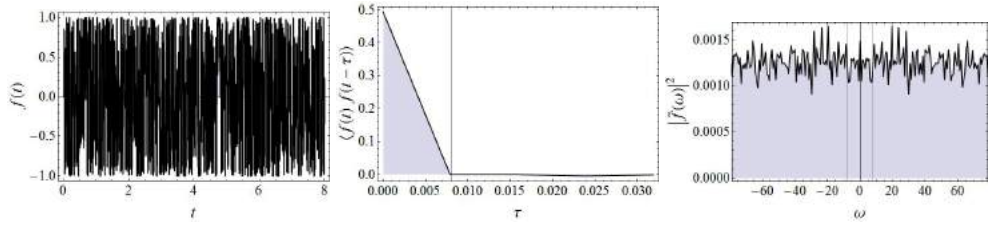

Figure 4.5: $f(t)$, correlation function $g(\tau)$ and power spectrum $|\tilde{f}(\omega)|^2$ in the case of T_d very short compared to T_0, in the specific $T_d = T_0/100$. As expected the changes of phase are so frequent that we fall into the white noise, i.e. flat spectrum, regime. The values for the parameters used here are the same as in Fig. (4.4).

reach situations of very wide spectra, which means that we can not have a real broadband noise, provided that $\Delta\omega \ll \omega_0$. The last sentence underline that in that kind of noise we have to deal mainly with two parameter: dephasing T_d and frequency interval $\Delta\omega$; here we will just give a qualitative description for the behavior of the noise for different parameters, reporting the results in Fig. (4.6), Fig. (4.7) and Fig. (4.8). Using a notation similar to the one introduced in 4.1.1, we can write

$$f(t) = \sum_{j=1}^{n_\phi} \sin(\omega_j t + \phi_j)\left[\Theta(t - jT_d) - \Theta(t - (j+1)T_d)\right] \equiv \sum_{j=1}^{n_\phi} f_j(t)\,.$$

In a single step $jT_d < t < (j+1)T_d$ we can compute the Fourier transform $\tilde{f}_j(\omega)$ as done in Eq. (4.10), noticing that in both cases they have the same form. Then we obtain

$$\tilde{f}_j(\omega) = \frac{iT_d}{2} e^{i\left(j+\frac{1}{2}\right)\omega T_d}\left\{ e^{-i\left[\left(j+\frac{1}{2}\right)\omega_j T_d + \phi_j\right]}\ \mathrm{sinc}\left[\frac{(\omega-\omega_j)T_d}{2}\right] + \right.$$
$$\left. - e^{i\left[\left(j+\frac{1}{2}\right)\omega_j T_d + \phi_j\right]}\ \mathrm{sinc}\left[\frac{(\omega+\omega_j)T_d}{2}\right]\right\}.$$

Once we have to find the total power spectrum, i.e. $|\tilde{f}(\omega)|^2 = |\sum_j \tilde{f}_j(\omega)|^2$, we have here a different result compared to the phase noise. As first, notice that with this noise we have to deal with many many frequencies, so in principle we have as many delta peaks as the number of them; in addition to this we have to take into account the broadening of each peak do to the sinc arising from the step function. So we have a spectrum that enlarges with increasing $\Delta\omega$, because we can span a large interval of frequencies. In the previous case of phase noise, we had shown that decreasing T_d drives $f(t)$ into a regime which is comparable to the white noise, in principle one can think that the same could be done also for the frequency noise but with the prescription of the continuity of $f(t)$ it becomes impossible. Suppose to deal with not too large $\Delta\omega$, i.e. $\Delta\omega = \omega_0/5$ which a typical value used in the experiment presented in [87], so the ω_j are not too far one from the other. Then, if we change it very frequently with a T_d much smaller than T_0 we create a series of $f_j(t)$ that have similar frequencies and match one another due to Eq.

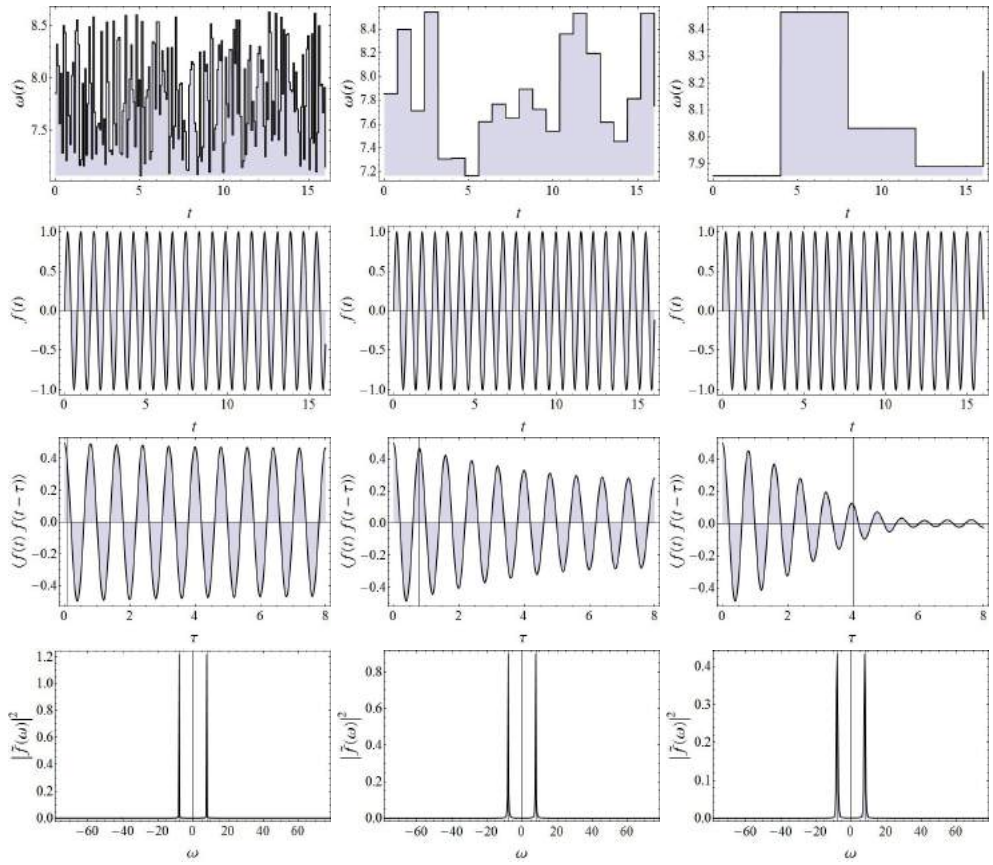

Figure 4.6: Noise characteristic for $T_0 = 4/5$, i.e. $\omega_0 = 2\pi \times 5/4$, $\Delta\omega = 0.1\omega_0$. From left to right we set $T_d = 0.1T_0$, T_0 and $5T_0$. From top to bottom we plot the following quantity: $\omega(t)$, $f(t)$, $\langle g(\tau)\rangle$ and $\langle|\tilde{f}(\omega)|^2\rangle$. Average performed over 100 realizations.

(4.13). Practically this results into a $f(t)$ which is closer to $\sin(\omega_0 t + \phi_0)$ (ϕ_0 being the initial phase), so instead of enlarging the spectrum we have come back to the perfect periodic case. With this in mind we can state that *for* $\Delta\omega \ll \omega_0$ $f(t)$ *is the same both in the limit of* $T_d \gg T_0$ *and* $T_d \ll T_0$. This is also shown in Fig. (4.6) where it is clear that whatever T_d is chosen (there we have $T_d/T_0 = 0.1$, 1 and 5) the spectrum does not differs too much from the one of a perfect $\sin(\omega_0 t)$ function. If one wants to obtain broad spectrum in the case of frequency noise the only possibility is to select $\Delta\omega \gg \omega_0$ and $T_d \simeq T_0$. Although we have just shown that this type of noise does not allow a wide range of possible spectra, the possibility of avoid any sudden changes of $f(t)$ makes it very interesting for the experimental physicists, which have implemented it in a series of recent experiment [87]. This because the bandwidth they can reach by using the frequency noise is sufficient in order to reach their goals, and the continuity of $f(t)$ is also important for them otherwise there should be a series of problem arising from this sharp variation of the external potential. In Fig. (4.9) we report the figure in [87] in

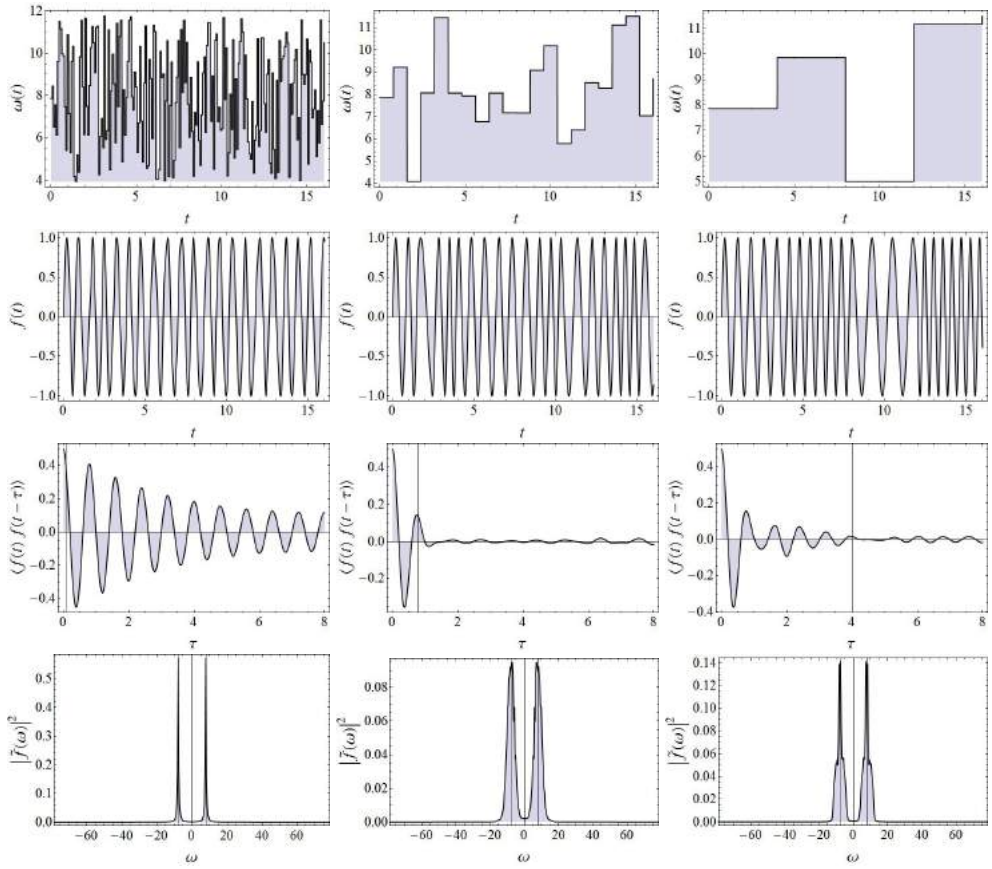

Figure 4.7: Same as Fig. (4.6) for $\Delta\omega = 0.5\omega_0$.

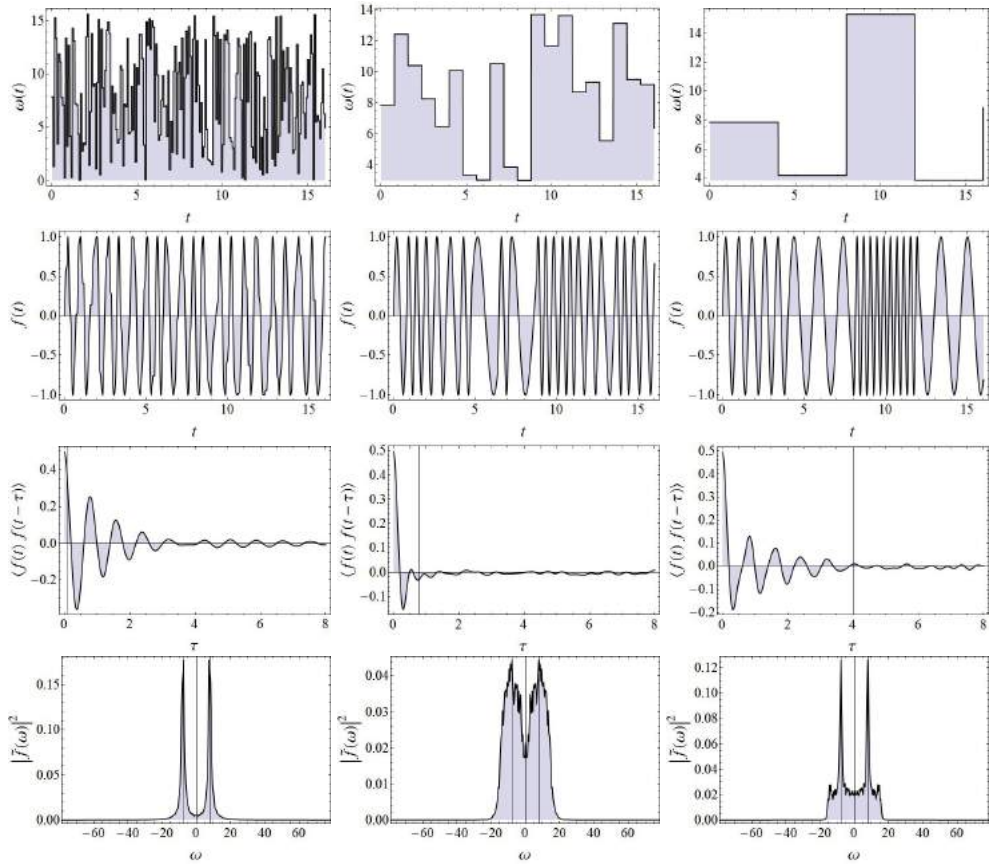

Figure 4.8: Same as Fig. (4.6) for $\Delta\omega = \omega_0$.

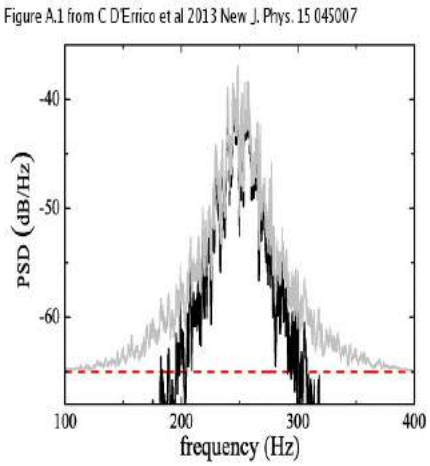

Figure 4.9: Typical power spectrum for the noise the author use in their experiments, obtained with the frequency noise method [87]. Figure extracted from [87].

which the authors shows a typical power spectrum of the noise they had used.

4.2 Noise-induced normal diffusion

In the previous chapter we have studied how a one-dimensional wave packet Anderson localize in the presence of a static disordered potential. This a widely studied and now we want to study what happens if to it we superimpose a time dependent random potential as the one described before.

The model we are going to use is the one of Eq. (4.2), with the random potential defined in Eq. (4.3):

$$i\frac{d}{dt}\phi_l(t) = -\left[\phi_{l-1}(t) + \phi_{l+1}(t)\right] + V_l\phi_l(t) + AV_l f(t)\phi_l(t)\,. \tag{4.14}$$

In all the simulations we employ the phase noise scheme for $f(t)$, this is motivated also if one looks to [87] where, although the experiments was done by using the frequency noise scheme, the numerical results they used as comparison were obtained with the phase noise. As static disorder V_l we use here two type of disorder: Anderson and bichromatic. The first one allows us to perform faster simulations, while the second is interesting because of the recent experiment developed in Florence at LENS [87, 125].

As said in the introduction of this chapter, the motion of a particle in a potential which randomly changes in time has been faced since long ago, due to the fact that thermal bath for quantum particles, as phonons for an electron moving in a lattice, could me modeled like that. Thermal agitation has been shown to give rise to diffusion in a noninteracting tight-binding lattice [26, 27]. In those papers the thermal agitation was described as random disorder, uncorrelated in space and time, with zero mean. Because

of this a natural choice for the underling static disorder V_l is the Anderson model that we have explained to be uncorrelated in space, and then we modulate it by an $f(t)$ with sufficiently small correlations time. We demonstrate that this can be easily achieved by implementing the phase noise scheme. Also recently, in a paper by Quach [46], a similar problem was studied regarding a series of coupled optical cavities with a two-level atom.

In order to study and characterize the dynamics of a wave packet it is useful to consider two quantities: the width $\sigma(t)$ and the partecipation ratio $\mathrm{PR}(t)$, respectively defined as

$$\sigma(t) = \sqrt{m_2(t)}\,, \tag{4.15}$$

where

$$m_2(t) = \sum_l l^2 |\phi_l(t)|^2 - \left(\sum_l l |\phi_l(t)|^2 \right)^2 , \tag{4.16}$$

and

$$\mathrm{PR}(t) = \frac{1}{\sum_l |\phi_l(t)|^4}\ ; \tag{4.17}$$

the first gives informations about the spatial spreading of the density $\rho_l(t) = |\phi_l(t)|^2$, while the second could be regarded as the number of sites significantly populated.

Despite these two seems to be linked, and one could expect that larger packets occupy a grater number of sites, there is some situations in which looking just at one of them one could reach to incorrect interpretation. This is the case of self trapping, in which $\sigma(t)$ increases in time but $\mathrm{PR}(t)$ stays more or less constant, meaning that $\phi_l(t)$ has a frozen bulk that does not evolve and that is responsible for the high occupation of some sites, while the tails of the density still moves and lead to an increasing width. This peculiar case is reasonably described as a localized state, because most of the particles do not move, but it is not Anderson localization. We will show later that this phenomenon occurs in interacting system and we find that, once a noise is added to the system, the interplay between self trapping and delocalization induced by the noise ends up in some interesting features.

Here we just recall the statistical properties of the Anderson disorder

$$V_l \in [-W, W]\,, \qquad \mathcal{P}(V_l) = \frac{1}{W}[\Theta(V + W) - \Theta(V - W)]\,,$$

and the definition of a quasi-periodic lattice

$$V_l = \frac{\Delta}{J} \cos(2\pi\beta l + \theta)\,,$$

which are the two kind of disorder used in our simulations. In all the cases we take into account we uses as initial state a Guassian defined as

$$\phi_l(t = 0) = A \exp\left[-\frac{(l - L/2)^2}{4\sigma_0^2} \right] , \tag{4.18}$$

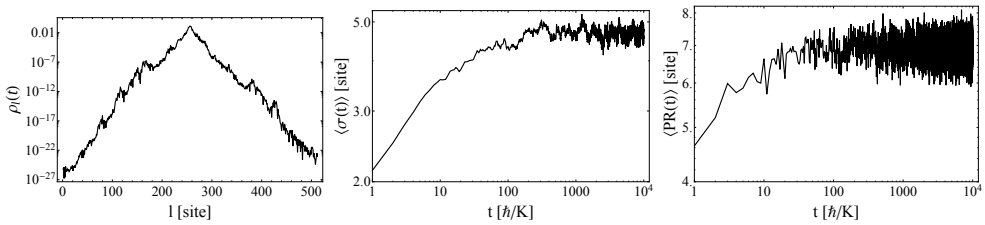

Figure 4.10: Example of Anderson localization. First panel shows the density profile (log scale), second and third panel $\sigma(t)$ and PR(t), respectively. As expected after an initial stage those quantities do not evolve. Using expression in Eq. (4.19) we have $\sigma(t) \approx t^{\alpha}$, with $\alpha = 0$.

where L is the number of lattice sites, so the Guassian is centered in the middle of the lattice, σ_0 is the initial width and we always set $\sigma_0 = 2$. In Eq. (4.18) we just indicate a proportionality because we also fix the density

$$\sum_{l=1}^{L} |\phi_l(0)|^2 = 1\,,$$

from which we get A. For very large system A approaches the values it should have in a continuous system, i.e. $A^2 = 1/\sigma_0\sqrt{2\pi}$. When such a wave packet is loaded onto a disordered potential we known from literature [1, 2, 68, 94] and previous chapter that it exponentially localizes. A consequence of this is well explained in the title of the milestone paper of Anderson [2]: the absence of diffusion. Using (4.15) and (4.17) this will be simply visible: after an initial dynamics in which the density profile $\rho_l(t) = |\phi_l(t)|^2$ rearranges, in particular the tails, then it stops all the expansion and both $\sigma(t)$ and PR(t) remains constant in average [55, 80, 90], as we also report in Fig. (4.10).

After having verified the appearance of Anderson localization (see Fig. (4.10) we turn on the temporal disorder, that we call also noise, $A \cdot f(t)$, and look to what happens. As predicted in several papers (e.g. [26–29, 46]) dynamical disorder breaks localization and restore the expansion of the wave packet. One of the objective of this work is to characterize its spreading, in order to classify the dynamics of the packet. In general at larger time one finds that the width grows in time as a power of time, $\sigma(t) \propto t^{\alpha}$, depending on the exponent one deals with different dynamical regimes [55, 80]:

$$\sigma(t) \propto t^{\alpha} \begin{cases} \alpha = 0 & \text{localization,} \\ \alpha < 0.5 & \text{subdiffusive regime,} \\ \alpha = 0.5 & \text{normal diffusion,} \\ 0.5 < \alpha < 1 & \text{super-diffusive regime,} \\ \alpha = 1 & \text{ballistic regime.} \end{cases} \tag{4.19}$$

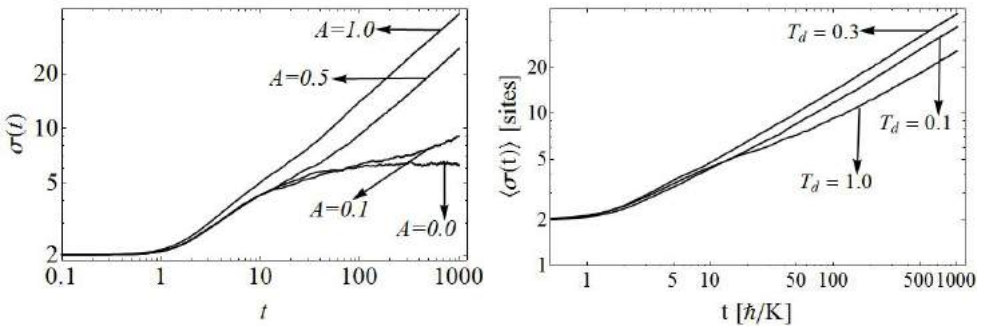

Figure 4.11: Evolution of $\sigma(t)$ for a Gaussian wave packet as in Eq. (4.18), with $\sigma_0 = 2$. Static disorder with an Anderson model of $W = 1.5$.
Left panel: simulations performed for fixed $T_d = 0.2$ and different amplitude A.
Right panel: here we present the $\sigma(t)$ in the case of fixed $A = 1.0$ and different T_d.

We start by considering the situations reported in Fig. (4.11): we keep constant the parameters which define the noisy behavior of $f(t)$, i.e. T_0 and T_d (we are working in the case of $T_{max} \gg T_0, T_d$ so it does influence $f(t)$) and vary its intensity A. As one could imagine, the more we perturb the system, the greater the expansion of $\rho_l(t)$ is. Another possibility is to keep fixed the intensity of the disorder, and change the degree of noisiness by varying T_d. A possible result is also plotted in Fig. (4.11). Comparing the plots in Fig. (4.11) we immediately notice that if for constant dephasing $\sigma(t)$ at fixed time increases with A, the same does not happens in the opposite situation, i.e. A fixed and different T_d. A more clear example is reported In Fig. (4.12) where $\sigma(t)$ at $t = 1000$ is plotted as function of T_d for different disorder amplitude W, while all other parameters are kept constant. In that figure we emphasize that $\sigma(t_{max})$ is not a monotonic function of T_d, but it has a maximum for certain values of dephasing. This suggests that the expansion depends onto spectrum $\mathrm{Sp}(\omega)$ of $f(t)$, which is itself a function of T_d as demonstrated in Eq. (4.11). An analogous result could be find in [46], where authors shows that the equivalent of $\sigma(t)$ as a maximum for certain values of the correlation time of the noise, when a disordered background is present.

In the following we will try to give an explanation of this peculiar behavior, as done in [87]. A good start point is the classical diffusion equation

$$\frac{\partial \rho(x,t)}{\partial t} = \frac{D}{2}\frac{\partial^2 \rho(x,t)}{\partial x^2}\,, \tag{4.20}$$

where D is the *diffusion coefficient* for the distribution $\rho(x,t)$. A possible solution of Eq. (4.20) is the Gaussian

$$\rho(x,t) = \frac{1}{\sigma(t)\sqrt{2\pi}}\, e^{-\frac{x^2}{2\sigma^2(t)}}\,, \tag{4.21}$$

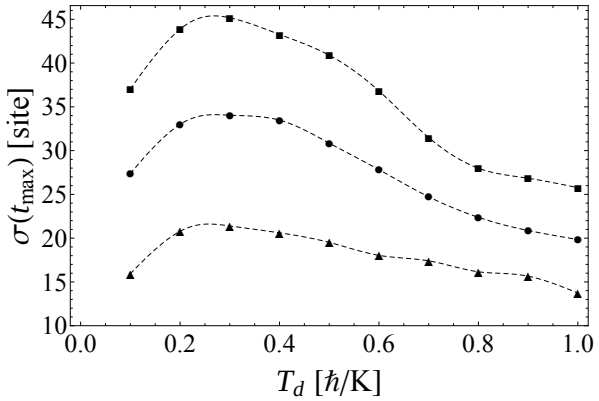

Figure 4.12: $\sigma(t)$ at $t = 1000$ as function of the dephsaing time T_d in the case of Anderson disorder with $W = 1.5$ (squares), $W = 2$ (circles) and $W = 4$ (triangles). Notice that the behavior of the curves is similar to the one of η in Fig. (4.18), suggesting that there is a connection between expansion and η. Moreover the greater W the smaller $\sigma(t_{max})$, this reflects that also the localization eigenstates, at least their overlaps, play a role. For stronger disorder, i.e. large W, states are more localized and their overlap become smaller and smaller, this suppresses transition between them driven by the noise, slowing down the diffusion process.

which is a self-similar solution in the sense that during the evolution $\rho(x, t)$ will keep a Gaussian shape but with a variance $\sigma(t)$ that is a function of time. Inserting Eq. (4.21) in Eq. (4.20) we obtain

$$2\sigma(t)\frac{d\sigma(t)}{dt} = D\,,$$

that is

$$\frac{d\sigma^2(t)}{dt} = D\,. \tag{4.22}$$

Eq. (4.22) is readily integrated, giving $\sigma^2(t) = \sigma_0^2 + Dt$ or, equivalently,

$$\sigma(t) = \sigma_0\sqrt{1 + \frac{t}{t_0}}\,. \tag{4.23}$$

In (4.23) we introduced $\sigma_0 = \sigma(0)$ that is the initial width of $\rho(x, t)$ and define $t_0 = D/\sigma_0^2$. We are interested in the asymptotic, i.e. large t, dynamics so Eq. (4.23) can be approximated with

$$\sigma(t) \approx \sqrt{D}\sqrt{t}\,. \tag{4.24}$$

We obviously obtain that the width of a Gaussian like the one in (4.21), which we recall is a solution of Eq. (4.20), grows in time as the square root of t so, in accordance with (4.19), it has diffusive dynamics.

As already mentioned, there are predictions about discrete system in the presence of an uncorrelated noise claiming that it will be driven into a diffusion regime. i.e. $\sigma \sim \sqrt{t}$ [27, 29, 46]. To verify this in our systems we integrate Eq. (4.2) up to mlarge

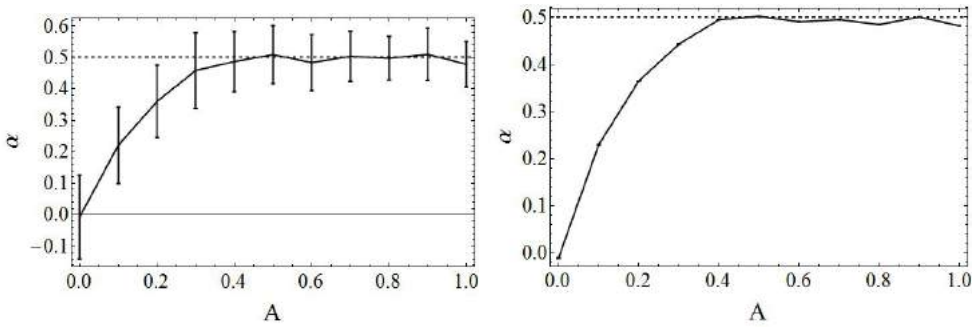

Figure 4.13: Exponent α of Eq. (4.25) for a noise with $A = 1$, $T_0 = 4/5$ and $T_d = 0.2$. Static disorder is an Anderson chain with $W = 1.5$. Simulations are performed up to $t = 10^3$, and we consider 100 realizations of disorder. Left and right panel differs only for the method use for determining α, but the two curves are compatible within errors.

times. Here by large we mean a time t at which $\rho_l(t)$ is expanded in such a way that one has there is a large time interval in which $\ln(\sigma(t))$ versus $\ln(t)$ is linear. Once we have the data set we fit them with a generalized version of (4.23)

$$\sigma(t) = \sigma_0 \left(1 + \frac{t}{t_0}\right)^{\alpha} , \tag{4.25}$$

with σ_0, t_0 and α being free parameters. At this stage we are only interested in α. We had largely investigated by a large amount of numerical simulations this problem, and in Fig. (4.13) we report an example that clarify what we have obtained. Fig. (4.13) shows that α is in accordance with the theory prediction; there we shown for completeness two way of extracting α from the data. In the left panel we fit every single realization of $\sigma(t)$ with (4.25) and at the end we calculate the weighted average, using the fit errors as weights. This is the reason of the error bars in left panel of Fig. (4.13). In the right panel, on the other hand, we first average the $\sigma(t)$ to obtain curves like the ones in Fig. (4.11) and then fit the realization-averaged $\langle\sigma(t)\rangle$. This last case is presented in Fig. (4.14) From (4.25) we can also extract both σ_0 and t_0, and combining them we can estimate the diffusion coefficient

$$D = \frac{\sigma_0^2}{t_0} , \tag{4.26}$$

we stress here that, although we get a different α for each fit of $\sigma(t)$, the diffusion coefficient is always defined with σ_0^2 in order to have the right physical dimensions, $[D] = [L^2][T^{-1}]$, which allows a comparison between D extracted from different sets of data. This procedure was implemented also in [87] to compare numerical and experimental data, and what they find is reported in Fig. (4.15). There they plot D as function of A^2 for different disorder strength, and what is important to notice is that each curves has a linear behavior with A^2 up to a certain values which depends on the disorder, and that the slope of $D(A^2)$ is a function of disorder strength too. We try to give some explanation of

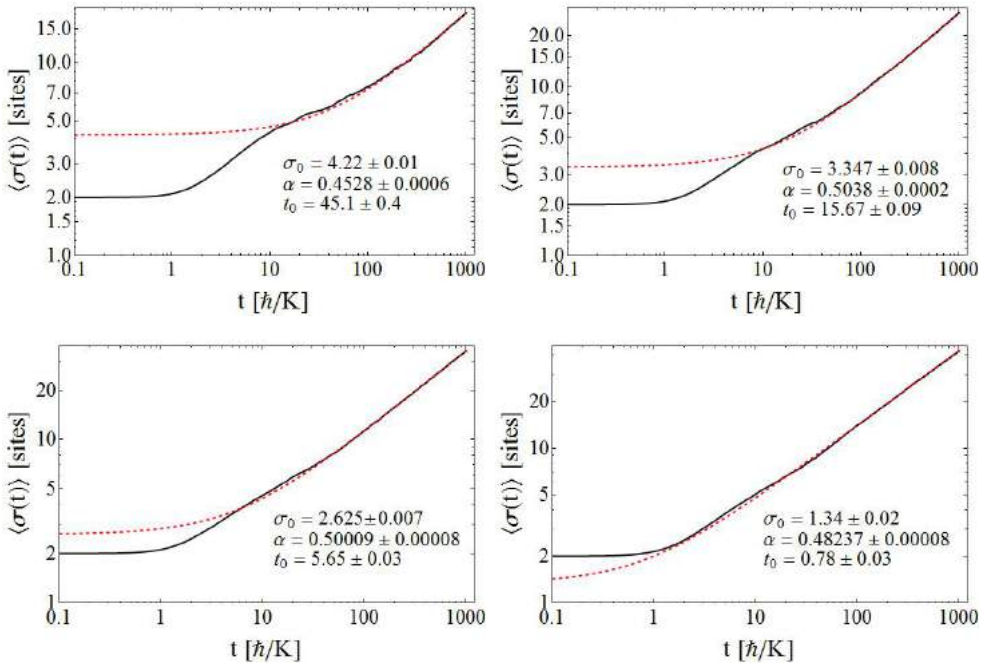

Figure 4.14: $\langle\sigma(t)\rangle$ averaged over 100 realizations of the disorder. The dashed red line is a fit of the data with (4.25). In each panel we put the results of the fit. Parameters used here are $W = 1.5$ for the Anderson noise, for the noise we set $T_0 = 4/5$, $T_d = 0.2$. From top left different A are considered: 0.3, 0.5, 0.7 and 1.0 (clockwise).

this dependence on both A^2 and the disorder by implementing a perturbative approach, which can give a clear, although not too detailed, idea of the mechanism underline the noise-driven diffusion.

The approach we use is based onto the standard perturbative method for linear system in the presence of time-dependent potential, i.e. on the transitions between states induced by the perturbation, and onto the prescription of [126]. In that paper author finds that $D \propto \Gamma\xi^2$ in which ξ is a characteristic length of the system and Γ is the transition rate within perturbative approach [127]; in the case of disordered system a good choice for ξ seems to be the localization length because, as we will show, it determines the length-scale for the spatial overlap between states, which is involved in the calculation of Γ [87].

Let us consider the quasi-periodic lattice, and suppose to be in the localized regime $\lambda > 2$. From previous chapters we know that fir a ginven λ all the eigenstates of the system are Anderson localized with the same localization length [55, 67, 68, 77, 80, 87]

$$\xi = \frac{1}{\ln(\lambda/2)} \; ; \tag{4.27}$$

now take a look to Eq. (4.1), together with Eq. (4.3) we can always write

$$H_l(t) = H_l^{(0)} + Af(t)V_l \, ,$$

where we divided the time independent part $H_l^{(0)}$, given by the Aubry-André model in Eq. 2.39 for $U = 0$, from the non stationary one. Thus we have

$$H_l^{(0)} = \sum_{l=1}^{M} \left[-\left(\phi_l \phi_{l+1}^* + \phi_l^* \phi_{l+1}\right) + \lambda \cos(2\pi\beta l + \theta)|\phi_l|^2 \right] \, .$$

In the regime of small noise amplitude, $A \ll 1$, it is true that $Af(t)V_l \ll H_l^{(0)}$ and we can assume that the only effect of noise is to induce hopping between different localized states of the unperturbed system. The coupling is driven by the frequency component of the noise spectrum that is resonant with the energy difference between states. For a proper choice of λ one can always obtain $\xi \sim 1$, i.e. states decays rapidly onto length scale comparable to the lattice spacing, then we can only consider coupling between neighboring sites, due to the fast decay of states.

The question is how to determine Γ which, in this perturbative regime, is defined by [87]

$$\Gamma \propto A^2 \eta \, |\langle i|V_l|f\rangle|^2 \, . \tag{4.28}$$

Let us explain a little bit more in details each terms of Eq. (4.28): $|\langle i|V_l|f\rangle|^2$ is the usual matrix element of the perturbation between $|i\rangle$ and $|f\rangle$. The term $A^2\eta$ arises from the time dependent $f(t)$; as already said the transition is be possible only if the right right

frequency $\omega_{if} = E_f - E_i$ is present into the spectrum of $f(t)$, $\mathrm{Sp}(\omega) = |\tilde{f}(\omega)|^2$. Because it is has its own dependence onto the frequency we have to take into account for the overlapping between the distribution of the eigenfrequencies of the system, $\mathcal{P}(\omega)$, and $\mathrm{Sp}(\omega)$. We thus define a quantity that can be linked to this

$$\eta \propto \int \mathcal{P}(\omega)\mathrm{Sp}(\omega)\, d\omega\,, \tag{4.29}$$

that we then introduce in Eq. (4.28). We use proportionality because the numerical value depends onto the normalization of both $\mathcal{P}(\omega)$ and $\mathrm{Sp}(\omega)$. A^2 in front of all measures the strength of the noise, i.e. it is proportional to the integrated power spectrum. In the experiments the time-varying field $Af(t)$ inject into the system a quantity of energy which is $\int \mathrm{Sp}(\omega)d\omega \propto A^2$; if one normalize $\mathrm{Sp}(\omega)$ to 1, as we do in all our calculations, then obtains the form we have just introduced with explicit A^2.

In the experiments described in [87] and here reported in 4.5 authors do not use η to give an estimation of this overlap because the definition in (4.29) is not directly measurable. They instead use the width of $\mathrm{Sp}(\omega)$,

$$\delta\omega \propto \int_{-\omega_{max}}^{\omega_{max}} \omega^2\mathrm{Sp}(\omega)\, d\omega\,,$$

or

$$\delta\nu = \frac{\delta\omega}{2\pi}\,.$$

They found that $\delta\nu$ which gives larger expansions is close to the inverse of the bandwidth $\mathcal{W}$ of the disorder, i.e. $\delta\nu \sim \mathcal{W}/h$, this agrees with what we find numerically for η. We had demonstrated that changing T_d modify $\mathrm{Sp}(\omega)$ and thus its width $\delta\omega$; comparing Fig. (4.12) with (4.16) it is possible to see that maximum for $\sigma(t_{max})$ is achieved for T_d of the order of $1/\mathcal{W}$, and for this values $\delta\nu \sim 1/T_d$. So we have exactly $\delta\nu \sim \mathcal{W}$ as the best conditions for expansion.

Regarding the overlapping integral we have to consider $|\lambda\langle i|\cos(2\pi\beta I + \theta)|f\rangle|^2$, to get an analytic prediction we use the strong assumptions

$$|\lambda\langle i|\cos(2\pi\beta I + \theta)|f\rangle|^2 \approx \lambda^2|\langle i|f\rangle|^2\,, \tag{4.30}$$

and assume the eigenstates $|n\rangle$ exponentially localizes as

$$\langle I|n\rangle \approx \frac{1}{\sqrt{\xi}}\exp\left(-\frac{|I - I_n|}{\xi}\right)\,, \tag{4.31}$$

where I_n is the localization center of the eigenstate. The approximation done before suggest to consider state for which $|I_i - I_f| \simeq 1$, and with this in mind one can readily find

$$\lambda^2|\langle i|f\rangle|^2 \approx \lambda^2\frac{(1+\xi)^2}{\xi^2}\,.$$

Now, using Eq. (4.27) one get [2]

$$\lambda^2 |\langle i|f\rangle|^2 \approx e^{2/\xi} \frac{(1+\xi)^2}{\xi^2} \,. \tag{4.32}$$

Finding an expression for η is little bit more difficult, because none of the function involved are known exactly. However we could approximate the density of state of $H_l^{(0)}$ as a box distribution large $\mathcal{W} = 1 + \lambda/2$, which is the width of the energy spectrum for a quasi-periodic lattice:

$$\rho(E_n) = \frac{1}{\mathcal{W}} \left[\Theta\left(E_n + \frac{\mathcal{W}}{2}\right) - \Theta\left(E_n - \frac{\mathcal{W}}{2}\right) \right] ;$$

this description differs from the real due to the fact that it does not consider any gap present in the spectrum, which instead could play a role [80, 128]. This hypothesis turns in a eigenfrequencies distribution

$$\mathcal{P}(\omega) \approx \frac{2}{\mathcal{W}} \left[\Theta(\omega + \mathcal{W}) - \Theta(\omega - \mathcal{W}) \right] . \tag{4.33}$$

Working in the strong noise limit, i.e. $T_d \ll T_0$, we find that the optimal condition for the diffusion is obtained for $T_d = 2\pi/\mathcal{W}$, which means (see Eq. (4.11) that $\mathrm{Sp}(\omega)$ has its first minima in $\omega = \pm\mathcal{W}/2$ and could be identified with

$$\mathrm{Sp}(\omega) \propto \mathcal{W} \frac{1}{\mathcal{W}^2} \mathrm{sinc}^2 \left(\omega \frac{2\pi}{\mathcal{W}} \right) \,, \tag{4.34}$$

where the linear dependence on $\mathcal{W}$ coming from $\int \mathrm{Sp}(\omega) d\omega = 1$; we imposed this normalization to $\mathrm{Sp}(\omega)$ since we explicit the A^2 contribution in (4.28). Using the approximations (4.33) and (4.34) in (4.29) we obtain

$$\eta \propto \frac{1}{\mathcal{W}} \,. \tag{4.35}$$

Remembering that $\mathcal{W} = 1 + \lambda/2$ and $\lambda = 2\exp(1/\xi)$ we arrive to

$$\Gamma \propto A^2 \frac{(1+\xi)^2}{\xi^2 \left(1 + e^{1/\xi}\right)} \,. \tag{4.36}$$

Finally, to obtain an expression for D we recall what is written in [126]

$$D \propto \Gamma \xi^2 \,, \tag{4.37}$$

identifying ξ in that article with the localization length, so inserting (4.36) into (4.37)

[2] The calculation of the integral is based onto a semi-discrete approximation: we consider the eigenstates in the continuum as $\phi(x) = \exp(-|x|/\xi)/\sqrt{\xi}$, which is normalized to 1. Then we take $\langle i|f\rangle = \int \phi(x)\phi(x-1)dx$, where 1 is the lattice spacing, having set it as unit length.

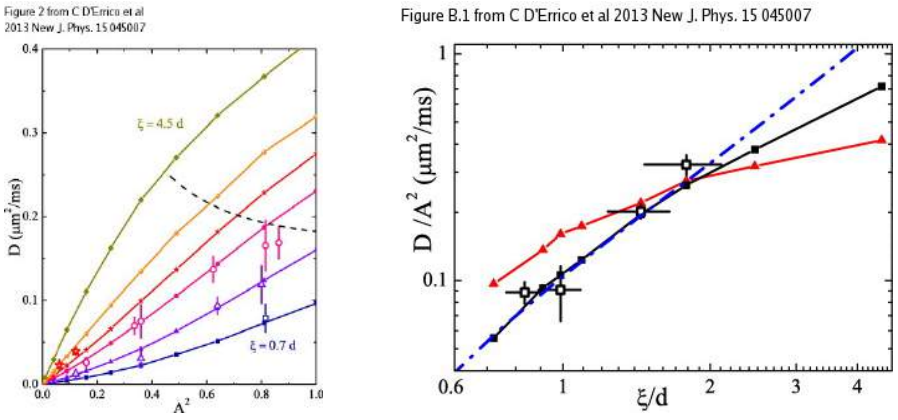

Figure 4.15: **Left panel:** measured D vs A^2, for different values of disorder strength. There the experiment performed with a quasi periodic lattice, from top to bottom : $\lambda = 2.5$ (rhombuses), 3 (spheres), 3.5 (stars) 4 (circles), 5.5 (triangles) and 8 (squares). Open symbols stand for the experimental measurements and filled ones for numerical simulations. Dashed line represents the critical values for A, i.e. A_c, and D above which perturbative approach fails.
Right panel: normalized diffusion coefficient D/A^2 vs. the localization length ξ, for the regime of small A in both experiment (open squares) and numerical simulations (filled squares), and for $A = 1$ in simulations (triangles). The dash-dotted line shows the prediction with perturbative approach (4.38). For numerical data, solid lines are just guide to the eye. Figure taken from [87].

the result is [87]

$$D \propto A^2 \frac{(1+\xi)^2}{1+e^{1/\xi}} \,. \tag{4.38}$$

A nice proof of this prescription could be find in [87], from which we take Fig. (4.15) Remaining in the perturbative approach we try explore a little bit more wider set of situations which can help us to better understand which role is played by each of terms involved in Γ. Eq. (4.28) shows that the transition rate is made as the product of two parts, one belonging to the spatial properties of the disorder $|V_{if}|^2$ and the other coming from interplay between the noise and twill be focused to the noise dependence. As widely shown in 4.1.1, in particular Eq. (4.11), $\mathrm{Sp}(\omega)$ is a function of T_d, $\omega_0 = 2\pi/T_0$ and its shape will suffer sensible changes as one of those parameters is varied, see Fig. (4.4). In Fig. (4.16) and Fig. (4.17) we will consider the case of two different disorder and various noisy functions $f(t)$: the former define the energy spectra, i.e. the eigenfrequencies of V_l, the latter gives $\mathrm{Sp}(\omega)$. In those figures it is immediately visible that the overlap between $\mathrm{Sp}(\omega)$ and $\mathcal{P}(\omega)$ could be very different and to confirm it we numerical compute η and show it in the left panel of Fig. (4.18). There we show also the plot of Fig. (4.12); comparing the two panels, in particular those data that are computed for the same value of T_0, we see that the behavior of $\eta(T_d)$ is the same of $\sigma(t_{max})$ versus T_d. This is a

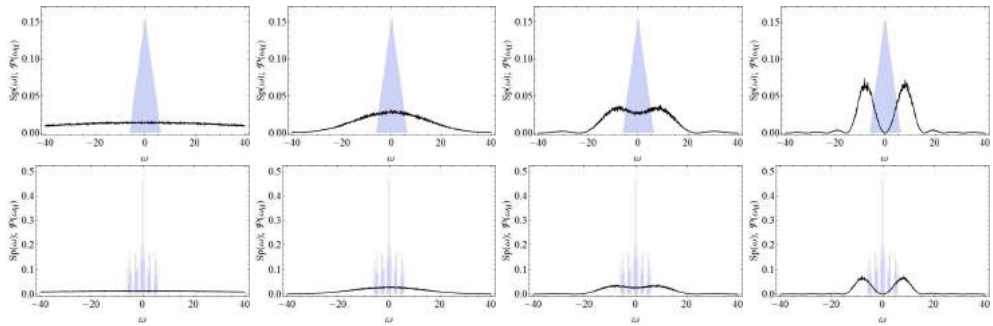

Figure 4.16: Comparison between the power spectrum of the noise with $T_0 = 0.2$ and the distribution of eigenfrequencies $\omega_{if} = E_i - E_f$ for the Anderson model with $W = 2$ (top row) and quasi-periodic lattice with $\Delta/J = 2.5$ (bottom row). From left ot right we consider different dephasing time T_d: 0.05, 0.2, 0.4 and 0.8.

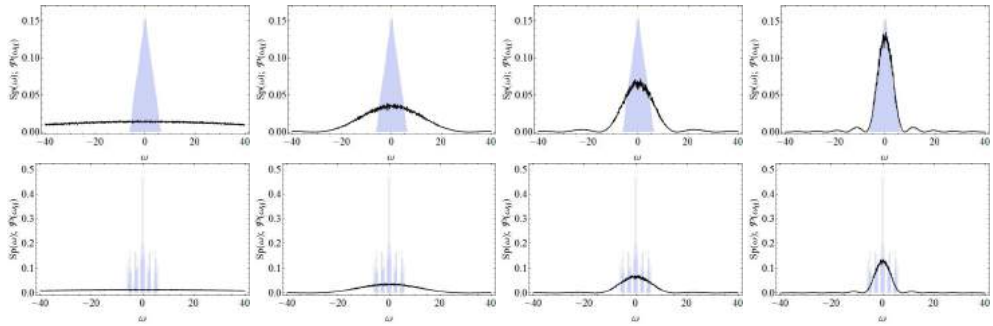

Figure 4.17: Comparison between the power spectrum of the noise with $T_0 = 31.5$ and the distribution of eigenfrequencies $\omega_{if} = E_i - E_f$ for the Anderson model with $W = 2$ (top row) and quasi-periodic lattice with $\Delta/J = 2.5$ (bottom row). From left to right we consider different dephasing time T_d: 0.05, 0.2, 0.4 and 0.8.

clear proof that our picture describing noise induced expansion for the wave packet as the transitions between states works properly.

A better study will go into the direction of also finding the dependence of $|V_{if}|^2$ onto the type of disorder, but this is not a goal of this work. Future development will go into that direction.

4.3 Interacting wave packet in a random potential

Up to now we have only considered the dynamics of a wave packet driven by a linear, although complicated, time-dependent Hamiltonian. We have demonstrated that if the behavior in time of the Hamiltonian is comparable to some noise a wave packet will shows a normal diffusive dynamics, increasing its width as the square root of time; this type of system is quite diffuse in nature once one deals with some random vibration or thermal bath. Another interesting aspect of nature is that among particles there could

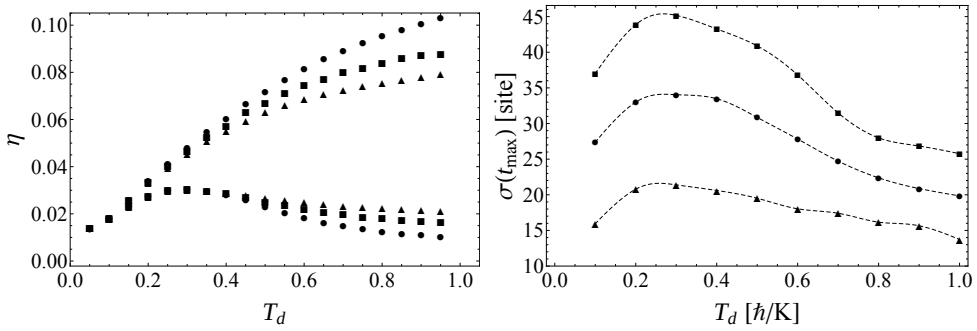

Figure 4.18: **Left panel:** η defined in Eq. (4.29) against T_d for different types of disorder and noise frequency $\omega_o = 2\pi/T_0$. We consider Anderson disorder with $W = 2$ (circles), $W = 4$ (triangles) and quasi-periodic lattice of $\Delta/J = 2.5$ (squares). Upper data for $T_0 = 31.5$ and lower for $T_0 = 0.2$.
Right panel: $\sigma(t_{max})$ versus T_d as in Fig. (4.12). Notice that the lower set of data for η and $\sigma(t_{max})$, which are computed for the same T_0, behave exactly in the same manner.

be interactions that can not be avoided, even if small. The study of their influence on the expansion of a wave packet is a field of research belonging to different branches of physics: from nonlinear science to atomic physics. As described in previous chapter the use of Fano-Feshbach [107–109] magnetic resonance in ultracold atomic gases open a wide range of possibilities for studying those phenomena that until now were just treated from a theoretical point of view.

The microscopic dynamics is governed by the Eq. (2.34), in which we have to add the explicit time dependence of V_l, thus

$$i\frac{d\phi_l(t)}{dt} = -\left[\phi_{l-1}(t) + \phi_{l+1}(t)\right] + V_l\left[1 + Af(t)\right]\phi_l(t) + U\left|\phi_l(t)\right|^2\phi_l(t)\,. \qquad (4.39)$$

4.3.1 Repulsive interactions: subdiffusion

Solving Eq. (4.39) without the noise, i.e. $f(t) = 0$ or for us simply $A = 0$, is the subject of many theoretical papers [49–58, 60] and recently it was also investigated experimentally with cold atoms [88]. Is is not our aim to give e review of those theories, we just put our attention on the fact that in this case interactions lead to a subdiffusive expansion of the wave packet: its width grows in time as t^α with $\alpha < 0.5$, as indicated in (4.19). To give a simple explanation one can say that the finite interaction energy breaks the orthogonality of the single-particle eigenstates of the linear system, weakening the localization. In this case one can describe the resulting dynamics by the mean of perturbative theory as an interaction-assisted coherent hopping between localized states, with a coupling strength that decreases as the sample expand, since the density and hence the interaction energy decreases [87,88]. This is the usual description of the process from a microscopic point of view, but in general one can also try to give a picture of what is

going on taking into account the macroscopic quantities that are, in principle, accessible to experiment. We have exactly done this in 4.2, where we have analyzed the effect of the noisy $V_l(t)$ by looking at $\sigma(t)$ and PR(t): we consider that the wave packet, which at $t = 0$ is taken to be Gaussian (4.18), expands maintaining its shape but increasing σ and this was derived from the classical diffusion Eq. (4.20). Something similar has been done also in the case of finite repulsive interaction, $U > 0$, again without noise. In that case the density profile does not evolves following (4.20), being the observed expansion subdiffusive, and then one has to consider a generalized nonlinear diffusion equation (NDE) in which the diffusion coefficient is not a constant D but depends onto the density, i.e. $D(n(x,t))$ and so decreases as the wave packet spreads. This results in a slowing of the process with respect to the case of normal diffusion with $\alpha = 0.5$. For reasons of completeness we want just to report that a suitable microscopic model for this kind of dynamics relies onto a scheme similar to that one used in the case of the noise-assisted diffusion. The diffusion coefficient is taken to be $D \sim \Gamma\xi^2$, with ξ characteristic localization length of the disordered potential, and the transition rate is defined as (using dimensional units) [125]

$$\Gamma_{if} = \frac{2\pi}{\hbar} \frac{|\langle i|H_{int}|f\rangle|^2}{|E_i - E_f|} , \tag{4.40}$$

where $H_{int} \propto \int \rho(x)^2 dx$ is term in the Hamiltonian describing the interactions; $|i\rangle$ and $|f\rangle$ represent generic initial and final states or, better, quadruplets of them due to the structure of H_{int}. For suitable values of the disorder strength only long-distance couplings are allowed, which tend to decrease with decreasing interactions energy; in this case one recovers that $D \propto \sigma^{-\beta}$, with $\beta > 2$.

Let us introduce the NDE as in [125]:

$$\frac{\partial \rho(x,t)}{\partial t} = \frac{\partial}{\partial x}\left[D_0 \rho^a(x,t) \frac{\partial \rho(x,t)}{\partial x}\right] , \tag{4.41}$$

which takes explicitly into account the density-dependent diffusion coefficient. In the usual solving of this problem the asymptotic one searches for solution at asymptotic time, i.e $t \gg 1$, and it has been demonstrated that a good set of solutions is made by the self-similar functions [125, 129]:

$$\rho(x,t) \propto \left[1 - \frac{x^2}{w(t)}\right]^{1/a} \Theta\left(w(t) - |x|\right) . \tag{4.42}$$

From (4.42) it comes from that both $w(t)$ and $\sigma(t)$ evolves as $t^{1/(2+a)}$ with $a \geq 2$. Although (4.42) gives good results as $t \gg 1$, it does not describe short-time dynamics and, moreover, in real experiments the $\rho(x,0)$ is better approximated by a Gaussian rather than a function like that. In [125] authors suggest a simple and clear way to retain the already known results but with the corrections needed in order to take into

account the aspects just mentioned. They express a Gaussian as certain limit of function like the one in (4.42), namely

$$\exp\left(-\frac{x^2}{w^2}\right) = \lim_{b\to 0}\left(1-\frac{bx^2}{w^2}\right)^{\frac{1}{b}} , \tag{4.43}$$

and then use for the solutions of (4.41) the following ansatz[3]

$$\rho(x,t) = A\left[1-\frac{b(t)x^2}{w(t)^2}\right]^{1/b(t)} \Theta\left(\frac{w(t)}{\sqrt{b(t)}}-|x|\right) , \tag{4.44}$$

which should be good at short times. In (4.44) $A(b,w)$ is an appropriate normalization constant and for the exponent they assume

$$b(t) = a[1-\exp(-t/\tau)] . \tag{4.45}$$

Within this framework they found that the width $\rho(x,t)$ evolves in time as (4.25) with a diffusion exponent $\alpha = 1/(a+2)$ [125], that is in accordance with the predictions of [129].

Finally, we had obtained that an interacting wave packet expanding onto a disordered lattice has a width that spreads in time as

$$\sigma(t) \propto D(t)\, t^{\alpha} , \tag{4.46}$$

with a diffusion coefficient given by

$$D_{int}(t) = 2\alpha\frac{\sigma_0^{1/\alpha}}{t_0}\sigma(t)^{2\left(1-\frac{1}{2\alpha}\right)} . \tag{4.47}$$

Eq. (4.46) and Eq. (4.47) are consistent with a generalized version of the classical diffusion equation (4.22). Indeed inserting (4.47) in $d\sigma^2(t)/dt = D_{int}(t)$ and solving for $\sigma^2(t)$ one gets at the end

$$\sigma(t) = \sigma_0\left(1+\frac{t}{t_0}\right)^{\alpha} ,$$

which is again the function of Eq. (4.25).

[3] Complete expression for the approximation of (4.42) could be found in [125]:

$$\rho(x,t) = \frac{b(t)^{3/2}\Gamma(1/b+3/2)}{\sqrt{\pi}w(t)\Gamma(1/b)}\left(1-\frac{b(t)x^2}{w(t)}\right)^{\frac{1}{b(t)}}\Theta\left(\frac{w(t)}{\sqrt{b(t)}}-|x|\right)$$

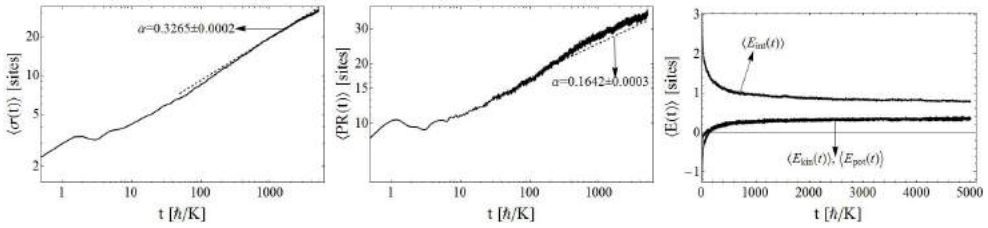

Figure 4.19: From left to right: width $\langle\sigma(t)\rangle$, partecipation ratio $\langle \mathrm{PR}(t)\rangle$ and energies in the case of DNLS with an Anderson disorder with $W = 2$. Data averages over 50 realizations. When interesting we put on the graphs also the values of the diffusion exponent obtained from a fit with the function in (4.23). Here is important to notice that $\sigma(t) \propto t^{\alpha}$ with $\alpha = 0.3625 \pm 0.0003$, so the expansion is clearly subdiffusive. The nonlinear parameter is set to $U = 50$. Data are averaged over 50 realizations of the disorder.

4.3.2 Attractive interaction: self trapping

Self-trapping is a localization phenomenon that arise in non interacting system, and it is totally different from the Anderson localization. First of all there is the possibility of having it also in pure periodic systems and in a double well potential [130–133]. The explanation of this phenomenon could be find with very simple arguments based on energy conservation [50]: all start from the fact that Eq. (4.39) in absence of the noise, i.e. $A = 0$, is describes a closed system in which both norm $\sum_l |\phi_l(t)|^2$ and energy are conserved. Let us focus on the energy; as we already noticed the underlying periodic potential modify the energy spectrum of non interacting particle by opening gaps of forbidden energies between regions of allowed energies. Moreover, the discrete version of (correspond to the tight binding approximation (see . . .) in which one has to deal with just the lowest band of the lattice; due to this the energy of the linear system is bounded both from bottom and above. If we create an initial localized state (as the Gaussian we always use) the energy of which is quite far from those boundaries one can prove that self trapping mechanism set in: the system is unable to transfer energy from interaction to kinetic an potential and the only way it has to preserve the total energy is to keep the density peaked in some region of the (one dimensional) space. This high peaks brings the high contribution from interaction energy (proportional to on site density) while the phases of $\phi_l(t)$ runs following their dynamics.

A signature of self trapping could be find looking to both the width $\sigma(t)$ and the partecipation number $\mathrm{PR}(t)$, following the ideas we draw few line before we expect that $\sigma(t)$ could evolves, even increasing in time due to the dynamics of non self-trapped atoms in the tails of $\rho_l(t)$ [50, 134], but the $\mathrm{PR}(t)$, which we remind measures the number of significantly populated sites, should remains constant in average because the bulk of $\phi_(t)$

does not expand. In our case the state is prepared as usual:

$$\phi_l(0) = N \exp\left[-\frac{(l-l_c)^2}{4\sigma_0^2}\right],$$

without any additional phase $\exp(i\theta_l(0))$ (i denotes the imaginary units), and N a real constant fixing the normalization of the wave function. If we write the wave function in the usual modulus phase representation, remembering that $|\phi_l(t)|^2 = \rho_l(t)$,

$$\phi_l(t) = \sqrt{\rho_l(t)} e^{i\theta_l(t)},$$

and put it into the definition of the kinetic energy, we have

$$\begin{aligned} E_{kin}(t) &= -\sum_l \left[\phi_l(t)\phi^*_{l+1}(t) + h.c.\right] \\ &= -2\sum_l \sqrt{\rho_l(0)\rho_{l+1}(0)}\cos[\theta_l(t) - \theta_{l+1}(t)], \end{aligned} \tag{4.48}$$

For our choice of the initial conditions the initial kinetic energy becomes

$$E_{kin}(0) = -2\sum_l \sqrt{\rho_l(0)\rho_{l+1}(0)},$$

which is the minimum value accessible. When the wave packet evolves each $\phi_l(t)$ acquire a certain phase and $E_{kin}(t)$ grows going to 0 which correspond to complete uncorrelated phase differences between nearest sites, i.e. all the free particle state of the first band are populated. We show this behavior for the kinetic energy because we can now better understand what we have state at the beginning: in this case if we choose $U < 0$ strong enough the kinetic energy goes again to 0, and to ensure energy conservation the interaction energy and potential energy have to compensate the increasing of E_{kin} and the only possibility is to generate regions of high density which carry a lot of interaction energy. In Fig. (4.20) we plot ρ_l, $\sigma(t)$ and PR(t) which give a clear signature of the self trapping mechanism. We stress here that the self trapping is a localization phenomenon which arises from the interplay between interactions and the bounded spectrum of the linear system, so it is totally a different mechanism from Anderson localization: self trapping does not depends onto the disorder, it is possible to observe it also in perfectly periodic system with appropriate nonlinear terms. On the other hand Anderson localization is a single particle behavior, and it appears only if a disordered potential is present: it depend just on the nature of the system. In one dimension every disorder lead to localization, not all interaction gives self trapping. Moreover self trapping and Anderson localization influence different parts of the wave packet: the former acts onto a finite region where density is higher and its a macroscopic phenomenon, the latter instead generate exponential decay on the tails. An outline of this is reported in Fig. (4.21), where $\rho_l(t)$ for the bare disordered system and with strong attractive interactions are compared.

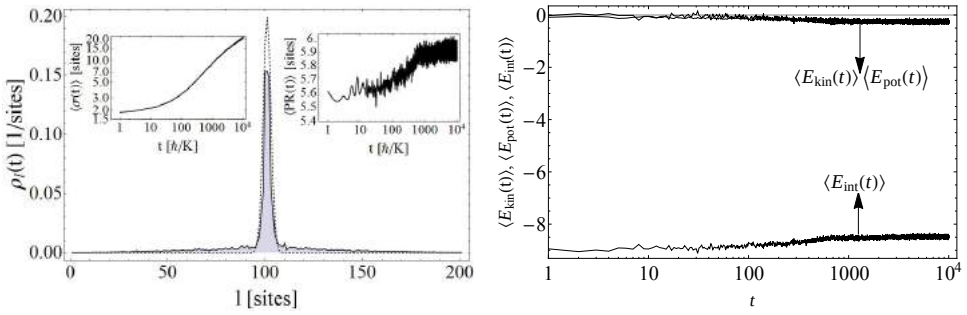

Figure 4.20: **Left panel:** at the center $\langle\rho_l(0)\rangle$ (dashed line) and $\langle\rho_l(t)\rangle$ (solid line, colored area used to evidence it) for $t = 10^4$. Initial and final density do not differs a lot, there is a high-density frozen bulk, while few atoms move in the tails of the distribution. Inset: $\langle\sigma(t)\rangle$ (left) and $\langle \mathrm{PR}(t)\rangle$ (right); while the first increases to the particle in the wings of the density the second reaches a situation in which it is constant in average. This is a signature of self trapping: $\rho_l(t)$ has a bulk that does not spread, and that accounts for the number of significantly occupied sites.
Right panel: Evolution in time of the energies in the case of self trapping. Top data are the kinetic and potential energies, the bottom data is the interaction energy. It stops increasing when self-trapping sets in.

4.4 Interplay between noise and interactions

In 4.2 and 4.3 we had illustrated that a wave packet loaded onto a disordered potential shows different type of spreading depending on the terms that are added to the linear, stationary, Hamiltonian:

- only noise: the expansion is diffusive, i.e. $\sigma(t) \propto D_{noise}\sqrt{t}$, with a diffusion coefficient D_{noise} that is constant and depends onto the both the properties of disorder and noise;
- only interactions: the expansion is subdiffusive, i.e. $\sigma(t) \propto D_{int}(t)\, t^{\alpha}$, with $\alpha < 0.5$ and $D_{int}(t)$ which implicitly depends on time through the width σ, i.e. $D(\sigma(t))$.

In this section we will take into account the interesting situation of both of them present in the system, i.e. we will numerically study the whole (4.39). The presence of both this sources of Anderson localization breaking (we specify that is the Anderson localization that disappears because we have seen that other type of localization, i.e. self-trapping, could exist) lead to different situations, in particular when one considers repulsive or attractive interactions. A summary of various situations is reported in Fig. (4.22), for the case of Anderson model. We can observe that the system still expands with a dynamics that at large times is diffusive, meaning that for $t > t^* \ll t_0$ (t_0 is the activation time in (4.25) the noise dominates over all other processes inducing delocalization, but for $t < t^*$ U and $f(t)$ works together and, depending onto the sign of U, the influences the

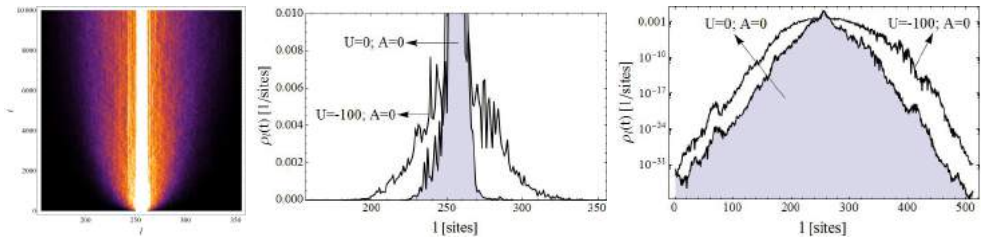

Figure 4.21: **Left panel:** surface plot of $\langle \rho_l(t) \rangle$, averaged over 50 realizations of the disorder. Here the self-trapping is extremely evident: the center of the distribution does not evolve, while its wings spread wilt time passes.
Central and Rigth panel: $\rho_l(t)$ in the case of only disorder and of disorder with $U \ll 0$, as indicated into the plots. Shaded area correspond to the Anderson localized wave packet.

dynamics differently. Very shortly: if $U > 0$ and noise and interactions cooperate and the observed $\sigma(t)$ is always equal or larger than the one observed in the case of noise or interactions alone, depending on their values; if $U \ll 0$ interactions contribute to the appearance of an initial expansion faster than diffusive, and after that the system shows an interesting contemporary presence of both diffusion and self-trapping.

4.4.1 Repulsive interactions and noise: cooperation

In the first two row of both Fig. (4.22) we observe that when noise and interactions are introduced together the expansion in globally faster compared to the case of noise or interactions alone. At final time, $\langle \sigma(t) \rangle$ of the weave packet subject to both U and $A \cdot f(t)$ (blue lines) is equal or larger than the other two cases of noise alone (red lines) and interactions alone (green lines), but with an exponent α of (4.25) that is intermediate between the previous, i.e. $0.25 \leq \alpha \leq 0.5$. This indicates that both the delocalization mechanism are playing a role which depends onto the relative strength of the two.

We have discussed before that the expansion in nonlinear disordered lattices (interactions) and random potential in time (noise) have been studied extensively in theory and experiments in different fields, but up to now we are not aware of any theory for this combined problem. Recently was published a paper regarding it [87] in which some of the results of this work has been reported.

In order to derive a simple model which can give a description for what observed we suppose that the width of the wave packet evolves in time as (4.25) and obeys an equation that takes into account both the mechanism acting onto the system, i.e. noise and interactions. Because of this, we state that the evolution in time of $\sigma^2(t)$ depends onto the linear combination of (4.22) and (4.47):

$$\frac{d\sigma^2(t)}{dt} = D_{noise} + D_{int}(t)\,, \tag{4.49}$$

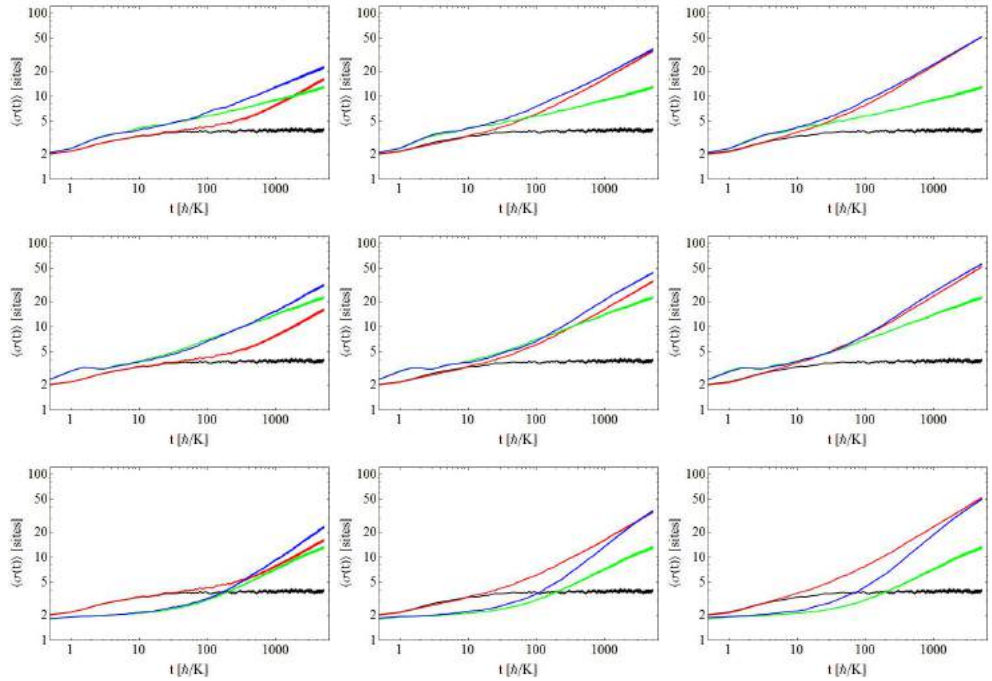

Figure 4.22: $\langle\sigma(t)\rangle$ evolution for different situation of noise and interactions interplay. In each panel we consider the case of only noise (red), only interactions (green) and both of them (blue) present in the Hamiltonian (4.39). Black curve correspond to the case of neither noise nor interactions acting, i.e. Anderson localization set in. From left to right we conisder increasing noise amplitude $A = 0.1$, 0.5 and 0.8, while going from top to bottom we have two cases with repulsive interactions $U = 10$ (first row), $U = 50$ (second row) and one with repulsive interactions $U = -100$ (third row). The static potential V_l is and Anderson disorder with $W = 2.5$; for the noise $f(t)$ we set $T_0 = 4/5$ and $T_d = 0.2$. Data averaged over 50 realizations of disorder.

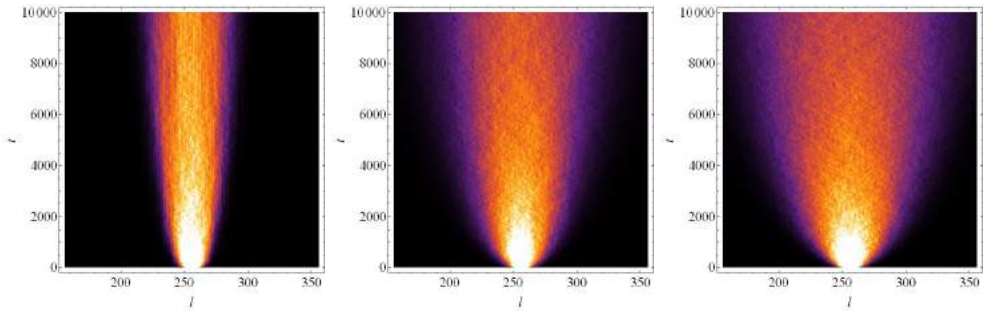

Figure 4.23: Surface plot for the evolution of $\rho_l(t)$, averaged over 50 realizations of $V_l(t)$. From left to right: interactions alone, noise alone and both of them acting simultaneously. For V_l we use a quasi-periodic lattice $\lambda\cos(2\pi\beta l+\phi)$ with $\lambda=2.5$ and $\beta=(\sqrt{5}-1)/2$. Noise parameters are $A=0.5$, $T_d=0.2$, $\omega_0=2\pi\times 5/4$, nonlinear term is $U=+50$.

where we stress that the constant part arises from the noise, while the time dependent part from the interaction. This is again reasonable if compared with the models discussed in 4.2 and 4.3: expansion induced by noise or interactions is driven by two different microscopic mechanism. The first give rise to a constant D_{noise} due to the fact the transition rate between state depends only onto the parameters of the system (noise amplitude and power spectrum, disorder strength which fixes ξ and the energy spectrum), while interactions introduces a $D_{int}(t)$ that depends implicitly on time through the density. This is still true when they are both present, and so we are reasonably confident in using (4.49) to describe the overall process. We have performed a lot of simulations for two types of disorder (Anderson and quasi-periodic) and for a wide range of parameters (in Fig. (4.23) and (4.24) we report the plot of the evolution of $\rho_l(t)$ in two of them) and we find that Eq. (4.49) is valid in most of the cases. Moreover, we have to say that an equation similar to (4.49) has been theoretically predicted in [135] for Brownian motion of classical interacting particle.

In order to verify the goodness of (4.49) we first extract D_{noise} and D_{int} from the respective case of noise and interactions alone by fitting data with (4.25), then results are used to numerically solve (4.49) with the appropriate initial condition (i.e. as σ_0 we use the one extracted from the fit of the case with both noise and interactions with (4.25)). The numerical solution of Eq. (4.49) is actually in good agreement with the experimental data and also with the numerical results coming from the integration of Eq. (4.39). In Fig. (4.25) we show it together with an example over many of the observation done. The examples of the experimental observations and numerical simulations reported in Fig. (4.25) strongly support the hypothesis of additivity of the two delocalization mechanisms, at least at first order. In the experimental data (see left panel of Fig. (4.25)) typically one observes a slightly faster diffusion with noise and interaction. This difference is due to the axial excitation in presence of noise, which in

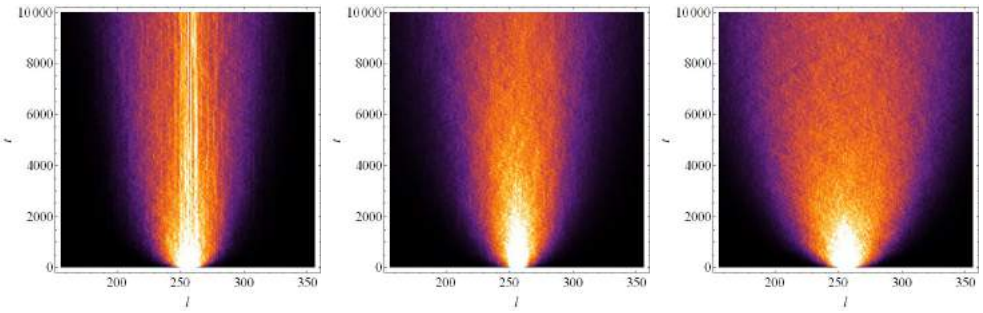

Figure 4.24: Surface plot for the evolution of the density $\rho_l(t)$, averaged over 50 realizations of the random potential $V_l(t)$. From left to right we consider the case of interaction alone, noise alone and both of them acting simultaneously. Underling static disorder is an Anderson lattice characterized by $W = 2$. Noise parameters are $A = 0.5$, $T_d = 0.2$, $\omega_0 = 2\pi \times 5/4$, while for the interaction we set $U = +50$.

turn excites the radial degrees of freedom in presence of interaction [88] and produces the increased expansion shown in Fig. (4.25). On the contrary, in numerical simulations, which neglect the axial-to-radial coupling, there are much smaller deviations from the solution of Eq. (4.49), of the order of a few lattice constants (see right panel of Fig. (4.25)).

The good agreement between the experimental data and the prediction of Eq. (4.49) persists for the whole range of A and E_{int} that are accessible in the experiment, with A ranging from 0.4 to 1 and E_{int} adjustable up to $\approx J$. Furthermore, as we described above in Fig. (4.15), in numerical simulations we can explore the region of large A and/or ξ, where the perturbative description of the noise effect fails. Interestingly enough, although this regime is not perturbative, we find the additivity of noise and interaction mechanisms also in this case. An investigation over a broad range of parameters in theory indicates that the system should behave in a fully symmetric way for attractive and repulsive interaction, provided that also the energy distribution is reversed when changing the sign of the interaction. For example, the diffusion dynamics for a repulsive system initially prepared in a potential minimum is equivalent to the one of an attractive system initially prepared in a potential maximum.

Therefore, the large region of validity of Eq. (4.49) supports the idea that the observed anomalous diffusion is driven by the additivity of the two delocalization mechanisms, which indeed act independently. Note that the interaction-assisted diffusion tends to vanish as the sample expands, so that one should expect a long-time crossover to a regime where interaction effects are negligible, and the system diffuses normally due to noise alone. While we can clearly observe this crossover in the simulations, its experimental characterization is prevented by the limited observation time. Although this, numerical simulations indicate that deviation from this behavior might appear and Eq. (4.49) does not describes the expansion of the wave packet in the proper way. We had

Figure 3 from C D'Errico et al 2013 New J. Phys. 15 045007

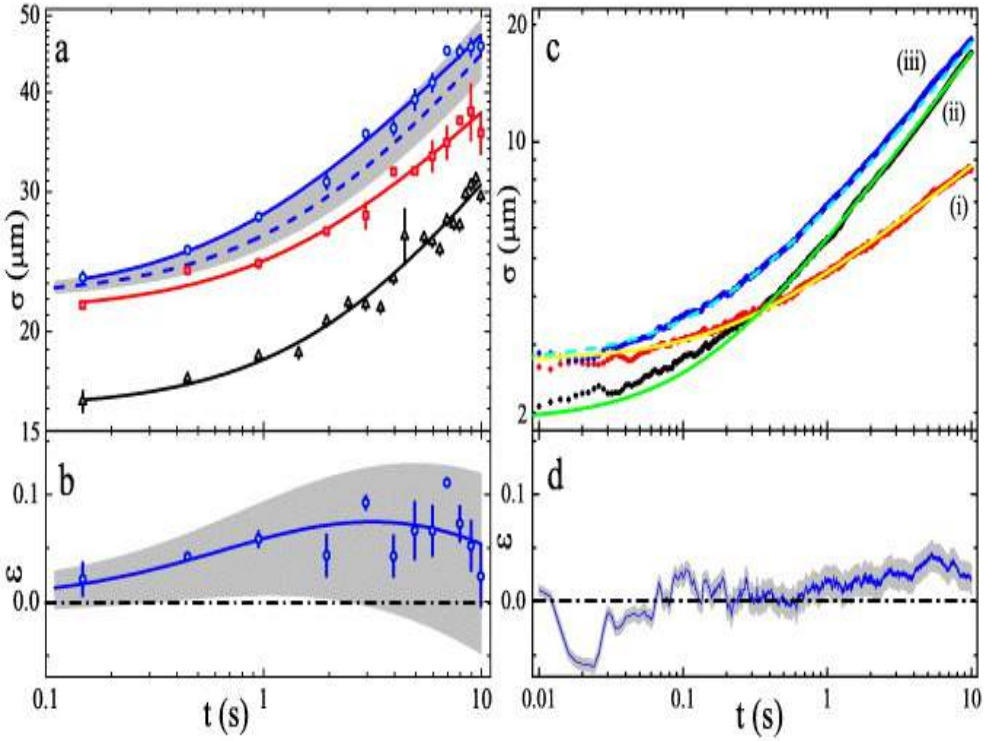

Figure 4.25: **Noise and interaction additive anomalous diffusion.**
a) Measured time evolution of the width for noise alone (triangles), interaction alone (squares), or both (circles), for $\Delta/J = 4$. The noise amplitude is $A = 0.6$, while the interaction strength is $E_{int} \sim 0.8J$. The experimental data are fitted with Eq. (4.25) (solid lines). The dashed line is the numerical solution of Eq. (4.49) using the extracted diffusion coefficients from the fits, with the confidence interval shown as a gray area.
b) Relative residuals of the fit, for the case with noise and interaction, and the solution of Eq. (4.49), with the associated confidence interval (gray area).
c) Numerical simulation of the time evolution of the width for interaction alone (i), noise alone (ii), and both (iii), for $\Delta/J = 2.5$, $J = 180$ Hz, $A = 0.195$, $T = 1$ ms and $E_{int} = 1.6J$. The numerical data are fitted with Eq. (4.25) (solid lines), whereas the dashed line is the numerical solution of Eq. (4.49).
d) Relative residuals of the numerical $\sigma(t)$ with noise and interaction (iii) and the solution of Eq. (4.49). The gray area represents the confidence level of 2 standard deviations.
Figure taken from [87].

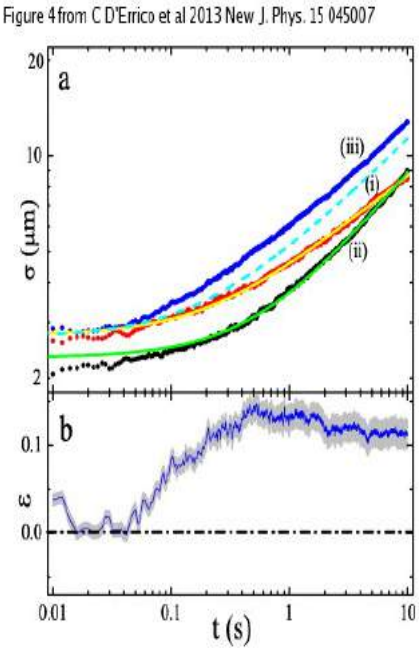

Figure 4.26: Deviations from additivity with a narrowband noise. Numerical simulation of the time evolution of the width (top panel) and relative residuals (bottom panel) with the same parameters of Fig. (4.25), but with $T_d = 10\,\text{ms}$. Deviations from additivity are evident in the discrepancy between the curve with noise and interaction (blu line) and the solution of Eq. (4.49) (dashed line).

observed those deviation into two different situations: a noise with a bandwidth much smaller than the eigengrequencies distribution width, which implies that the parameter η in (4.29) becomes very small, or when interactions are strong enough (both in the repulsive and attractive regime, depending on the initial conditions) to generate trapping mechanism (see 4.4.2). For small η the diffusion is much slower than the case of greater one (see Fig. (4.18)), and we describe this in 4.2 using the idea that narrower $\text{Sp}(\omega)$ can not couple many localized states due to the fact that $\text{Sp}(\omega)$ does not posses the appropriate ω associated to that transition. Very interestingly the addition of interactions seems to restore a fast expansion in this regime, as if the additional coupling mechanism between states due to H_{int} generates an effective broader spectrum $\text{Sp}(\omega)$. An example of this is reported in Fig. (4.26), where we use for $f(t)$ a dephasing time T_d 10 times smaller than the one sued in the simulations reported in Fig. (4.25). One observes a D_{noise} smaller than int the case of broadband noise; interactions are able to restore a diffusion comparable with the one the one obtained in the case of both interactions and broadband noise, therefore much faster than the one predicted by the additive conjecture in Eq. (4.49).

It is important to notice that in this regime the additive hypotesis in Eq. (4.49) fails although the diffusion mechanism is well described by the perturbative model in

4.2. This example together with its complementary case of strong noise which manifests additivity to the interactions, despite the perturbative model is no longer valid, indicates an independence of the hypothesis (4.49) from the validity of the perturbative description given by Eq. (4.36), Eq. (4.37) and Eq. (4.38).

4.4.2 Attractive interactions and noise

The second regime in which (4.49) does not work is the one observes the appearance of self-trapping, as described in 4.3.2, E_{int} is too large to be transformed into kinetic energy during the expansion [55, 132], and the bulk of the system is effectively localized. A couple of examples are shown in Fig. (4.28) and Fig. (4.29), in which self-trapping in achieved by the mean of a strong attractive U onto the initial state (4.18), close to the ground state of the system. Here, we observe an interplay of noise and interaction resulting in a breakdown of the additivity (4.49) and in a transient super-diffusive behavior, i.e. an expansion with $\alpha > 0.5$. In absence of noise, the central part of the distribution, where E_{int} is large, cannot expand, and therefore $\sigma(t)$ increases slower than normal (see 4.3.2 and figures therein). Noise can break this trapping by providing the necessary energy to couple the interaction-shifted states to the lattice band. This causes the fast expansion at short times, which is even faster than normal diffusion. We note that related super-diffusion effects have been predicted in linear systems with varying energy [136]. An analogous effect might arise when the noise is able to release the large kinetic energy associated to the self-trapped part of the system, but further studies are needed to clarify this mechanism.

4.5 Random system with interactions: experimental realization

In all the previous sections we have considered theoretical models and numerical simulations which are linked to a specific Hamiltonian or, equivalently, to a given equation of motion (e.g. (4.39), and we have stressed many times that the possible experimental study of this kind of systems is not simple do to the fact that all the terms involved in Eq. (4.39) are not easy to control, or impossible. Because of this it is hard to build up an experiment that could analyzed both the single effects of noise and interactions, and the combinations of them. This is true when one deals with condensed matter system, in which parameters defining the problem are not totally accessible. A great jump to skip those difficulties was done when ultracold atomic system became realizable. The power of those system is that one can, at least in principle, model an experiment starting from the Hamiltonian due the possibility of controlling and tuning different parameters, as we have already described. With ultracold atoms one can select the confining potential defining the dimensionality of the system, the external potential acting on the atoms

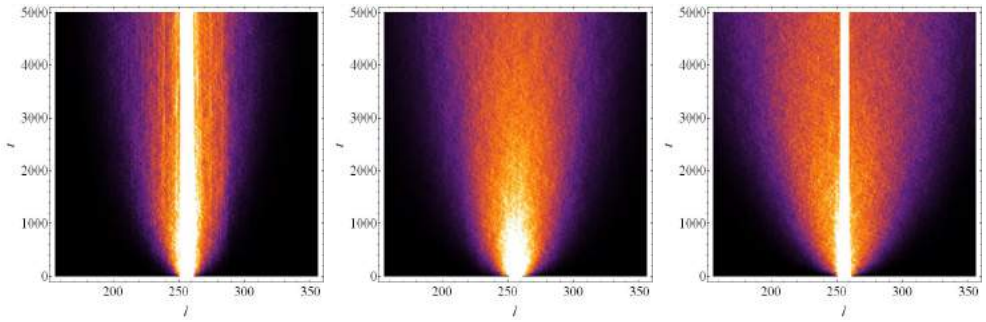

Figure 4.27: Surface plot for the evolution of the density $\rho_l(t)$, averaged over 50 realizations of the random potential $V_l(t)$, in the case of strong attractive interactions.
Left panel: only interactions. Bulk of ρ_l does not move: the self trapping. Tails spreads leading to a subdiffusive regime.
Central panel: only noise. $\rho_l(t)$ expands following Eq. (4.20): $\sigma(t) \propto \sqrt{t}$.
Right panel: noise and interactions. $U < 0$ works to create self-trap atoms in the bulk of $\rho_l(t)$, as in the first panel; noise allows low density tails to expand. Comparing with central panel one observes that, although the width is smaller, the enlargement of the whole distribution is faster.
Parameters for static disorder, noise and interactions are the same as in Fig. (4.28).

and last but not least the interactions among atoms. This peculiarity give to ultracold atoms a role of privilege into the wide world of investigation of quantum world.

In this thesis we will refer to the recent work by the Florence group at LENS [87]. Here we report what they describe in that paper, to which we gave our contribution with numerical simulations and theoretical analysis.

4.5.1 Static disorder

In these experiments the static disorder is created by the mean of a quasi-periodic potential that we know is

$$V(x) = V_1 \sin^2(k_1 x + \theta_1) + V_2 \beta^2 \sin^2(\beta k_1 x + \theta_2)\,.$$

The relevant length scale is given by the period of the main lattice, i.e. $d = \lambda_1/2$, while for energies the two important scales are the tunneling energy J, which typically is of the order of 150Hz, and the disorder strength Δ, proportional to V_2 (see [67, 68] and 1.2.1).

4.5.2 Noise implementation

In the experiment of [87] the frequency noise scheme described in 4.1.2 is used to generate $V_l(t)$. The noise has a sufficiently broad spectrum in order to couple as many state as possible within the lattice bandwidth $\mathcal{W}/h \approx (2\Delta + 4J)/\hbar$), but with the prescription that excitations of radial modes (see 2.3) and transition to the first

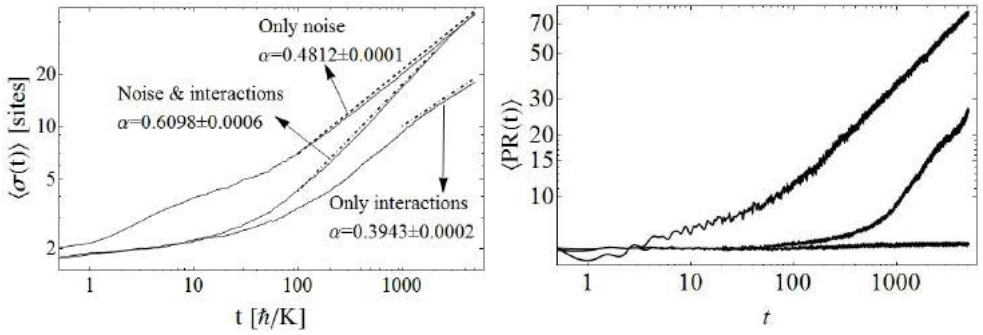

Figure 4.28: $\langle\sigma(t)\rangle$ and $\langle \mathrm{PR}(t)\rangle$ (averaged over 50 realizations of disorder) in the case of both attractive interactions $U = -100$ and noise ($T_0 = 4/5$, $T_d = 0.2$, $A = 0.5$). Underling static disorder is an Anderson potential with $W = 2$.
Left panel: $\langle\sigma(t)\rangle$. Dashed lines correspond to fit with (4.25). Only noise (top curve) and only interactions (bottom curve) gives diffusive and sub-diffusive expansion, respectively. Middle curve: combined action of $U < 0$ and $f(t)$ lead to an expansion with an exponent $\alpha > 0.5$, i.e. faster than diffusive. At the end of which $\sigma(t)$ again goes diffusively.
Right panel: $\langle \mathrm{PR}(t)\rangle$. For only interactions (bottom curve) self-trapping is evident. For only noise (top curve) $\mathrm{PR}(t)$ grows. Noise and interactions together: initially interactions are so strong that dominate, $\mathrm{PR}(t)$ lies onto the curve of the only interactions case, then $\rho_l(t)$ starts to spreads and populates more sites.

excited band of the lattice will be avoided; the frequencies associated to those process are $\omega_r = 2\pi \times 50\,\mathrm{Hz}$ for the radial modes and $\Delta E_{gap}/h \approx 3 - 5\,\mathrm{KHz}$ for the first band state excitation.

Typical values for the parameter in $f(t)$ are $\omega_0/2\pi = 250\,\mathrm{Hz}$, $\Delta\omega_0/2\pi = 50\,\mathrm{Hz}$ and $T_d \sim 5\,\mathrm{ms}$. This choice result in a spectrum that for $t \gg T_d$ decays exponentially outside the band $[\omega_0 - \Delta\omega_0, \omega_0 + \Delta\omega_0]$, on a frequency scale $\approx 1/T_d$, as shown in Fig. (4.9). We recall (see 4.1.2) that this kind of noise is easier to realize and introduces less disturbance in the system due to the fact that at each change of frequency also phase varies in order to keep $f(t)$ continuous. Moreover we have shown in 4.1.2 that for $t \approx T_d$ $\mathrm{Sp}(\omega)$ contains only few frequencies around ω_0, this might results in an inefficient coupling between states, as the parameter η assumes very small values, in order to provide diffusion [87, 137]. This aspect which is clearly visible numerically it is not observed in the experiment, a possible explanation is that in experiments the relative phase between the two lattices is not completely fixed, but it changes in time due to external factor such as mirror vibrations, this introduces into the system a small, but not negligible phase noise which leads to a small expansion also in the absence of controlled noise. Numerical simulations performed with a phase noise with small A and $2\pi/T_d \approx 440\,\mathrm{Hz}$ (assuming this as a typical frequency for mechanical vibration) are in accordance with the measured increasing of $\sigma(t)$ of the order of 1μm of an experiment

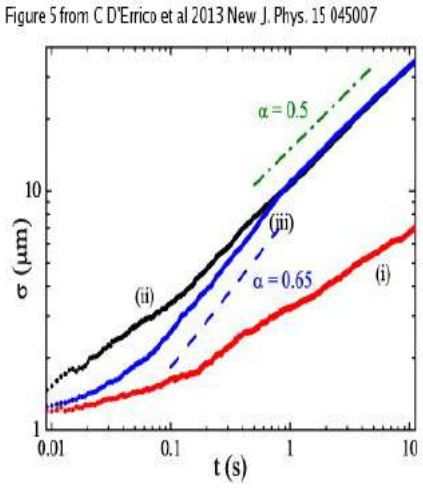

Figure 4.29: Numerical simulations for $\langle\sigma(t)\rangle$ for attractive interaction alone (red curve), noise alone (black curve) or both (blue curve) in the case of an underlying quasi-periodic potential with $\Delta/J = 2.5$, $J = 180\,\text{Hz}$, $A = 0.4$, $U = -35$ and $T_d = 0.6\,\text{ms}$. As in Fig. (4.28) an intermediate super-diffusive ($\alpha > 0.5$) seems to be induced by self-trapping, while asymptotically one recovers normal diffusion with exponent $\alpha \sim 0.5$. Dashed and dot-dashed lines shows the the diffusive and super-diffusive slope, respectively. Figure taken from [87].

in which $A = 0$.

4.5.3 Interaction energy

Regarding the interactions, they are tuned by changing the scattering length a_s by the mean of a Fano-Feshbach resonance, and they obtain values within $0.1a_0$ and $300a_0$ [138]. The mean interaction energy per atom is defined as

$$E_{int} = \frac{2\pi\hbar a_s}{m}\bar{n}\,,$$

where $\bar{n}$ is the mean on-site density. This quantity can be related to the nonlinear parameter in (4.39) approximatively by

$$E_{int} \approx \frac{2JU}{\bar{n}_s}\,,$$

where $\bar{n}_s$ stand for the mean number of sites occupied by the atomic distribution [55, 68, 87].

In order to create quasi 1D samples atoms are trapped by a radial frequency of $\omega_r = 2\pi \times 50\,\text{Hz}$. This radial degree of freedom limits the possible range for E_{int} to value not much larger than J or Δ.

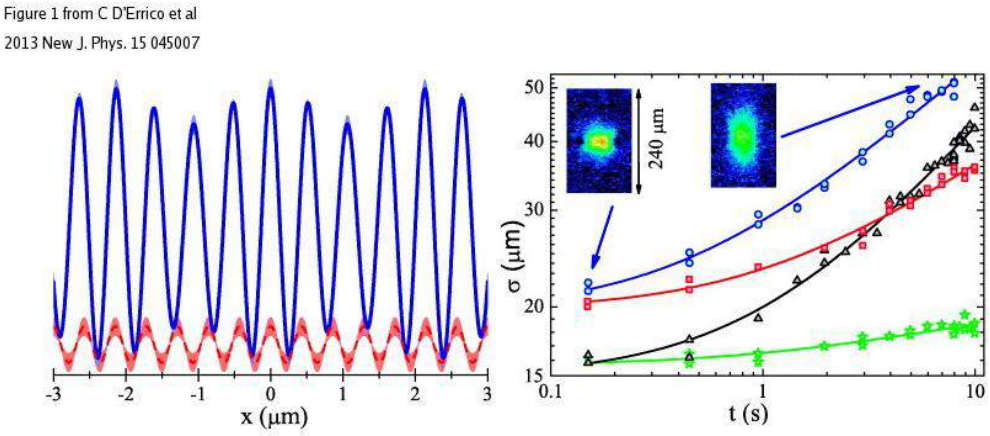

Figure 4.30: **Left panel:** noisy quasi-periodic potential (blue line), realized by a static main optical lattice overlapped with a secondary one (red line) with a broadband amplitude modulation.
Right panel: measured $\sigma(t)$ for different values of noise amplitude and interaction energy: $A = 0$ and $E_{int} \sim 0$ (stars), $A = 0.9$ and $E_{int} \sim 0$ (triangles), $A = 0$ and $E_{int} \sim 0.8J$ (squares) and $A = 0.8$ and $E_{int} \sim 0.8J$ (circles). Solid lines correspond to fit of data with (4.25). The quasi-periodic potential ha $\Delta/J = 4$.
Figure taken from [87].

4.6 Summary and outlook

An effective overview of the extensive investigation done can be achieved by looking to the partecipation number PR(t) (4.17) for varying A, E_{int} (U) and Sp(ω) in numerical simulations. The specific diagram in Fig. (4.31), which shows the calculated PR(t) at $t = 10\,\mathrm{s}$, for the expansion of a particular Gaussian initial distribution (4.18), can be used to summarize general properties investigated with our system.

For a broadband noise (width of Sp(ω) comparable to the bandwidth of the underlying disordered potential, see left panel in Fig. (4.31)), one finds again that Anderson localization is suppressed by either noise or interaction, with both leading to an expansion of the system. We remark that the underlaying mechanisms for these two expansions are quite different: weak interaction produces a coherent coupling of single-particle localized states; the resulting transport can be modeled as a coherent hopping between such states, with a characteristic sub-diffusive behavior that is determined by the changing density (see 4.3). Noise instead drives an incoherent hopping between localized states, which result in a diffusive expansion (see 4.2). Once both transport mechanisms are combined, one sees an enhanced expansion, as highlighted by the increasing width in the left panel of Fig. (4.31) for finite A and E_{int}. Our detailed time-dependent analysis indicates that this combined diffusion is well modeled by the generalized, additive diffusion model of Eq. (4.49). This surprisingly simple results seems not to be limited to the

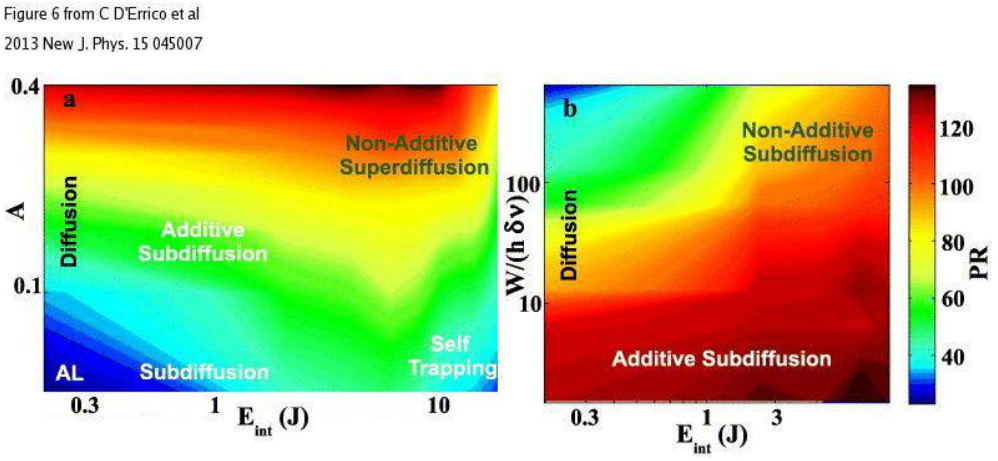

Figure 4.31: Generalized diffusion regimes. The color scale represents the number of significantly occupied sites after 10 sec of our numerically simulated expansion, for $\Delta = 2.5J$, $J = 180$ Hz and a Gaussian wave packet initially distributed over ≈ 13 lattice sites.
Left panel: dependence on A and E_{int} for a broadband noise ($T_d \approx h/\mathcal{W}$).
Right panel: dependence on E_{int} and $\delta\nu$ (i.e. the width of $\mathrm{Sp}(\omega/2\pi)$), for a fixed noise strength $A = 0.4$.
Figure taken from [87].

region of parameters where the noise- or interaction-induced diffusions can be modeled by perturbative approaches.

Numerical simulations reveal also a region of stronger interaction, where the interaction itself prevents expansion, because of the self trapping-mechanism. This is visible as a reduction of the $\mathrm{PR}(t)$ for increasing E_{int} (U) in Fig. (4.31). Here, the addition of noise restores a diffusion, which our time-dependent analysis has shown to have an anomalous super-diffusive nature. In this regime, the model of Eq. (4.49) clearly breaks down.

Finally, an interplay of noise and interaction is seen also in presence of narrowband noise, as shown in right panel of Fig. (4.31): here expansion is studied for different η (defined in Eq. (4.29)), and E_{int}, for a fixed value of the noise strength (i.e. $A = 0.4$). In the non interacting regime, the diffusion constant decreases for increasing η. The addition of the interaction recovers a faster expansion, which however cannot be described by Eq. (4.49). In this chapter we have studied the transport of a wave-packet in presence of controllable disorder, noise (see 4.1), and interaction. Most of the work has been done numerically, and from the result we get we build up a model that explains what one observes in some interesting situations. One of the possible realizations for the model studied has been realized by an ultracold atomic system (see 4.5) [87]. Most of the results reported in [87] are reported here, because the numerical simulations used in that paper are one of the main subject of this work.

We have characterized the noise induced diffusion and its interplay with an interaction induced subdiffusion by studying the evolution of the wave packet width $\sigma(t)$, supposing that it is described by Eq. (4.25). We have observed that the complex anomalous diffusion resulting by the simultaneous presence of the two processes, can be remarkably explained by a simple generalized diffusion equation (4.49) in a wide range of parameters. Finally, we have numerically observed also regimes where the presence of trapping phenomena produce a more complex interplay between the noise and interaction induced diffusion mechanisms (see 4.4.2). It is interesting to note that a quasi-periodic lattice might allow to study also a different regime that has been extensively analyzed in theory [29, 139, 140], in which in absence of noise all the eigenstates are extended, while the noisy potential is disordered. This regime can be achieved simply by using a weaker disorder, below the localization threshold, $\lambda < 2$. Preliminary numerical simulations we have performed show that in this case the noise slows the dynamics from ballistic to diffusive, which are in perfect accordance with the recent results published in [46].

In 4.5 we recall [87], and show how the combination of an ultracold atomic system with optical lattices can be effectively employed to study quantum phenomena related to noise. In the future study of lattice systems with higher dimensionality or in reduced dimensions will allow to explore the regime of strong correlations, and again in this case one can face the problem from a theoretical point of view but also the numerics could eventually be supported by experiments. Here there is a strong interest in understanding the behavior of open quantum systems [141], and how quantum phase transitions are affected by noise [142]. An interesting alternative to the use of a noisy optical potential is to employ a large sample of a second atomic species with a controllable thermal distribution, which is coupled via resonant elastic scattering to the atomic system under study. This approach might allow to introduce a noise in thermal equilibrium, and to simulate phonon-related phenomena [26, 143, 144].

Furthermore, an experiment like the one in [87] could be easily used to control the temperature of our weakly interacting bosons in presence of disorder, to investigate the many-body metal-insulator transitions at finite temperatures [145], and in this direction could also be interesting to perform a systematic theoretical investigation.

5

Disorder and localization with two interacting condensates

5.1 Basic Ideas

In this chapter we describe how Anderson localization could be obtained in a system made by two interacting condensates.

We find a seminal idea in a paper by Gavish and Castin [146] in which authors propose to cerate a Bose-Einstein condensate loaded into an optical lattice in such a way that only some randomly chosen sites will be populated with a large number of atoms. Then a second condensate is loaded onto this array of randomly distributed delta peaks which clearly is a realization of a disordered potential. Because atoms creating the disorder are frozen, i.e. once they occupy the sites they will not move any more, we are in the presence of a static disorder. We follow this idea of using two condensate one of which has a non uniform spatial distribution that act onto the second as a disordered potential but, instead of the method suggested in [146], we want the disorder potential to be generated by the condensate itself without any external trapping.

This is possible because in an optical lattice, under some conditions which are theoretically well-known [117, 147–149, 149–152] and experimentally verified [153, 154], an uniform distributed interacting condensate (described as a plane wave of well defined momentum) when slightly perturbed starts to evolve in time creating fluctuations and breaking its flat density: this is known as modulation-instability phenomenon and it arises from the interplay between the lattice and the interactions among atoms [117].

First we consider just one BEC and study the properties of the disorder it generates, in particular the dependence onto the ratio between the self-interaction strength and the tunneling rate which turns out to be the only important parameter of this problem. Then we take into account the second condensate, interacting with the first but not with itself, and study Anderson localization.

5.2 Model

the system is well described by two coupled discrete nonlinear Schrödinger equations:

$$\begin{aligned} i\hbar\dot{\psi}_l^D(t) &= -K_D\left(\psi_{l-1}^D(t)+\psi_{l+1}^D(t)\right)+\left[U_{DD}|\psi_l^D(t)|^2+\Lambda|\psi_l^L(t)|^2\right]\psi_l^D(t) \\ i\hbar\dot{\psi}_l^L(t) &= -K_L\left(\psi_{l-1}^L(t)+\psi_{l+1}^L(t)\right)+\Lambda|\psi_l^D(t)|^2\psi_l^L(t)\,, \end{aligned} \tag{5.1}$$

here we use dimensional units. Note that the coupling between ψ^D and ψ^L has a mean filed form analogous to the single specie term in the Gross-Pitaevskii equation. In (5.1) D, L stand for *disordered* and *localized*, respectively, meaning that the first equation describes the condensate which is dynamically unstable and which will be considered as the disorder, while the second equation describes the condensate that could Anderson localize because of the presence of the other. We set the self-interaction term of the second (L) species to zero because we want it just to feel the presence of the first one, which acts like an external potential by the mean of $\Lambda|\psi_l^D(t)|^2$.

Problem is thus characterized by four explicit parameters:

- Tunneling rates: $K_{D,L}$;
- Self interaction strength: U_{DD};
- Interspecies interaction strength: Λ;

moreover we have to take into account he total number of particles for each condensate or, more correctly, the *filling factor* which is defined as the ratio between the total number of particle $N_{D,L}=\sum_{l=1,M}|\psi_l^{D,L}(t)|^2$ and the number of lattice sites M: $\bar{\rho}^{D,L}=N_{D,L}/M$.

It is possible to perform a rescaling of those equations by defining two new wave function as $\psi_l^{D,L}=\sqrt{N_{D,L}}\phi_l^{D,L}$, in such a way that $\sum_{l=1}^{M}|\phi_l^{D,L}|^2=1$. Moreover it will be useful to measure time in units of $\hbar/K_L$, and the reason it will be explained in the following. Defining the new parameters

$$g=\frac{U_{DD}N_D}{K_L};\quad \alpha=\frac{K_D}{K_L};\quad \eta=\sqrt{\frac{N_L}{N_D}};\quad \lambda=\frac{\Lambda\sqrt{N_DN_L}}{K_L}\,, \tag{5.2}$$

we get

$$\begin{aligned} i\dot{\phi}_l^D(t) &= -\alpha\left(\phi_{l-1}^D(t)+\phi_{l-1}^D(t)\right)+g|\phi_l^D(t)|^2\phi_l^D(t)+\lambda\eta|\phi_l^L(t)|^2\phi_l^D(t)\,, \\ i\dot{\phi}_l^L(t) &= -\left(\phi_{l-1}^L(t)+\phi_{l-1}^L(t)\right)+\frac{\lambda}{\eta}|\phi_l^D(t)|^2\phi_l^L(t)\,. \end{aligned} \tag{5.3}$$

Equations (5.3) could be useful becouse they contains constants that depend explicitly on the parameters of the problem, such as the number of atoms.

5.3 Disorder creation and characterization

Now we will consider the evolution of a single interacting condensate in a lattice, the dynamics of which is driven by the DNLS in Eq. (2.34), in order to look to the density profile $\rho_l(t) = |\phi_l(t)|^2$ and study some of its statistical properties in particular the probability distribution function and the autocorrelations function. As in Chap. 4 we are dealing with

$$i\dot{\phi}_l(t) = -\left(\phi_{l-1}(t) + \phi_{l+1}(t)\right) + g|\phi_l(t)|^2\phi_l(t)\,, \tag{5.4}$$

where the field $\phi_l(t)$ is normalized to 1, and is g defined in (5.2).

5.3.1 Dynamical instability of DNLS

Starting from Eq. (5.4) we will show how from a uniform density a disordered one can be obtained. The method is extremely simple and it lies onto the interplay between lattice, which introduce not only discretization of space but also fundamental changes in the dispersion law of free particle (i.e. band structure), and nonlinearity coming from interactions among particles. This means that, in order to create a disordered density, we have just to take a uniform ditribution, slightly perturb it, and than let it evolves following Eq. (5.4).

Stationary Solution

First we recall that Eq. (5.4) has stationary solutions that are plane waves:

$$\phi_l(t) = \phi_0 \exp\left[i(pl - \nu t)\right]\,; \tag{5.5}$$

each corresponding to an energy[1]

$$\omega = -2\cos(p) + \frac{g}{M}\,, \tag{5.6}$$

where we use the fact that $\sum_{l=1}^{M} |\phi_l|^2 = 1$ ends up in $\phi_0 = \sqrt{1/M}$, and $g = UN/K$. Eq. (5.5) readily gives the on-site density $\rho_l(t) \equiv |\phi_l(t)|^2 = 1/M$, which is uniform in space and constant in time: the condensate will remain uniformly distributed over all the lattice.

Stability Analysis

Once we have stationary solutions of Eq. (5.5) we want to investigate if they are stable or not under the influence of small perturbations. This is a widely studied problem,

[1] Because we are using dimensionless equations, energy and frequencies are equivalent.

both in free space and in the presence of a lattice, by the mean of stability analysis method in combination with the Bogoliubov theory of condensate (see for example [103, 104, 147–150, 155]); here we briefly report results presented in [149]. First we need to introduce the Bogoliubov formalism

$$\phi_l(t) = (\phi_0 + \delta\phi_l)\ e^{i(pl-\nu t)} \equiv \left(\phi_0 + u_l(t)e^{iql} + v_l(t)^* e^{-iql}\right)\ e^{i(pl-\nu t)}\,, \tag{5.7}$$

with q being the perturbation's momentum, notice that here only a single q is considered. Putting together Eq. (5.7) and Eq. (5.4) we get, at first order in u/ψ_0, a matrix equation for the time-derivative of the perturbation modes u and v:

$$i\frac{d}{dt}\begin{pmatrix} u \\ v \end{pmatrix} = \begin{pmatrix} a & c \\ -c^* & a-b \end{pmatrix}\begin{pmatrix} u \\ v \end{pmatrix} = \omega\begin{pmatrix} u \\ v \end{pmatrix}\,, \tag{5.8}$$

with $a = 2\sin p \sin q$, $b = 2\cos p - 2\cos p\cos q$ and $c = g$. Eigenvalues $\omega_\pm$ of Eq. (5.8) form the excitation spectrum of the condensate. The secular equation associated to Eq. (5.8) is

$$\omega^2 - 2a\omega + a^2 - b^2 + c^2 = 0\,,$$

which has two solutions: $\omega_\pm = a \pm \sqrt{b^2 - c^2}$. Using the extended form for a b and c we obtain

$$\omega_\pm = 2\sin p \sin q \pm 2\left|\sin\frac{q}{2}\right|\sqrt{2\cos p\left(2\cos p\sin^2\frac{q}{2} + \frac{g}{M}\right)}\,. \tag{5.9}$$

When $\omega_\pm$ are complex the wave function become *dinamically*, or *modulationally*, *unstable*. This because

$$u_l(t) \propto \exp(i\omega t) = \exp(i\Re(\omega_\pm)t)\exp(-\Im(\omega_\pm)t)\,,$$

then, if $\Im(\omega_\pm) < 0$, amplitude of u_l exponentially grows in time.

In order to observe those instabilities we need the expression under the square root to be negative, and finding the set of parameters for which this happens is quite complicated because they are a lot. As first simplification **from now on we will only consider** $U > 0$, i.e. $g > 0$, meaning that we will work only with system composed by particles with **repulsive interactions**. With this assumptions we have that waves in Eq. (5.7) will be unstable only for $\cos p < 0$, which means $-\pi < p < -\pi/2$ and $\pi/2 < p < \pi$, and this can be demonstrated by simple arguments:

- $\cos p < 0$ implies $-2|\cos p|\sin^2(q/2) + g/M > 0$. This, solved for q, could have solutions, at least in principle;
- $\cos p > 0$ suggests $\sin^2(q/2) < -(g/2M\cos p)$. This has no solution because the r.h.s is always negative, due the fact that we impose $g > 0$.

From the first condition we can determine a value for g above which all q are unstable.

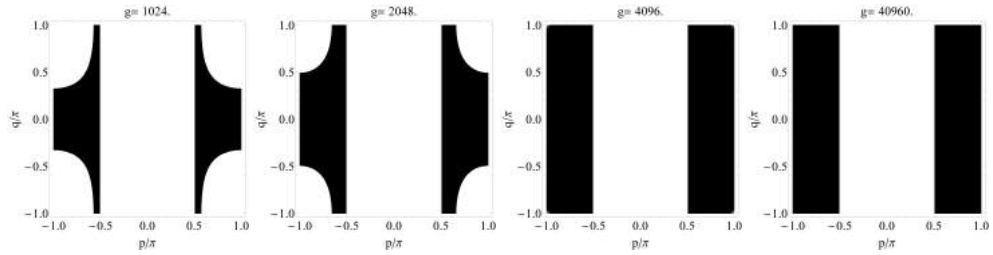

Figure 5.1: Surface plot of Sgn $\left[2\cos p\left(2\cos p\sin^2\frac{q}{2}+\frac{g}{M}\right)\right]$ as function of (p,q) for different values of g (indicated on the graphs) and a lattice of $M=2^{11}$ sites. Black regions correspond to negative values of the function, white region to positive. As determined in the text negative values, and then instability, are confined in interval $-\pi<p<-\pi/2$ and $\pi/2<p<\pi$. It is important to notice that for $g\geq 2M$, i.e. $g\geq 2^{12}$, all q's are unstable while for $g<2M$ some white region (i.e. stable q) are still present.

Looking at the previous results we have that for $\cos p<0$ instabilities appear when $\sin^2(q/2)<g/2M|\cos p|$. Because $\sin x$ is limited the inequality is alway satisfied for $g/2M|\cos p|>1$ so, because $|\cos x|\leq 1$, we obtain that

if $g>2M$ any perturbation we put on the large amplitude wave of momentum $-\pi<p<-\pi/2$ or $\pi/2<p<\pi$ is unstable.

Perturbing stationary solutions

We have just shown that amplitude of unstable modes exponentially grows in time, so in order to create a disordered density profile we need to perturb an initial wave function with the largest possible number of unstable modes. We try with two different methods: one consists in perturbing the momentum distribution, the other in disturbing directly the density. We find that both of them leads to disordered profiles that have the same properties, but for completeness we give a short description of both of them.

We start by creating the unperturbed carrying wave: $\phi_l=\sqrt{1/M}\exp(ip_0 l)$ with $p_0=2\pi l/M$, l being an integer. The latter definitions comes from our choice of using periodic boundary condition, $\phi_1=\phi_{M+1}$ and $\phi_0=\phi_M$. The Fourier transform of this wave is $\tilde{\phi}_p=\delta_{pp_0}$. Numerically, we first create $\tilde{\phi}_p(0)$, then we have two possibilities:

- Perturbing function in momentum space by adding a random background:

$$\tilde{\phi}_p(0)=\delta_{pp_0}+\epsilon\Delta[-\pi;\pi]\,,$$

  where $\epsilon\ll 1$ and $\Delta[a;b]$ is a random number between a and b, picked up from an uniform distribution. $\phi_l(t=0)$ is then obtained by applying a Fourier anti-transformation: $\phi_l(0)=\mathcal{F}^{-1}[\tilde{\phi}_p(0)]$.

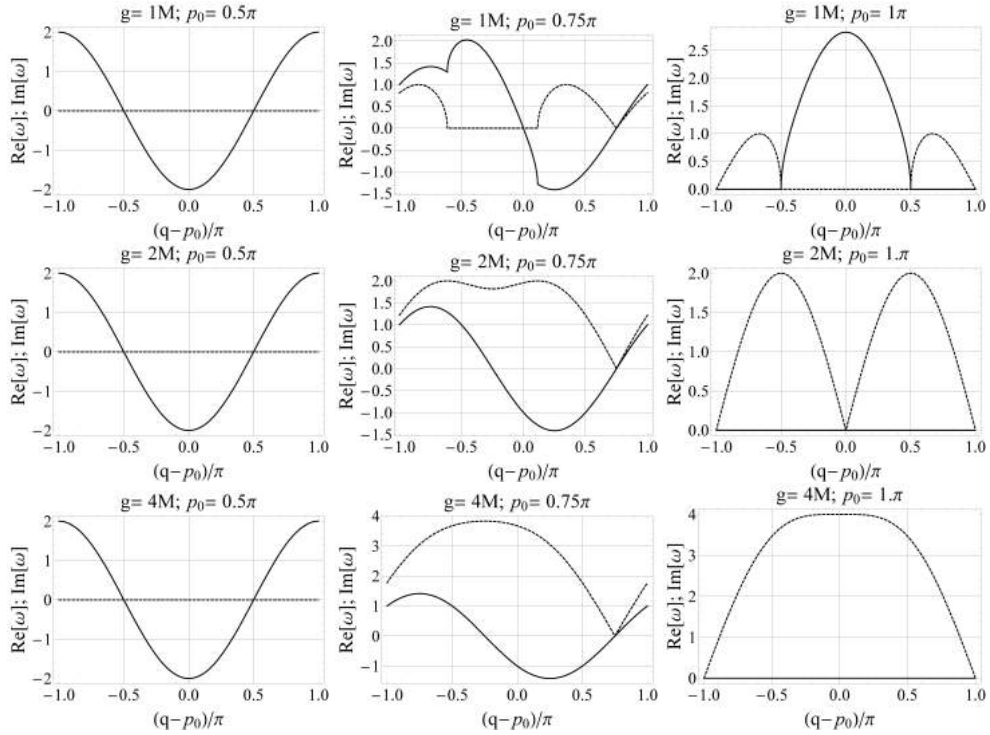

Figure 5.2: $\Re(\omega)$ (solid line) and $\Im(\omega)$ (dashed line) as function of $q - p_0$ for different nonlinearities g and carrying wave momenta p_0 and fixed $M = 2^{11}$. It is evident that the imaginary part becomes nonzero for $p_0 > \pi/2$ and its value, as well as the one of the real part, depends on g. Meaning that in order to have dynamical instabilities we need to set $p_0 > \pi/2$ but which of perturbation modes are unstable depend on the nonlinearity.

- Perturbing function in real space. The idea is to write down initial function as $\phi_l(0) + \delta\phi_l$ in order to obtain small perturbation on the density: $\rho_l(0) + \delta\rho_l \equiv \rho_l(0) + \epsilon_l\rho_l(0)$ with $\epsilon_l = \epsilon\Delta[-1;1]$ as before. Taking the modulus square of the perturbed function, $|\phi_l(0) + \delta\phi_l|^2$, and equating it to the perturbed density $\rho_l(0) + \delta\rho_l$, up to first order in $\delta\phi_l$ we get $\delta\rho_l = \delta\phi_l^*\phi_l + \delta\phi_l\phi_l^*$.

At the end we normalize $\phi_l(0) + \delta\phi_l(0)$ to 1. After various simulations we choose to perturb the density, because we have seen that acting directly on $\tilde{\phi}_p(0)$, if ϵ is not small enough, could lead to a density which is not close to a uniform value already at $t = 0$. On the other hand, using the second method we anyway obtain a momentum distribution peaked on p_0 with a small background but $\rho_l(0)$ is as close as we want to the constant value $1/M$. $\phi_l(0)$ is then used as initial condition to solve Eq. (5.4).

Short-time dynamics: Bogoliubov theory

Once the regions of stability of the perturbation have been found, we numerically integrate Eq. (5.4) and check if the scheme of previous section works well. First we put our attention on short-time scale, at which the Bogoliubov perturbation method should work properly. In Fig. (5.3) we report our results: there we compare the momentum distribution, defined as the squared modulus of the Fourier transform of the wave function, at some short time (in units of $\hbar/K$) with the imaginary part of ω in Eq. (5.9). Because $\{u(t), v(t)\} \propto \exp(\Im(\omega)t)$, $\omega \equiv 1/\tau_0$ defines a timescale τ_0 at which the perturbation of (quasi)momentum q has significantly increased its amplitude and so the greater $\Im(\omega)$ the shorter the time at which that perturbation could play a relevant role. Of course this two quantities could not be compared directly, but $\Im(\omega)$ gives a clear guide to the eye that shows us which result we have to expect.

First we fix the carrying wave momentum $p_0 = \pi$, and $N = 100M$ in order to be in the regime where DNLS well describes a condensate, then we consider values of g below and above the threshold, results for two of them are presented in Fig. (5.3). As expected, apart from the highest peak at $p/\pi = 1$ which correspond to the unperturbed wave, the momentum distribution follows the prediction of Bogoliubov. For $g < 2M$ we could see a region where perturbation do not increase their amplitude while for $g > 2M$ all q are unstable, it is also evident the local maxima of $\tilde{\phi}_p$ correspond to the maxima of $\Im(\omega)$, i.e. to the fastest increasing perturbation.

5.3.2 Disordered density profiles

Although the short time dynamics could be interesting by itself, we want to study the behavior of the condensate at time much larger than the one at which Bogoliubov theory still works. This is motivated by the fact that we have to wait a certain amount of time in order to let the perturbations grow and brake the uniform density. Very naively

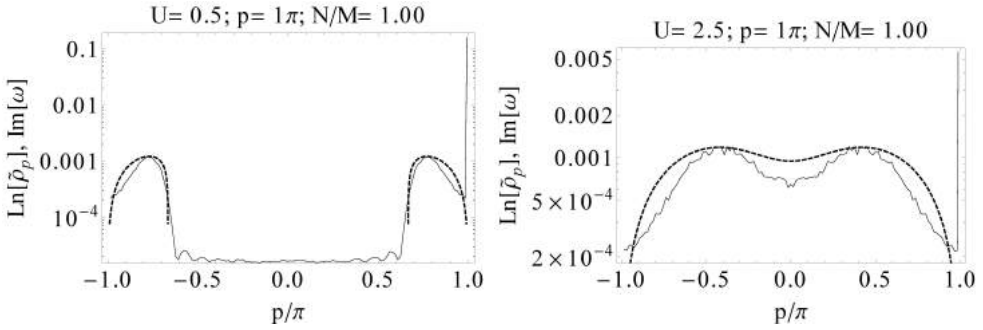

Figure 5.3: Momentum distribution (in logarithmic scale) after a short time interval for two different values of U: 0.5 on the left panel, and 2.5 on the right. Black dashed line are the imaginary part of the Bogoliubov frequencies, $\Im(\omega)$. Here they are just guide to the eye, but the fact that shape of $\tilde{\rho}_p$ recalls $\Im(\omega)$ confirms the population of single momenta evolves following Bogolibuov prediction.

we could imagine that if we wait for a sufficient long time all the momentum component start to being populate, without following Boboliugobv prescription, and we loose the initial uniform density profile $|\phi_l(0)|^2 = 1/M$; at this stage we are dealing with a new density that is, somehow, disordered. In order to confirm or not our idea we have to perform a statistical analysis over a certain amount of profiles. Our studies has been done by considering a large set of different parameters, in particular we try with different p_0 and g. We numerically integrate Eq. (5.4) by a standard 4^{th} order Runge-Kutta method, and look to three quantities, two more linked to the definition of a disorder,

- Probability Distribution Function (PDF) $\mathcal{P}[\rho_l(t)]$ (where $\rho_l(t) = |\phi(t)|^2$),
- Correlation function $g_i^{(1)}(t) = \sum_{l=1}^{M} \rho_l(t)\rho_{l+1}(t)$,

and the third one that could tell us something interesting on the physics of the system

- $\tilde{\rho}_p(t) = |\mathcal{F}[\phi_l(t)]|^2$.

To obtain a significant number of densities we consider different realizations of initial condition $\psi_l(0)$, which differ one from the other because of the random choice of the background perturbation.

By analyzing our data we observe an interesting feature of this system: a crossover between two different type of disorder. The first one is characterized by a PDF with Gaussian shape and $\tilde{\rho}_p(t)$ is nicely fitted Gaussian centered around $p = 0$, the second has a PDF which shows an exponential decay at small ρ together with small populated region of higher ρ, moreover its the momentum distribution has two maxima in $p = \pm\pi$ and a minimum at $p = 0$. This feature seems quite peculiar and we want to study it with a little bit more attention by performing a series of simulations for various sets of parameters (p_0, g), in order to characterize the crossover. We initially do not find a clear

way to explain this, also because we find that the crossover depends on both p_0 and g, but then we find in literature something very interesting concerning *system with negative temperature*.

Are we dealing with negative temperature?

Our attention were captured by the shape of the momentum distribution, which changes from a Gaussian centered around 0 to a shape with two peaks at $\pm\pi$. This behavior recall us a recent paper by Bloch [156] where the authors built up a very fascinating experiment to create a system that shows negative absolute temperature for some of its degrees of freedom. We than find some other articles in literature, in particular [157–159], where the idea of negative temperature where presented and [160] in which authors study a system directly linkable with the one presented here.

The main idea is that *a system which energy spectrum is bounded from above has states with negative temperature*, and one of the first example was an ensemble of nuclear spin [157]. It is evident that, because of the lattice, our system is energetically bounded, moreover we are working in tight-binding approximation, which enforce this fact considering just the first Bloch band. As we showd in Chap. 2 Eq. (5.4) is derived from the Hamiltonian

$$\mathcal{H} = -\sum_{l=1}^{M}(\phi_l\phi_{l+1}^* + c.c.) + \frac{g}{2}\sum_{l=1}^{M}|\phi_l|^4\,; \tag{5.10}$$

inserting in it a stationary solution $\phi_l = \sqrt{1/M}\exp[i(p_0 l - \nu t)]$ we get the energy density, i.e. energy per site,

$$h \equiv \frac{\mathcal{H}}{M} = -\frac{2}{M}\cos p_0 + \frac{g}{2M^2}\,. \tag{5.11}$$

In [159] the author find a combination of parameters which defines a threshold for the transition from $T > 0$ to $T < 0$, this threshold is written in terms of energy density and it is $h_c = g/M^2$. So we have that

if $h < h_c$ system has $T > 0$ while for higher energy, $h > h_c$, system has $T < 0$;

transition point is defined by $h = h_c$ which, in our case, becomes

$$\cos p_0 = -\frac{g}{4M}\,. \tag{5.12}$$

In [160] authors shows also that at negative temperature system shows peculiar dynamical structure called breathers, which are very high density peak with a very long life-time, that is exactly the situation which we find and is also described in [159]. In situations where $h > h_c$ the PDF $\mathcal{P}(\rho_l)$ (which in [159] is called $p(a)$) has apparently an exponential decaying shape meaning that there are some few sites occupied with a large number of particles, while most of the sites are populated by a small amount of them; in that

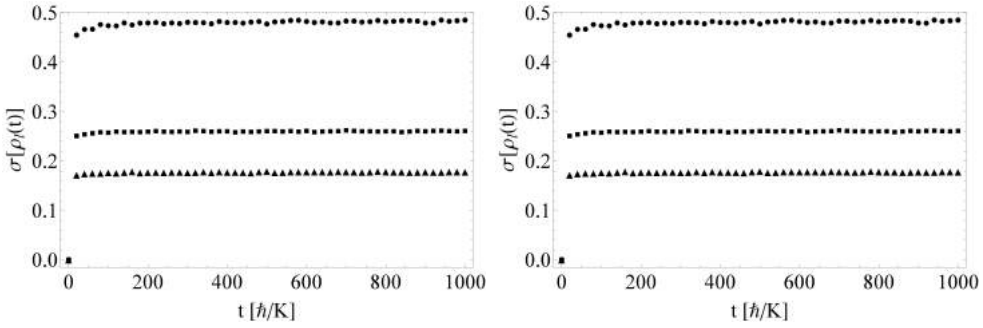

Figure 5.4: Standard deviation of $\langle\sigma[\rho_l(t)]\rangle$ versus time, averaged over 10 realizations of the disorder.

case Rasmussen et al in [159] conclude that the system is in a state with negative temperature. They are working in the grandcanonical ensemble while we are in the microcanonical one, having a well defined value of energy and particles number. In [160] authors find a functional method to determine a temperature also in the microcanonical ensemble, and this turns out to be again negative in this situation.

A possible way to visualize this change of temperature is to plot the distribution of energy $n(E_p)$ instead of the momentum distribution n_p, that is similar to what has been done in [156]. In that paper, and in the following, E_p does not refer do the real energy level of the system, but rather to energies of the free particle which, in the presence of a lattice, are $E_p = -2\cos p$. We will show that the logarithm of $n(E_p)$ versus E_p changes slope going from a side of h_c to the other. If, naively but we think not correctly because we are microcanical, we interpret this slope as $\ln(n(E_p)) \propto -E_p/T$ the changes in temperature will become more clear.

To compute the PDF for each value of g we take into account not only different realizations for a fixed time t, but also densities at different times. The reason of this choice lie on observation that from a certain t_0 many quantities of interest, such as PDF, the standard deviation of ρ_l (see Fig. (5.4) and the momentum distribution $\tilde{\rho}_p$, reach a regime in which they do not evolve macroscopically, i.e. change shape, but fluctuate around a mean value. This could be interpreted as a thermalization of the system, and this sentence becomes more meaningful if interpreted in the sense described before, i.e. if we associate to the momentum distribution a temperature (whatever this means in our case).

$h < h_c$: Gaussian disorder

From Eq. (5.12) $h < h_c$ becomes $g > 4M|\cos(p_0)|$: in this regime we are considering large enough interactions. Although Eq. (5.4) does not take into account quantum fluctuations, thus it is not strictly possible to speak about superfluid-insulator transition, we can argue from simple energetic arguments what could happen in this case. Because

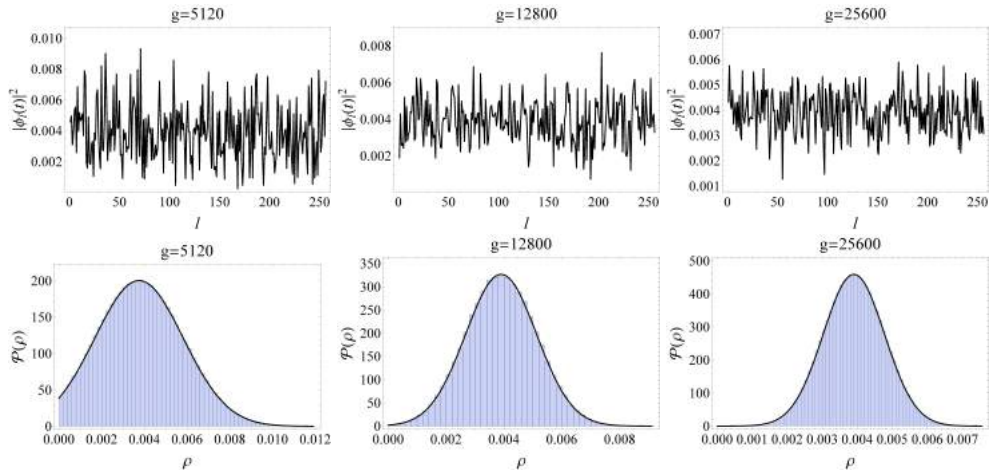

Figure 5.5: Top row: density profile $\rho_l = |\phi_l(t)|^2$ at $t = 10^4\hbar/K$ for $p_0 = \pi$ and a lattice size $M = 256$ sites. Bottom row: probability density function $\mathcal{P}(\rho)$, computed over 100 realizations. Here we consider $g = 5120$, 12800 and 25600. Black lines corresponds to fits of the data with a Gaussian $\propto \exp[-(\rho_l - a)^2/2\sigma^2]$. We can observe that the Gaussian shrinks with increasing g.

$E_{int} > E_{kin}$ tunneling between neighboring sites is not favorite because the energy cost due to repulsion is too high to avoid. A clear consequence could be understood in the limit $g = UN/K \ll 1$: tunneling is suppressed and then $\rho_l(t)$ is frozen to $\rho_l(0)$. If we now slightly decrease g tunneling becomes possible but, because it is too small, only few particles can move around the lattice. Some examples are reported in Fig. (5.5). This behavior could be inferred also looking at the probability distribution function (PDF), $\mathcal{P}(\rho_l)$, which remains Gaussian but enlarges for decreasing g, as shown in Fig. (5.5) by the black lines which are data fit with $\mathcal{P}(\rho_l) \propto \exp(-(\rho - a)^2/2\sigma^2)$.

$h > h_c$: Exponential decaying disorder

In the opposite limit of small U one observes a very peculiar dynamical behavior: the creation of peculiar structures in the density called breathers [159, 160]. A clear example of this is shown in Fig. (5.6); in each density plotted there is a certain amount, generally small, of high peaks where the density is ten times larger than the average value, those are the breathers. Their formation is possible because the energy cost the system has to pay is not too large, due to the very small interactions among particles, which is a mechanism similar to the self-trapping described in Chap. 4. This situations is very similar to the one proposed in [146], but the important difference between that paper and our system is that here this array of high peaks randomly distributed is self-generated by the condensate itself, just because it is dynamically unstable.

Once generated the density profile we again perform a statistical analysis in order to characterize it, focusing first on $\mathcal{P}(\rho_l)$, as shown in Fig. (5.6). The distribution of density

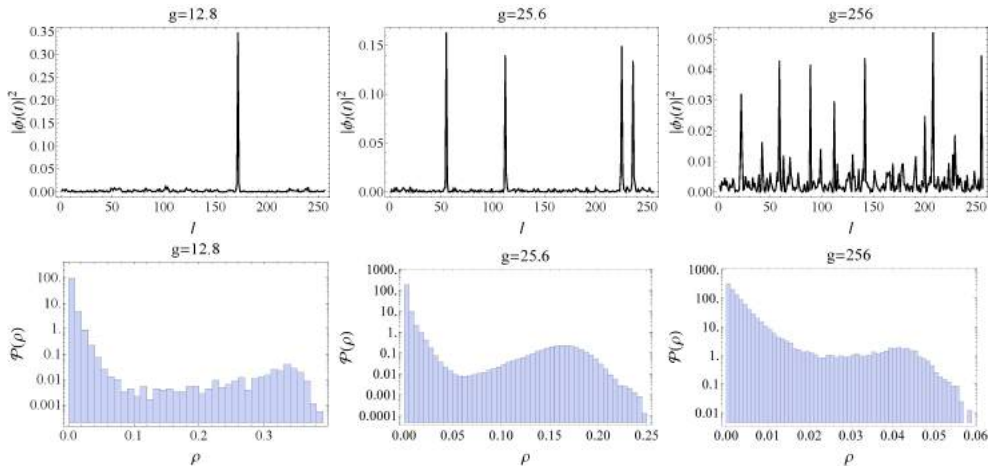

Figure 5.6: Top row: density profile $\rho_l = |\phi_l(t)|^2$ at $t = 10^4\hbar/K$ for $p_0 = \pi$ and a lattice size $M = 256$ sites. Formation of breathers, few peaks of height much larger then the average density $1/M$, is evident. Bottom row: probability density function $\mathcal{P}(\rho)$, computed over 100 realizations. Its behavior stress presence of breathers: for small ρ it decay exponentially, but for higher values a small peak is present. Here we consider $g = 12.8$, $g = 25.6$, $g = 256$.

profile reflect the formation of breathers-like structure: each PDF has an exponential decaying shape for low values ρ_l, i.e. a large fraction of lattice site are populated by a small amount of particle, but there is a small amount of sites where ρ_l are much much higher.

5.4 Interacting BECs: Anderson localization

We have shown that an interacting condensate loaded into a lattice, because of the modulation instabilities, assumes during its dynamics a nonuniform density profile. Now we go further and introduce a second condensate which interact with the first one by a mean field term, but does not interact with itself. This scheme is well described by Eq. (5.1), and in particular the second equation describe a condensate moving in a lattice to which a potential $V_l(t) = (\lambda/\eta)|\phi_l^D(t)|^2$ is superimposed. This is key point: use a condensate $\phi_l^D(t)$ to generate a disordered, even time-dependent, potential $V_l(t) \propto \rho_l^D(t)$ which will be seen by a second condensate described by the wave function $\phi_l^L(t)$.

As shown in Chap. 1 and 3 a wave packet loaded onto a one dimensional static disordered potential will become Anderson localized, and the localization properties (in particular the localization length) depend on the disorder parameters, i.e. distribution function, correlations, amplitude and mean. In our system we need to create disordered potentials with different characteristics and, moreover, we want these to be controllable; let us start to look how it is made possible.

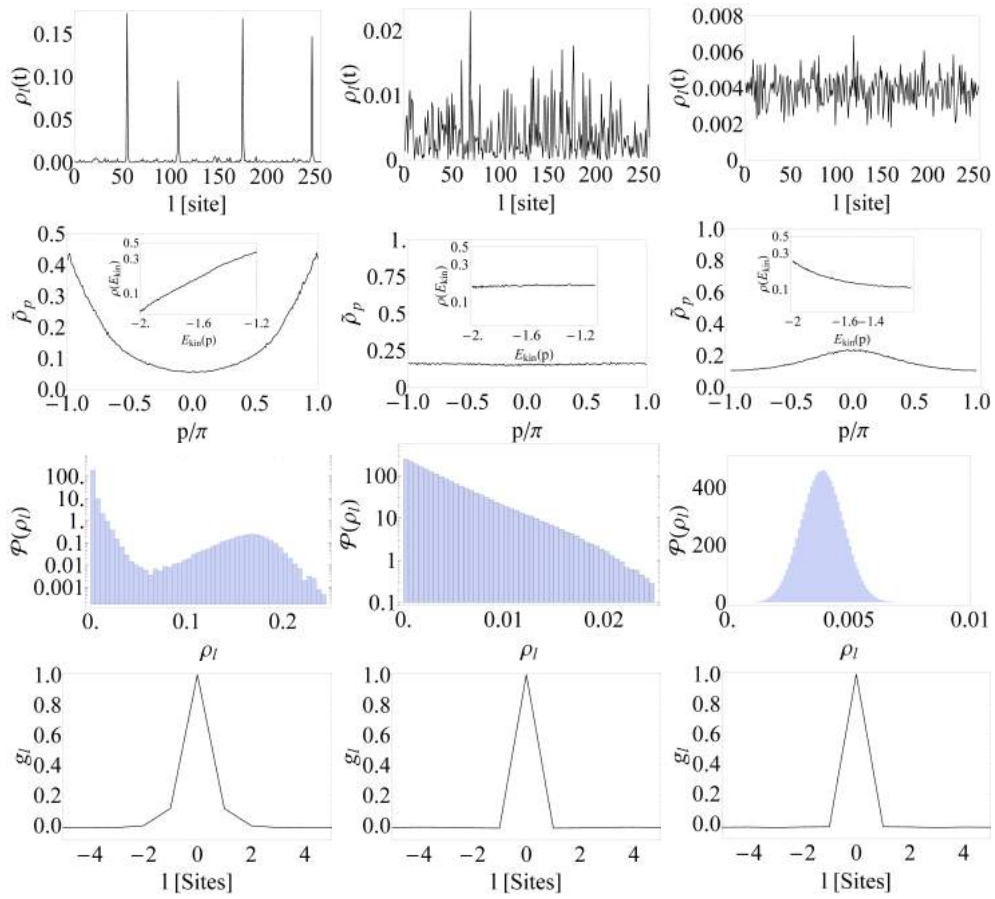

Figure 5.7: Simulations for three different values of initial energy: $h > h_c$, $h = h_c$ and $h < h_c$. From left to right we increase g. Without any perturbation of the initial state the critical energy density corresponding to $T = 0$ is $h_c = g/4M^2$. In the first and last column we select g far from this vales: under and above it, respectively. Second column shows the case of $h = h_c$, we reach that situation by numerically finding g from that condition. Each g correspond to a different disorder: first row shows the density profile for a single realization while in the two last rows we report the density distribution function $\mathcal{P}(\rho)$ and the density-density correlation function. In the second row momentum and energy (inset) distribution are plotted. Is is clear that $\tilde{\rho}_p$ changes its shape, and because of this also the non interacting particle energy distribution shows different slope (in log scale). We could interpret this as a changing of the system's temperature.

First we suppose to work with two species with a different number of atoms $N^D \ll N^L$, i.e. the specie which creates the disorder is more abundant then the other. Furthermore, looking at Eq. (5.1), we see that the effective disordered potential is

$$V_l(t) = \Lambda \rho_l^D(t)\,,$$

where Λ is proportional to the interspecies scattering length. A change in Λ implies a scaling of ρ_l^D, this means that we can modify both the mean value and the standard deviation of the disorder by setting Λ; notice that this scaling does not affect the distribution of the disorder: if $\mathcal{P}(\rho_l^D)$ is Gaussian or exponentially decaying it keeps its shape. This ensure that we deal with the same kind of disorder created by the initial choice of U.

The second important point is the time dependence of $V_l(t)$. The theory of localization deals of course with static potentials and we see in Chap. 4 that if stationarity is not satisfied Anderson localization could be modified or even destroyed and a spreading of $\psi_l^L(t)$ is restored. Here we focus on Anderson localization, considering static potentials, i.e. $dV(t)/t = 0$. How can we control this? Numerically it is very easy, and again evident in Eq. (5.1); $\rho_l(t)$ change in time because the tunneling between sites, in our case nearest neighboring sites, is possible. If particles can not jump from one site to the nearest and density does not evolve any more. Tunneling rate is determined by parameters $\alpha(t)$ thus the easiest way to obtain a static disorder is to set it to zero, i.e. in our equation we have

$$\alpha(t) = \Theta\left(t_{dis} - t\right)\,.$$

This choice for α lies on the fact that, for our convenience, we measure time in units of $\hbar/K_L$ thus, because single species simulations were performed by using $\hbar/K$ to measure time, the natural choice is to set $K_D = K_L$, so we are in the same situations analyzed before. The value of t_{dis} is selected by looking at previous results: as we shown in Fig. 5.4, depending on g, the density profile evolution take some times in order to reach a situation of quasi-stationary disorder properties: because we want a disorder with well-defined characteristics we have to wait a time longer, or at least equal, to this. At $t = t_{dis}$ interaction between species L and D is turned on, i.e.

$$\Lambda \equiv \Lambda(t) = \Lambda\Theta(t - t_{dis})\,.$$

We have now introduced the last parameter we can manipulate, the interspecies interaction strength Λ. We use for Λ values determinate as follows: for a specific realization of ρ_l^D we have that at $t = t_{dis}$ it has a standard deviation defined by

$$\sigma_R = \sqrt{\langle \rho_l^2\left(t_{dis}\right)\rangle - \langle \rho_l\left(t_{dis}\right)\rangle^2}\,. \tag{5.13}$$

We want to create a disorder with unitary standard deviation: this uniquely fixes this

parameters

$$\Lambda(t) = \frac{1}{\sigma_R}\Theta(t - t_{dis})\,; \tag{5.14}$$

by this definition the disordered potential has

$$\langle V_l(t_{dis})\rangle = \Lambda\rho_L\,; \quad \sigma(V_l(t_{dis})) = \sqrt{\langle V_l^2(t_{dis})\rangle - \langle V_l(t_{dis})\rangle^2} = 1\,,$$

where we set $\rho_L = N^L/M$.

We have created a system in which, when the interaction between species is turned on, density $\rho_l^D(\tau_d)$ is frozen by suppressing the tunneling between sites. This configuration correspond the problem of an expanding wave packet (species L) in the presence of a disordered potential, $\Lambda\rho_l^D(\tau_D)$, considered also in Chap. 3. Because our system is one dimensional we are sure that Anderson localization has to take place, and so the tails of $\rho_l^L(\tau)$ must become exponentially decaying and, moreover, the expansion of the wave packet should be suppressed. To prove that tis is true we perform a complete simulations of this situations for different disorder realizations, i.e. different initial conditions $\psi_l^D(0)$, and then we apply again what described in Chapter 1 to put in evidence the robustness of our hypothesis.

First we determinate how in the presence of this specific disorder a wave packet should localize or, in order to give a more direct observable quantity, an estimation of the localization length. This is possible to do, and particularly easy in one dimension, by implementing the so-called Transfer Matrix method (see 1.3.2 and [62, 80, 98, 100]) which is based on a physical-mathematical theorem involving random matrices, and it is also useful due to the fact that localization length is a strong self-averaging quantity, this means that we could determine it onto a sufficiently large system instead of performing averages over many disorder realizations, however in numerical simulation we can not implement too large lattices, so we have to take into account this kind of averaging also because density is not a self-averaging quantity. In Fig. 5.9 and Fig. 5.8 we report the result obtained with the two type of disorder described before, moreover we compare them with the method of Chap. 3 to confirm its validity also in this case. In those figures we can see that finite size effects play a significant role in measuring L_{loc} onto disorder-averaged densities: due the finite length of the array each realizations of the disorder gives $L_{loc}(E)$ that is not exactly the one predicted with the mentioned transfer-matrix method, but there are fluctuations which becomes larger for small systems. Because of this the averaged density will show a localization length comparable the largest between all the realization taken into account: $L_{loc}(E)$ for a single realizations and the same quantity averaged over disorder gives, in those cases, quite different results.

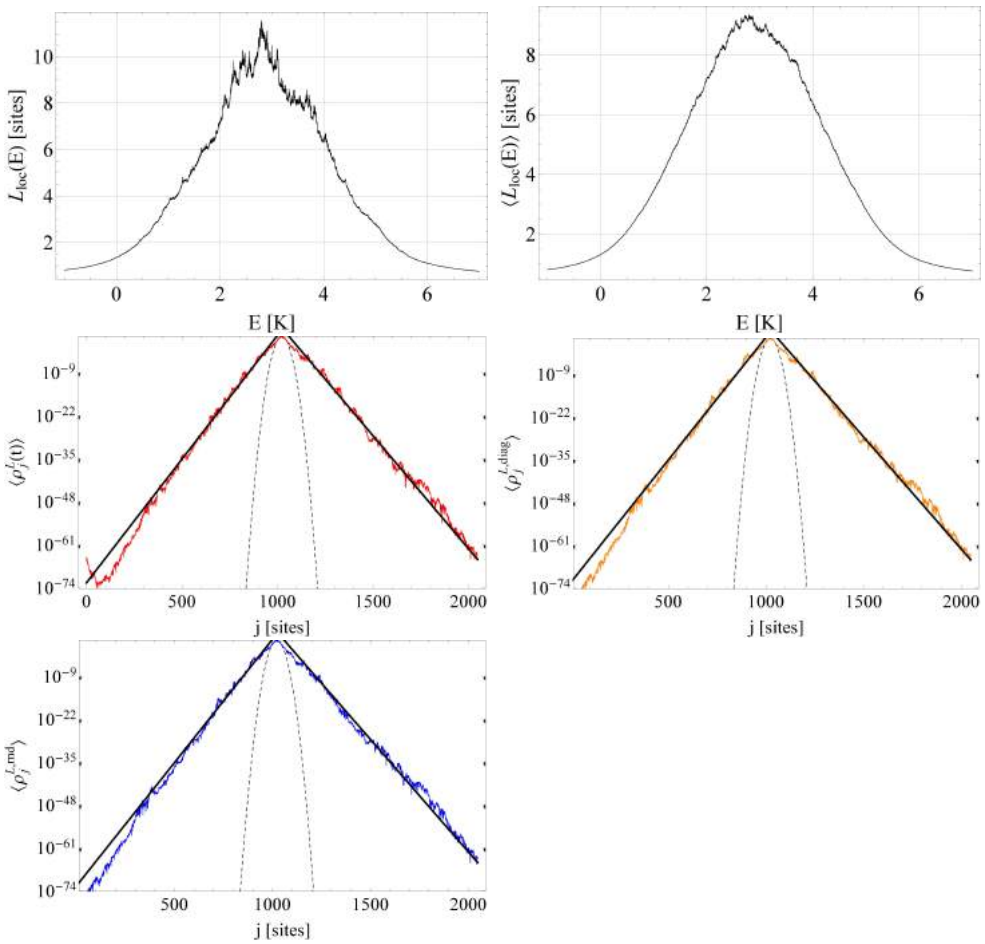

Figure 5.8: Top row: localization length as function of energy for the disorder used in our simulations. We consider 10 realizations of disorder for a lattice of $M = 2048$ sites. Other parameters are $N^L = M$, $N^D = 4M$ and $U = 10$. On the left $L_{loc}(E)$ for a single realization, on the right the same quantity averaged over 10 realizations, $\langle L_{loc}(E)\rangle$. This gives a smooth curve, but ti does not describe properly the properties of the system: each realization has indeed its own maximum L_{loc}, the greatest of them will dominate when we average density profiles. Remaining panels shows density profiles of an initially Gaussian wave packet of width 10 sites. Central row: on the left we put $\langle \rho^L(t)\rangle$ at $t = 5000\hbar/K$; in the right one the diagonal part of the density. Last panels shows $\langle \rho_l^L\rangle$ obtained with the random-phases ansatz as described in Chap. 3. Each plot is obtained by averaging over 10 realizations of the disorder. Dashed line correspond to the initial wave packet while the others are fits of the tails with $\exp(-2|x|/\xi)$. Left and right tails are fitted separately and we get: $\xi_L = 11.62 \pm 0.05$ and $\xi_R = 12.7 \pm 0.1$. Those values are compatible with the maximum values of $L_{l}ocE = 11.6$ obtained with the transfer matrix method. Notice that left and right tails do not have the same localization length, this is because each of them is dominated, in average, by the tail of the realization with the largest L_{loc}.

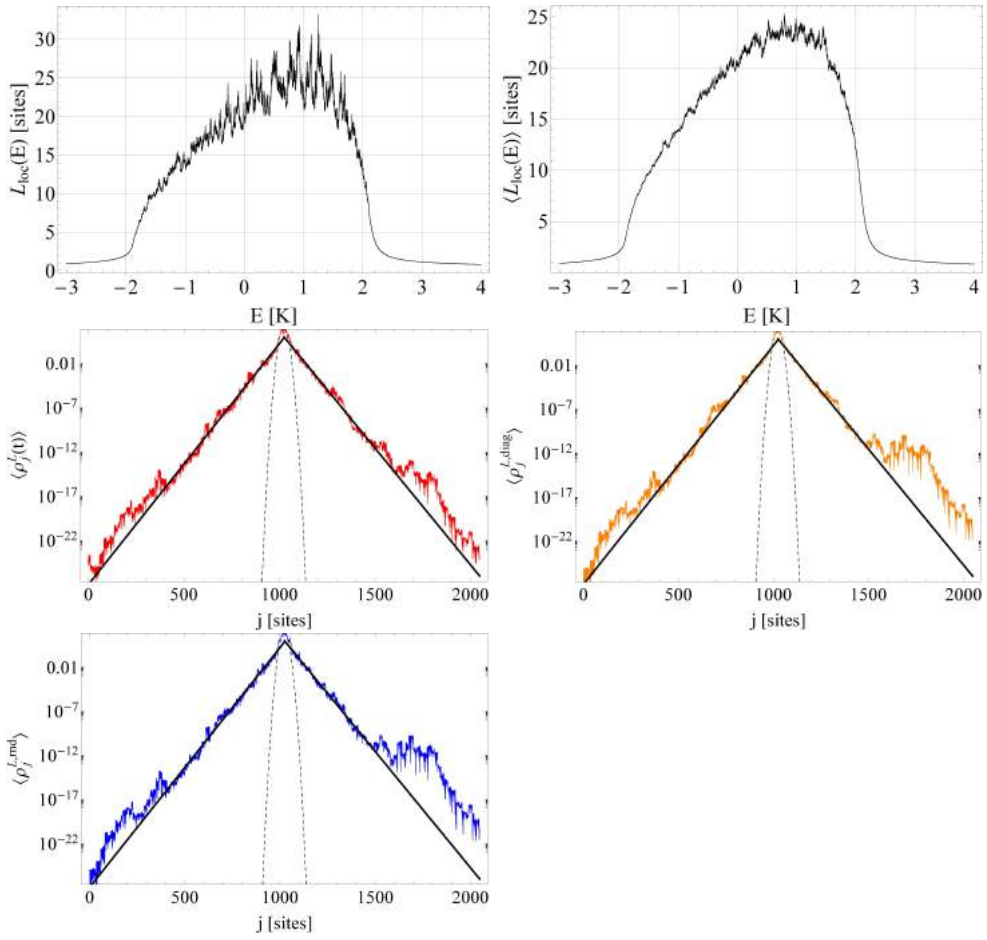

Figure 5.9: Same quantities of Fig. (5.8) for the case $U = 0.1K$. Fitting left and right tails of $\langle\rho(t)\rangle$ with $\exp(-2|x|/\xi)$ gives $\xi_L = 32.0 \pm 0.2$ and $\xi_R = 33.0 \pm 0.2$. Maximum values of $L_{loc}(E)$ for those 10 realizations of disorder is 32.2 which is reasonably close to the fitted values.

6 Conclusions

In this thesis I have reported the results of my studies about the dynamics of a wave packet loaded into disordered potential in the intriguing case of both nonlinearity and stochastic time-dependent potentials acting on it. I have been stimulated by the fact that, although many real systems can be described by models involving them, I do not find a clear understating of their interplay. I investigate it mainly from a theoretical point of view, but I also collaborated with ultracold atoms experiment in Florence [87] for which I realize numerical simulations and analytical models.

This works starts dealing with Anderson localization of non interacting particles in static disorder: this is the basic phenomenon that characterize those systems and it will be present in all the model we consider. I try to interpret it giving a simple picture of what happens to a wave packet when it localizes; I do not search for the origins of the exponential decay of the tails, but rather find a suitable description of why it assumes this special shape. Recalling the possibility of using eigenstates of a potentials as a basis for the state of a system, we show that the interference between them leads to a suppression of the macroscopic dynamics, at least in the tails of the wave packet that are the parts where Anderson localization manifests. This is a complementary point of view with respect to all the others interpretations given until now, typically based on the idea that plane waves of certain momentum will become localized due to the scattering with defects of the random potential. I found that in disordered systems the random structure of energy spectrum leads to destructive interference between eigenstates. Because this interference describes the dynamics of a wave packet, its disappearance results in a quasi static profiles: system is localized. More in the specific it is Anderson localized because the tails shows exponential decay, but this comes from the underlying shape of eigenstates which form the wave packet. We suppose that if one finds potentials the eigenenergies of which are distributed in a random way any wave packet moving on it will stops its dynamics and becomes localized with a shape that is specific of a given potential. Results reported in the thesis have been published in [161].

I apply those methods also to system of coupled Bose-Einstein condensate, using a model in which one condensate evolves in time assuming a spatial density profile which is not uniform. This is a good proposal and I do not find anything similar in literature. Some papers deal with the idea of using one condensate to Anderson localize another, but the one which is used as disorder is simply trapped by external potentials. Here I suggest that disorder is created by the condensate just because it follows its natural evolution so, at least in principle, no trapping is needed. Then I analyze these profiles looking to their spatial correlations and probability density function. I found that two classes of disorder can be created, both of them uncorrelated in space, but with density peaks that are distributed according to different distributions. Which type is generated depends on the strength of interactions, which we assume to be always repulsive. Small interactions lead to a potentials with few high peaks and all the other sites of the lattice are almost empty, this is described by an exponential decaying distribution functions. For large interactions, on the other hand, probability distribution function is found to be Gaussian; at each sites density shows fluctuations around its mean value. In addition to this I take into account the momentum distribution of the disordered condensate and the results I obtained are quite interesting. Each disorder corresponds to a specific momentum distribution: Gaussian disorder has a momentum distribution which is also a Gaussian centered around the zero momentum while exponential decaying disorder has a momentum distribution with two pronounced peaks at the highest momenta, i.e. at the boundaries of the Brillouin zone. When I found it I was advised that such a behavior could be related to a change in temperature, the particular intriguing aspect is that these kind of systems could show absolute negative temperature. This is due to the presence of the lattice that introduces an upper bound to the energy spectrum; it has been demonstrated that this allows the systems to achieve negative temperature. In cold atoms it has been observed in the last years but with a slightly more complicated scheme: here it seem that it derives naturally from the evolution of the system. After having studied the disorder I consider the localization of a wave packet, which represents the second specie, onto it. First I determine the possible localization length then compare the result obtained for a complete integration of the equations of motion with the scheme previously discussed. The results are in complete accordance once finite size effects are taken into account.

So fare I have only spoken about localization which is of great interest, both theoretical because of its deep quantum origin and practical do to the fact that disorder are ubiquitous in nature. But it is also true that localization has to fight against different processes that tend to destroy it. Two typical examples are interaction among particles and time-dependent potentials. Both of them goes into the direction of destroying Anderson localization and restoring macroscopic dynamics, and I study this dynamics looking to the evolution of the width of the wave packet and to the mean number of sites it occupies. About noise I discuss possible method to create and control a stochastic time-dependent potential and study how changing the parameters that define it could

influences the dynamics of the whole wave packet. I found that correlation time of the disorder plays a role, and it could be understood when its inverse is compared to the typical energy differences between eigenstates; because correlation time is related to the width of frequency spectrum of the potential, the more this machetes the distribution of eigenfrequencies for the underlying static disorder, the more the wave packet expand. I also find that, with all types of noise considered, results into a diffusive behavior of the wave packet, which is in accordance with most of the known results for these systems. In the case of only interactions existing theories predict a subdiffusive regime and indeed it is what I recover. I review some of the basic models that gives an explanation of this and then I discuss the peculiar phenomenon of self-trapping, which set in for strong enough interactions. It is also interesting to say that there are in literature papers that describe interactions acting as an effective noise, under this light the two effect we consider are more closer then one can think. After having analyzed them separately I start to consider the combined effect of the two; this leads to a large number of possible situations. I always get result indicating that a wave packet expand more under the contemporary actions of the noise and interactions then in the case of only one of them present. I build up a simple model that works properly in a wide range of parameter, model that lies onto the simple idea that expansion is driven by a linear combinations, i.e. the sum, of the single effects. I apply this model both on numerical simulations but also to experimental results coming from measurements on ultracold atomic samples, again I recover that it well describes the dynamics for a large interval of the parameters involved in the systems, but there are also situation in which the models does not work. I also try t give an explanation to it. At the end I report some numerical results of a fascinating effect predicted for the interplay of noise and self-trapping: a transient super diffusion before the system slows down to normal diffusive behavior. This type of anomalous diffusion is not new in random time-dependent potentials, but I do not find any works dealing with its appearance in systems similar to the one I have considered. Many of the results I presented here are published in [87, 125]

Finally I want to say that, although we find interesting result which are supported also by experimental observations, there are still opens questions. Regarding the specific subject of this thesis, some parts are still under study: the interplay between self-trapping and noise, or the possibility of create a more complete model for the diffusions. Another interesting development will concern the two species localization: what could happens if the one that generates the disorder will evolve in time? Is Anderson localization robust against this? Moreover we remark that all the results in this thesis are derived in a mean field regime, the most intriguing future studies go into the direction of taking into account the full quantum problem, by implementing Bose-Hubbard like Hamiltonians. Counting for quantum fluctuations could give new results about which we do not have any idea up to now, but the possibility of investigating different states of matter and transitions between them, under the light of the idea of various insulating-superfluid

crossover, will be in our opinion a fruitful field of research.

A

Wannier function

In this appendix we will shortly reports basic theory of Wannier functions, which is important when a link between discrete systems and continuous systems in the presence of periodic lattices is needed.

What will be write in the following is the subject of many of textbook in solid state physics, in particular we will refer to [91].

Let us consider a single particle 1D Hamiltonian with a periodic potential of period d, i.e. $U(x) = U(x + jd)$ with $j \in \mathbb{N}$:

$$H = -\frac{\hbar^2}{2m}\frac{d^2}{dx^2} + U(x)\,.$$

The Bloch's theorem [91] states that eigenstates of H have the form

$$\psi_{n,k}(x) = e^{ikx}u_{n,k}(x)\,, \tag{A.1}$$

where k is the quasi-momentum, n is the band index and $u_{n,k}(x)$ is a function with the same periodicity of $U(x)$, i.e. $u_{n,k}(x + jd) = u_{n,k}(x)$. Quasi momentum is restricted to the first Brillouin zone $k \in [-\pi/d, \pi/d]$ and, in a system of finite length can assume N possible values, N being the number of periods of $U(x)$ present in the system. Because this periodicity, it follows from (A.1) that

$$\psi_{n,k}(x + jd) = e^{ijnd}\psi_{n,k}(x)\,. \tag{A.2}$$

If one considers any of the $\psi_{n,k}(x)$ as a function of k for fixed x, he recovers again a periodic function with period $2\pi/d$. This means that it has a Fourier series expansion in plane waves with wave vectors in real space. Keeping x fixed we therefore are allowed to write

$$\psi_{n,k}(x) = \frac{1}{\sqrt{N}}\sum_j w_{n,j}(x)e^{ijkd}\,. \tag{A.3}$$

The Fourier components $w_{n,j}(x)$ are called Wannier functions and they depend on x, on the sites j and onto the band n; they are of coure defined by an inverse Fourier transform

$$w_{n,j}(x) = \frac{1}{\sqrt{N}} \sum_k \psi_{n,k}(x) e^{-ijkd} \,, \tag{A.4}$$

where summation over k is limited to the fist Brillouin zone; for very large systems the summation could be substituted by an integral.

Now we report some of the main properties of those functions:

- As a consequence of Bolch's theorem and of (A.4) all the functions have the same shape:
$$w_{n,j+l}(x + ld) = w_{n,j}(x) \,, \tag{A.5}$$
so we will use the notation
$$w_{n,j}(x) = w_{n,j}(x - jd) \,. \tag{A.6}$$

- They form a complete and orthonormal set of functions. Completeness follows from the fact that we expressed the basis of the Bloch functions (which we remember are eigenstates of H) as linear combination of $w_{n,j}(x)$. Orthogonality is given by
$$\int w^*_{n,j}(x) w_{m,l}(x) = \delta_{nm}\delta_{jl} \,. \tag{A.7}$$
Again, this can be demonstrated using (A.4) and the fact that (A.1) are othogonal.

- It is well known that the energy spectrum of H is formed by a series of bands separated by gaps of forbidden energies. Wannier functions of the lowest energy band are centered around the lattice sites jd. Moreover for suitable choice for the phases of (A.1) one can always consider real $w_{n,j}(x)$, symmetric around jd and they rapidly go to zero away from the site [162].

Bibliography

[1] Ilya M. Lifshits, Sergej A. Gredskul, and Leonid A. Pasteur. *Introduction to the theory of disordered systems*. Wiley, New York, 1988.

[2] P. W. Anderson. Absence of diffusion in certain random lattices. *Phys. Rev.*, 109:1492–1505, Mar 1958.

[3] Patrick A. Lee and T. V. Ramakrishnan. Disordered electronic systems. *Rev. Mod. Phys.*, 57:287–337, Apr 1985.

[4] B. Kramer and A. MacKinnon. Localization: theory and experiment. *Reports on Progress in Physics*, 56(12):1469, 1993.

[5] Shanjin He and J. D. Maynard. Detailed measurements of inelastic scattering in anderson localization. *Phys. Rev. Lett.*, 57:3171–3174, Dec 1986.

[6] Diederik S. Wiersma, Paolo Bartolini, Ad Lagendijk, and Roberto Righini. Localization of light in a disordered medium. *Nature*, 390:671, December 1997.

[7] Frank Scheffold, Ralf Lenk, Ralf Tweer, and Georg Maret. Localization or classical diffusion of light? *Nature*, 398:206, March 1999.

[8] Martin Störzer, Peter Gross, Christof M. Aegerter, and Georg Maret. Observation of the critical regime near anderson localization of light. *Phys. Rev. Lett.*, 96:063904, Feb 2006.

[9] Tal Schwartz, Guy Bartal, Shumel Fishman, and Mordechai Segev. Transport and anderson localization in disordered two-dimensional photonic lattices. *Nature*, 446:52, March 2007.

[10] Liad Levi, Yevgeny Krivolapov, Shmuel Fishman, and Segev Mordechai. Hyper-transport of light and stochastic acceleration by evolving disorder. *Nat. Phys.*, 8:912, November 2012.

[11] Valery E. Lobanov, Yaroslav V. Kartashov, Victor A. Vysloukh, and Lluis Torner. Anderson localization of light with topological dislocations. *Phys. Rev. A*, 88:053829, Nov 2013.

[12] Alexander Figotin and Abel Klein. Localization of classical waves i: Acoustic waves. *Communications in Mathematical Physics*, 180(2):439–482, 1996.

[13] Hefei Hu, A. Strybulevych, J. H. Page, S. E. Skipetrov, and B. A. van Tiggelen. Localization of ultrasound in a three-dimensional elastic network. *Nat. Phys.*, 4:945, October 2008.

[14] E. Larose, L. Margerin, B. A. van Tiggelen, and M. Campillo. Weak localization of seismic waves. *Phys. Rev. Lett.*, 93:048501, Jul 2004.

[15] M. H. Anderson, J. R. Ensher, M. R. Matthews, C. E. Wieman, and E. A. Cornell. Observation of bose-einstein condensation in a dilute atomic vapor. *Science*, 269(5221):198–201, 1995.

[16] K. B. Davis, M. O. Mewes, M. R. Andrews, N. J. van Druten, D. S. Durfee, D. M. Kurn, and W. Ketterle. Bose-Einstein Condensation in a gas of sodium atoms. *Phys. Rev. Lett.*, 75:3969–3973, Nov 1995.

[17] C. C. Bradley, C. A. Sackett, J. J. Tollett, and R. G. Hulet. Evidence of Bose-Einstein Condensation in an atomic gas with attractive interactions. *Phys. Rev. Lett.*, 75:1687–1690, Aug 1995.

[18] C. C. Bradley, C. A. Sackett, and R. G. Hulet. Bose-Einstein Condensation of lithium: Observation of limited condensate number. *Phys. Rev. Lett.*, 78:985–989, Feb 1997.

[19] Giacomo Roati, Chiara D'Errico, Leonardo Fallani, Marco Fattori, Chiara Fort, Matteo Zaccanti, Giovanni Modugno, Michele Modugno, and Massimo Inguscio. Anderson localization of a non-interacting Bose-Einstein condensate. *Nature*, 453:895, June 2008.

[20] Juliette Billy, Vincent Josse, Zhanchun Zuo, Alain Bernard, Ben Hambrecht, Pierre Lugan, David Clément, Laurent Sanchez-Palencia, Philippe Bouyer, and Alain Aspect. Direct observation of Anderson localization of matter waves in a controlled disorder. *Nature*, 453:891, June 2008.

[21] Julien Chabé, Gabriel Lemarié, Beno^ Grémaud, Dominique Delande, Pascal Szriftgiser, and Jean Claude Garreau. Experimental observation of the anderson metal-insulator transition with atomic matter waves. *Phys. Rev. Lett.*, 101:255702, Dec 2008.

[22] Alain Aspect and Massimo Inguscio. Anderson localization of ultracold atoms. *Print edition*, 62(8):30–35, 2009.

[23] Giovanni Modugno. Anderson localization in Bose-Einstein Condensates. *Reports on Progress in Physics*, 73(10):102401, 2010.

[24] Laurent Sancez-Palencia and Maciej Lewenstein. Disordered quantum gases under control. *Nat. Phys.*, 6:87, February 2010.

[25] A. Einstein. über einen die erzeugung und verwandlung des lichtes betreffenden heuristischen gesichtspunkt. *Annalen der Physik*, 322(6):132–148, 1905.

[26] Anupam Madhukar and Morrel H. Cohen. Ideal resistivity in one dimension. *Phys. Rev. Lett.*, 38:85–88, Jan 1977.

[27] A. Madhukar and W. Post. Exact solution for the diffusion of a particle in a medium with site diagonal and off-diagonal dynamic disorder. *Phys. Rev. Lett.*, 39:1424–1427, Nov 1977.

[28] Andrei A. Gogolin, Vladimir I. Melnikov, and Emmanuel I. Rashba. Conductivity in a disordered one-dimensional system induced by electron-phonon interaction. *Zh. Eksp. Teor. Fiz.*, 69:327, Jul 1975.

[29] A. A. Ovchinnikov and N. S. Erikhman. *Zh. Eksp. Teor. Fiz.*, 40, 1975.

[30] H. Metiu, K. Kitahara, Robert Silbey, and John Ross. Coherent and diffusional motion of a chemisorbed atom. *Chemical Physics Letters*, 43(1):189 – 193, 1976.

[31] H. Scher and M. Lax. Stochastic transport in a disordered solid. i. theory. *Phys. Rev. B*, 7:4491–4502, May 1973.

[32] H. Scher and M. Lax. Stochastic transport in a disordered solid. ii. impurity conduction. *Phys. Rev. B*, 7:4502–4519, May 1973.

[33] Harvey Scher and Elliott W. Montroll. Anomalous transit-time dispersion in amorphous solids. *Phys. Rev. B*, 12:2455–2477, Sep 1975.

[34] A. M. Jayannavar and N. Kumar. Nondiffusive quantum transport in a dynamically disordered medium. *Phys. Rev. Lett.*, 48:553–556, Feb 1982.

[35] Leonardo Golubović, Shechao Feng, and Fan-An Zeng. Classical and quantum superdiffusion in a time-dependent random potential. *Phys. Rev. Lett.*, 67:2115–2118, Oct 1991.

[36] A. M. Jayannavar. Wave propagation and quantum superdiffusion in a rapidly varying random potential. *Phys. Rev. E*, 48:837–842, Aug 1993.

[37] Brian Berkowitz and Harvey Scher. Theory of anomalous chemical transport in random fracture networks. *Phys. Rev. E*, 57:5858–5869, May 1998.

[38] Devora Holder, Harvey Scher, and Brian Berkowitz. Numerical study of diffusion on a random-mixed-bond lattice. *Phys. Rev. E*, 77:031119, Mar 2008.

[39] Gennady Margolin and Brian Berkowitz. Spatial behavior of anomalous transport. *Phys. Rev. E*, 65:031101, Feb 2002.

[40] Marco Dentz and Brian Berkowitz. Exact effective transport dynamics in a one-dimensional random environment. *Phys. Rev. E*, 72:031110, Sep 2005.

[41] Brian Berkowitz and Harvey Scher. Anomalous transport in correlated velocity fields. *Phys. Rev. E*, 81:011128, Jan 2010.

[42] Harvey Scher, Karen Willbrand, and Brian Berkowitz. Transport in disordered media with spatially nonuniform fields. *Phys. Rev. E*, 81:031102, Mar 2010.

[43] Marco Dentz and Brian Berkowitz. Erratum: Exact effective transport dynamics in a one-dimensional random environment. *Phys. Rev. E*, 81:059901, May 2010.

[44] S.I. Denisov and Werner Horsthemke. Anomalous diffusion and stochastic localization of damped quantum particles. *Physics Letters A*, 282(6):367 – 372, 2001.

[45] A W Chin, A Datta, F Caruso, S F Huelga, and M B Plenio. Noise-assisted energy transfer in quantum networks and light-harvesting complexes. *New Journal of Physics*, 12(6):065002, 2010.

[46] James Q. Quach. Disorder-correlation-frequency-controlled diffusion in the Jaynes-Cummings-Hubbard model. *Phys. Rev. A*, 88:053843, Nov 2013.

[47] Thomas Wellens and Beno^Grémaud. Nonlinear coherent transport of waves in disordered media. *Phys. Rev. Lett.*, 100:033902, Jan 2008.

[48] Ignacio García-Mata and Dima L. Shepelyansky. Delocalization induced by nonlinearity in systems with disorder. *Phys. Rev. E*, 79:026205, Feb 2009.

[49] D. L. Shepelyansky. Delocalization of quantum chaos by weak nonlinearity. *Phys. Rev. Lett.*, 70:1787–1790, Mar 1993.

[50] G. Kopidakis, S. Komineas, S. Flach, and S. Aubry. Absence of wave packet diffusion in disordered nonlinear systems. *Phys. Rev. Lett.*, 100:084103, Feb 2008.

[51] A. S. Pikovsky and D. L. Shepelyansky. Destruction of anderson localization by a weak nonlinearity. *Phys. Rev. Lett.*, 100:094101, Mar 2008.

[52] S. Flach, D. O. Krimer, and Ch. Skokos. Universal spreading of wave packets in disordered nonlinear systems. *Phys. Rev. Lett.*, 102:024101, Jan 2009.

[53] Ch. Skokos, D. O. Krimer, S. Komineas, and S. Flach. Delocalization of wave packets in disordered nonlinear chains. *Phys. Rev. E*, 79:056211, May 2009.

[54] Hagar Veksler, Yevgeny Krivolapov, and Shmuel Fishman. Spreading for the generalized nonlinear schrödinger equation with disorder. *Phys. Rev. E*, 80:037201, Sep 2009.

[55] M. Larcher, F. Dalfovo, and M. Modugno. Effects of interaction on the diffusion of atomic matter waves in one-dimensional quasiperiodic potentials. *Phys. Rev. A*, 80:053606, Nov 2009.

[56] M. Mulansky and A. Pikovsky. Spreading in disordered lattices with different nonlinearities. *EPL (Europhysics Letters)*, 90(1):10015, 2010.

[57] T. V. Laptyeva, J. D. Bodyfelt, D. O. Krimer, Ch. Skokos, and S. Flach. The crossover from strong to weak chaos for nonlinear waves in disordered systems. *EPL (Europhysics Letters)*, 91(3):30001, 2010.

[58] Alexander Iomin. Subdiffusion in the nonlinear schrödinger equation with disorder. *Phys. Rev. E*, 81:017601, Jan 2010.

[59] J. D. Bodyfelt, T. V. Laptyeva, Ch. Skokos, D. O. Krimer, and S. Flach. Nonlinear waves in disordered chains: Probing the limits of chaos and spreading. *Phys. Rev. E*, 84:016205, Jul 2011.

[60] Bin Min, Tiejun Li, Matthias Rosenkranz, and Weizhu Bao. Subdiffusive spreading of a bose-einstein condensate in random potentials. *Phys. Rev. A*, 86:053612, Nov 2012.

[61] Ch. Skokos, I. Gkolias, and S. Flach. Nonequilibrium chaos of disordered nonlinear waves. *Phys. Rev. Lett.*, 111:064101, Aug 2013.

[62] Jacopo Giacomelli. Localizzazione di un condensato di bose-einstein in potenziali ottici disordinati unidimensionali. Master's thesis, Università degli Studi di Firenze, 2007.

[63] N.F. Mott and W.D. Twose. The theory of impurity conduction. *Advances in Physics*, 10(38):107–163, 1961.

[64] I.M. Lifshitz. The energy spectrum of disordered systems. *Advances in Physics*, 13(52):483–536, 1964.

[65] Ronald Fisch. Band tails, length scales, and localization. *Phys. Rev. B*, 53:6862–6864, Mar 1996.

[66] Joseph Goodman. *Speckle phenomena in optics*. Roberts and Co., Greenwood Village, 2010.

[67] Serge Aubry and G. André. Analyticity breaking and Anderson localization in incommensurate lattices. *Ann. Israel Phys. Soc.*, 3:133, 1980.

[68] Michele Modugno. Exponential localization in one-dimensional quasi-periodic optical lattices. *New Journal of Physics*, 11(3):033023, 2009.

[69] C. Fort, L. Fallani, V. Guarrera, J. E. Lye, M. Modugno, D. S. Wiersma, and M. Inguscio. Effect of optical disorder and single defects on the expansion of a Bose-Einstein Condensate in a one-dimensional waveguide. *Phys. Rev. Lett.*, 95:170410, Oct 2005.

[70] D. Clément, A. F. Varón, M. Hugbart, J. A. Retter, P. Bouyer, L. Sanchez-Palencia, D. M. Gangardt, G. V. Shlyapnikov, and A. Aspect. Suppression of transport of an interacting elongated Bose-Einstein Condensate in a random potential. *Phys. Rev. Lett.*, 95:170409, Oct 2005.

[71] D Clément, A F Varon, J A Retter, L Sanchez-Palencia, A Aspect, and P Bouyer. Experimental study of the transport of coherent interacting matter-waves in a 1d random potential induced by laser speckle. *New Journal of Physics*, 8(8):165, 2006.

[72] P. Lugan, D. Clément, P. Bouyer, A. Aspect, M. Lewenstein, and L. Sanchez-Palencia. Ultracold bose gases in 1d disorder: From lifshits glass to Bose-Einstein Condensate. *Phys. Rev. Lett.*, 98:170403, Apr 2007.

[73] L. Sanchez-Palencia, D. Clément, P. Lugan, P. Bouyer, G. V. Shlyapnikov, and A. Aspect. Anderson localization of expanding Bose-Einstein Condensates in random potentials. *Phys. Rev. Lett.*, 98:210401, May 2007.

[74] P. Lugan, D. Clément, P. Bouyer, A. Aspect, and L. Sanchez-Palencia. Anderson localization of bogolyubov quasiparticles in interacting Bose-Einstein Condensates. *Phys. Rev. Lett.*, 99:180402, Nov 2007.

[75] L Sanchez-Palencia, D Clément, P Lugan, P Bouyer, and A Aspect. Disorder-induced trapping versus anderson localization in bose-einstein condensates expanding in disordered potentials. *New Journal of Physics*, 10(4):045019, 2008.

[76] David Clément. *Static and dynamic properties of disordered Bose-Einstein condensates*. PhD thesis, Institute d'Optique d'Orsay, 2008.

[77] Chiara D'Errico. *Anderson localization of a weakly interacting Bose-Einstein condensate*. PhD thesis, Università degli Studi di Firenze, 2008.

[78] Gianpaolo Gobbo. Il teorema del limite centrale in meccanica statistica. Master's thesis, Università degli Studi di Padova, 2005.

[79] Aleksandr Y. Khinchin. *Mathematical Foundations of Statistical Mechanics*. Dover Pubns., New York, 1960.

[80] Marco Larcher. *Localization and spreading of matter waves in disordered potentials*. PhD thesis, Università degli Studi di Trento, 2013.

[81] E.I. Dinaburg and Ya.G. Sinai. The one-dimensional schrödinger equation with a quasiperiodic potential. *Functional Analysis and Its Applications*, 9(4):279–289, 1975.

[82] Joseph Avron and Barry Simon. Almost periodic schrödinger operators. *Communications in Mathematical Physics*, 82(1):101–120, 1981.

[83] Barry Simon. Almost periodic schrödinger operators: A review. *Advances in Applied Mathematics*, 3(4):463 – 490, 1982.

[84] Gerardo G. Naumis and F.J. Lopez-Rodriguez. The electronic spectrum of a quasiperiodic potential: From the hofstadter butterfly to the fibonacci chain. *Physica B: Condensed Matter*, 403(10 - 11):1755 – 1762, 2008.

[85] S. Jitomirskaya and C.A. Marx. Analytic quasi-periodic schrödinger operators and rational frequency approximants. *Geometric and Functional Analysis*, 22(5):1407–1443, 2012.

[86] Dov Levine and Paul Joseph Steinhardt. Quasicrystals: A new class of ordered structures. *Phys. Rev. Lett.*, 53:2477–2480, Dec 1984.

[87] C D'Errico, M Moratti, E Lucioni, L Tanzi, B Deissler, M Inguscio, G Modugno, M B Plenio, and F Caruso. Quantum diffusion with disorder, noise and interaction. *New Journal of Physics*, 15(4):045007, 2013.

[88] E. Lucioni, B. Deissler, L. Tanzi, G. Roati, M. Zaccanti, M. Modugno, M. Larcher, F. Dalfovo, M. Inguscio, and G. Modugno. Observation of subdiffusion in a disordered interacting system. *Phys. Rev. Lett.*, 106:230403, Jun 2011.

[89] Luca Tanzi, Eleonora Lucioni, Saptarishi Chaudhuri, Lorenzo Gori, Avinash Kumar, Chiara D'Errico, Massimo Inguscio, and Giovanni Modugno. Transport of a bose gas in 1d disordered lattices at the fluid-insulator transition. *Phys. Rev. Lett.*, 111:115301, Sep 2013.

[90] M. Larcher, M. Modugno, and F. Dalfovo. Localization in momentum space of ultracold atoms in incommensurate lattices. *Phys. Rev. A*, 83:013624, Jan 2011.

[91] Neil W. Ashcroft and David N. Mermin. *Solid State Physics*. Brooks/Cole, Pacifc Grove, 1976.

[92] R. Balian, R. Maynard, and Toulouse G., editors. *III-Condensed Matter*, Les Houches Summer School Proceedings, Amsterdam, 1979. North-Holland.

[93] K. Osterwalder and R. Stora, editors. *Critical phenomena, random systems, gauge theories*, Les Houches Summer School Proceedings, Amsterdam, 1986. North-Holland.

[94] Kazushige Ishii. Localization of eigenstates and transport phenomena in the one-dimensional disordered system. *Progress of Theoretical Physics Supplement*, 53:77–138, 1973.

[95] Rolf Landauer. Electrical resistance of disordered one-dimensional lattices. *Philosophical Magazine*, 21(172):863–867, 1970.

[96] P. W. Anderson, D. J. Thouless, E. Abrahams, and D. S. Fisher. New method for a scaling theory of localization. *Phys. Rev. B*, 22:3519–3526, Oct 1980.

[97] R. E. Borland. The nature of the electronic states in disordered one-dimensional systems. *Proceedings of the Royal Society of London. Series A. Mathematical and Physical Sciences*, 274(1359):529–545, 1963.

[98] V.I. Oseledec. A multiplicative ergodic theorem. Characteristic Ljapunov, exponents of dynamical systems. *Trans. Moscov. Math. Obsc.*, 19, 1968.

[99] Bertrand I. Halperin. *Properties of a Particle in a One-Dimensional Random Potential*, pages 123–177. John Wiley & Sons, Inc., 2007.

[100] Harry Furstenberg. Noncommuting random products. *Trans. Amer. Math. Soc.*, 108:377–428, 1963.

[101] D J Thouless. A relation between the density of states and range of localization for one dimensional random systems. *Journal of Physics C: Solid State Physics*, 5(1):77, 1972.

[102] D C Herbert and R Jones. Localized states in disordered systems. *Journal of Physics C: Solid State Physics*, 4(10):1145, 1971.

[103] Cristopher J. Pethick and Henrik Smith. *Bose-Einstein condensation in dilute gases*. Cambridge University Press, Cambdrige, second edition, 2008.

[104] Sandro Stringari and Lev P. Pitaevskii. *Bose-Eisntein Condenstation*. Oxford University Press, Oxford, 2003.

[105] Franco Dalfovo, Stefano Giorgini, Lev P. Pitaevskii, and Sandro Stringari. Theory of bose-einstein condensation in trapped gases. *Rev. Mod. Phys.*, 71:463–512, Apr 1999.

[106] James F. Annett. *Superconductiviy, Superfluids and Condensates*. Oxford University Press, Oxford, 2004.

[107] Ugo Fano. Sullo spettro di assorbimento dei gas nobili presso il limite dello spettro d'arco. *Il Nuovo Cimento*, 12(3):154–161, 1935.

[108] Herman Feshbach. Unified theory of nuclear reactions. *Annals of Physics*, 5(4):357 – 390, 1958.

[109] Herman Feshbach. A unified theory of nuclear reactions. {II}. *Annals of Physics*, 19(2):287 – 313, 1962.

[110] S. Inouye, M. R. Andrews, J. Stenger, H.-J. Miesner, D.M. Stamper-Kurn, and W. Ketterle. Observation of Feshbach resonances in a Bos-Einstein condensate. *Nature*, 392:151, March 1998.

[111] Cheng Chin, Vladan Vuletić, Andrew J. Kerman, and Steven Chu. High resolution feshbach spectroscopy of cesium. *Phys. Rev. Lett.*, 85:2717–2720, Sep 2000.

[112] S. L. Cornish, N. R. Claussen, J. L. Roberts, E. A. Cornell, and C. E. Wieman. Stable ^{85}Rb Bose-Einstein Condensates with widely tunable interactions. *Phys. Rev. Lett.*, 85:1795–1798, Aug 2000.

[113] E.P. Gross. Structure of a quantized vortex in boson systems. *Il Nuovo Cimento Series 10*, 20(3):454–477, 1961.

[114] Eugene P. Gross. Hydrodynamics of a superfluid condensate. *Journal of Mathematical Physics*, 4(2):195–207, 1963.

[115] Lev P. Pitaevskii. Vortex lines in an imperfect Bose gas. *Zh. Eksp. Teor. Fiz.*, 13:451, 1961.

[116] Fabrice Gerbier, Artur Widera, Simon Fölling, Olaf Mandel, Tatjana Gericke, and Immanuel Bloch. Interference pattern and visibility of a mott insulator. *Phys. Rev. A*, 72:053606, Nov 2005.

[117] Panayotis G. Kevrekidis. *The Discrete Nonlinear Schrödinger Equation*, volume 232 of *Springer Tracts in Modern Physics*. Springer, Berlin, 2009.

[118] Lev D. Landau and Evgeny M. Lifshitz. *Quantum Mechanics Non-Relativistic Thoery*. Buttworth-Heinemann, Oxford, third edition, 1981.

[119] Jun J. Sakurai. *Modern Quantum Mechanics*. Addison Wesley, Boston, 1993.

[120] Michele Modugno. Collective dynamics and expansion of a bose-einstein condensate in a random potential. *Phys. Rev. A*, 73:013606, Jan 2006.

[121] J. M. Huntley. Noise-immune phase unwrapping algorithm. *Appl. Opt.*, 28(16):3268–3270, Aug 1989.

[122] L Sanchez-Palencia, D Clément, P Lugan, P Bouyer, and A Aspect. Disorder-induced trapping versus anderson localization in bose-einstein condensates expanding in disordered potentials. *New Journal of Physics*, 10(4):045019, 2008.

[123] M. Piraud, P. Lugan, P. Bouyer, A. Aspect, and L. Sanchez-Palencia. Localization of a matter wave packet in a disordered potential. *Phys. Rev. A*, 83:031603, Mar 2011.

[124] S. Palpacelli and S. Succi. Quantum lattice boltzmann simulation of expanding bose-einstein condensates in random potentials. *Phys. Rev. E*, 77:066708, Jun 2008.

[125] E. Lucioni, L. Tanzi, C. D'Errico, M. Moratti, M. Inguscio, and G. Modugno. Modeling the transport of interacting matter waves in a disordered system by a nonlinear diffusion equation. *Phys. Rev. E*, 87:042922, Apr 2013.

[126] E. Ott, T. M. Antonsen, and J. D. Hanson. Effect of noise on time-dependent quantum chaos. *Phys. Rev. Lett.*, 53:2187–2190, Dec 1984.

[127] S. Fishman and D. L. Shepelyansky. Manifestation of localization in noise-induced ionization and dissociation. *EPL (Europhysics Letters)*, 16(7):643, 1991.

[128] D. O. Krimer and S. Flach. Statistics of wave interactions in nonlinear disordered systems. *Phys. Rev. E*, 82:046221, Oct 2010.

[129] B Tuck. Some explicit solutions to the non-linear diffusion equation. *Journal of Physics D: Applied Physics*, 9(11):1559, 1976.

[130] Andrea Trombettoni and Augusto Smerzi. Discrete solitons and breathers with dilute Bose-Einstein Condensates. *Phys. Rev. Lett.*, 86:2353–2356, Mar 2001.

[131] Th. Anker, M. Albiez, R. Gati, S. Hunsmann, B. Eiermann, A. Trombettoni, and M. K. Oberthaler. Nonlinear self-trapping of matter waves in periodic potentials. *Phys. Rev. Lett.*, 94:020403, Jan 2005.

[132] A. Smerzi, S. Fantoni, S. Giovanazzi, and S. R. Shenoy. Quantum coherent atomic tunneling between two trapped Bose-Einstein Condensates. *Phys. Rev. Lett.*, 79:4950–4953, Dec 1997.

[133] S. Raghavan, A. Smerzi, S. Fantoni, and S. R. Shenoy. Coherent oscillations between two weakly coupled bose-einstein condensates: Josephson effects, π-oscillations, and macroscopic quantum self-trapping. *Phys. Rev. A*, 59:620–633, Jan 1999.

[134] Magnus Johansson, Michael Hörnquist, and Rolf Riklund. Effects of nonlinearity on the time evolution of single-site localized states in periodic and aperiodic discrete systems. *Phys. Rev. B*, 52:231–240, Jul 1995.

[135] G. L. Aranovich and M. D. Donohue. Diffusion equation for interacting particles. *The Journal of Physical Chemistry B*, 109(33):16062–16069, 2005.

[136] P. Siegle, I. Goychuk, and P. Hänggi. Origin of hyperdiffusion in generalized brownian motion. *Phys. Rev. Lett.*, 105:100602, Sep 2010.

[137] Hiroaki Yamada and Kensuke S. Ikeda. Dynamical delocalization in one-dimensional disordered systems with oscillatory perturbation. *Phys. Rev. E*, 59:5214–5230, May 1999.

[138] G. Roati, M. Zaccanti, C. D'Errico, J. Catani, M. Modugno, A. Simoni, M. Inguscio, and G. Modugno. K^{39} Bose-Einstein Condensate with tunable interactions. *Phys. Rev. Lett.*, 99:010403, Jul 2007.

[139] J. P. Bouchaud, D. Touati, and D. Sornette. Waves in a rapidly varying random potential: A numerical study. *Phys. Rev. Lett.*, 68:1787–1790, Mar 1992.

[140] Lawrence Saul, Mehran Kardar, and N. Read. Directed waves in random media. *Phys. Rev. A*, 45:8859–8866, Jun 1992.

[141] S. Diehl, A. Micheli, A. Kantian, B. Kraus, H. P. Büchler, and P. Zoller. Quantum states and phases in driven open quantum systems with cold atoms. *Nat. Phys.*, 4:878, September 2008.

[142] Emanuele G. Dalla Torre, Eugene Demler, Thierry giamarchi, and Ehud Altman. Quantum critical states and phase transitions in the presence of non-equilibrium noise. *Nat. Phys.*, 6:806, August 2010.

[143] D.J. Thouless. Electrons in disordered systems and the theory of localization. *Physics Reports*, 13(3):93 – 142, 1974.

[144] Maciej Lewenstein, Anna Sanpera, Veronica Ahufinger, Bogdan Damski, Aditi Sen(De), and Ujjwal Sen. Ultracold atomic gases in optical lattices: mimicking condensed matter physics and beyond. *Advances in Physics*, 56(2):243–379, 2007.

[145] I. L. Aleinier, B. L. Altshuler, and G. V. Shlyapnikov. A finite-temperature phase transition for disordered weakly interacting bosons in one dimension. *Nat. Phys.*, 6:900, September 2010.

[146] Uri Gavish and Yvan Castin. Matter-wave localization in disordered cold atom lattices. *Phys. Rev. Lett.*, 95:020401, Jul 2005.

[147] Biao Wu and Qian Niu. Landau and dynamical instabilities of the superflow of bose-einstein condensates in optical lattices. *Phys. Rev. A*, 64:061603, Nov 2001.

[148] Biao Wu and Qian Niu. Superfluidity of Bose-Einstein condensate in an optical lattice: Landau-Zener tunneling and dynamical instability. *New Journal of Physics*, 5(1):104, 2003.

[149] A. Smerzi, A. Trombettoni, P. G. Kevrekidis, and A. R. Bishop. Dynamical superfluid-insulator transition in a chain of weakly coupled Bose-Einstein Condensates. *Phys. Rev. Lett.*, 89:170402, Oct 2002.

[150] G. Barontini and M. Modugno. Dynamical instability and dispersion management of an attractive condensate in an optical lattice. *Phys. Rev. A*, 76:041601, Oct 2007.

[151] C Menotti, A Smerzi, and A Trombettoni. Superfluid dynamics of a bose-einstein condensate in a periodic potential. *New Journal of Physics*, 5(1):112, 2003.

[152] Fedele, R. and Man'ko, M. A. Beam optics applications: quantumlike versus classical-like domains. *Eur. Phys. J. D*, 27(3):263–271, 2003.

[153] M. Cristiani, Oliver Morsch, N. Malossi, M. Jona-Lasinio, M. Anderlini, E. Courtade, and E. Arimondo. Instabilities of a bose-einstein condensate in a periodic potential: an experimental investigation. *Opt. Express*, 12(1):4–10, Jan 2004.

[154] L. Fallani, L. De Sarlo, J. E. Lye, M. Modugno, R. Saers, C. Fort, and M. Inguscio. Observation of dynamical instability for a Bose-Einstein Condensate in a moving 1d optical lattice. *Phys. Rev. Lett.*, 93:140406, Sep 2004.

[155] A. Smerzi and A. Trombettoni. Nonlinear tight-binding approximation for bose-einstein condensates in a lattice. *Phys. Rev. A*, 68:023613, Aug 2003.

[156] S. Braun, J. P. Ronzheimer, M. Schreiber, S. S. Hodgman, T. Rom, I. Bloch, and U. Schneider. Negative absolute temperature for motional degrees of freedom. *Science*, 339(6115):52–55, 2013.

[157] E. M. Purcell and R. V. Pound. A nuclear spin system at negative temperature. *Phys. Rev.*, 81:279–280, Jan 1951.

[158] Norman F. Ramsey. Thermodynamics and statistical mechanics at negative absolute temperatures. *Phys. Rev.*, 103:20–28, Jul 1956.

[159] K. Ø. Rasmussen, T. Cretegny, P. G. Kevrekidis, and Niels Grønbech-Jensen. Statistical mechanics of a discrete nonlinear system. *Phys. Rev. Lett.*, 84:3740–3743, Apr 2000.

[160] S. Iubini, R. Franzosi, R. Livi, G. L. Oppo, and A. Politi. Discrete breathers and negative-temperature states. *New Journal of Physics*, 15(2):023032, 2013.

[161] Moratti, M. and Modugno, M. Localization of a non interacting quantum wave packet in one-dimensional disordered potentials. *Eur. Phys. J. D*, 66(5):138, 2012.

[162] W. Kohn. Analytic properties of bloch waves and wannier functions. *Phys. Rev.*, 115:809–821, Aug 1959.

Acknowledgements

And finally let us switch to italian!

Il primo sentito ringraziamento va al prof. Massimo Inguscio, il quale mi ha dato la possibilità di poter entrare a far parte di questo grande gruppo. L'interesse e l'entusismo che ha sempre dimostrato sono di sprone per guardare sempre un poco più lontanto e proseguire verso nuovi traguardi.

Successivamente un enorme grazie va a Michele Modugno, con cui ho collaborato per più d'un anno. Suo il merito di avermi introdotto nel mondo della fisica degli atomi ultrafreddi applicata ai sistemi disordinati. Aiutandomi con costanti consigli, preziosi suggerimenti e proponendomi sempre nuvoi problemi da affrontare ha saputo darmi continui stimoli. Grazie anche per l'enorme disponibilità mostratami anche dopo la sua partenza per Bilbao, senza la quale gran parte di questo lavoro non sarebbe stata possibile.

Grazie a Giovanni Modugno, per avermi dato la possibilità di collaborare fianco a fianco con un grande gruppo sperimentale, potendo vedere come si fa la fisica vera, quella che si tocca con mano. Un sentito grazie per le numerose discussioni, ricche di idee stimolanti e non da ultimo per avermi aiutato a completare la scrittura della tesi. Ringrazio anche Filippo Caruso, per la collaborazione stretta e per tutti i consigli elargiti durante il periodo in cui si è collaborato.

Ringrazio Luca ed Augusto, che mi hanno accolto nella nuova famiglia del QSTAR ad Arcetri. Il lavoro in un gruppo di soli teorici mi ha permesso di imparare tantissime cose nuove. Grazie per la loro costante disponibilità, e per la fiducia affidatami nel collaborare ai loro progetti. La possibilità di affrontare i medesimi argomenti da punti di vista diversi è stata di fondamentale importanza per capire meglio il carattere interdisciplinare di quanto si sta facendo. Con loro ringrazio tutti gli altri membri del QSTAR!

Graze, grazie infinite a Chiara, Elenora, Luca, Lorenzo, Avinash e Marco. Prima di tutto amici, e poi compagni di lavoro. Il loro apporto è stato fondamentale, perché tre di questi quattro anni sono passati al loro fianco. Da ognuno di loro ho potuto imparare

qualche cosa. E senza di loro niente di questo sarebbe stato realizzato. Grazie di cuore ragazzi.

Se è vero che il Dottorato è l'ultimo gradino della scala degli studi, non resta che fare i ringraziamenti doverosi a chi sino qui mi ha accompagnato, magari evitando proprio di partire dalle elementari, anche se qualcuno più o meno già c'era allora.

Su tutti, prima di tutti, tutta la mia famiglia: i miei genitori e mio fratello. Spero di far futtare sempre i vostri insegamenti. I miei nonni, perché mi hanno inseganto che l'intelligenza non sta solo nelle lauree ma nel saper vivere onestamente. Perché va bene la fisica, ma al mondo bisogna sapere fare un po' di tutto, e un rastrello e una gerla di fieno talvolta contano tanto quanto un computer e un laser. Gli zii: sempre presenti e disponibili per tutto. Stefania e tutta l'allegra brigata: la vostra allegria è sempre contagiosa, per fortuna che ci siete. A Claudia, e ai cari piccoli Giovanni ed Anna: anche senza la dedica come qualche anno fa, vi porto sempre nel cuore. Come ebbi a dire allora, l'entusiasmo che vi contraddistingue è la vostra forza maggiore, e serve anche a noi grandi. Grazie.

Ora un immenso, sconfinato grazie alla mia seconda matta e unica famiglia: i miei amici di sempre, dalla A di Andrealuigi alla Z dei vari Zanga. Siete troppi per nominarvi tutti e rischierei di lascaire fuori qualcuno col rischio che per riparare debba esaurire le finanze a furia di birre offerte. Taglio la testa al toro e via, una volta finita offro ugulamente un giro a tutti!

E tra gli amici non posso non citare Lei... Grazie Vale! Ne metto solo uno, e non aggiungo altro. So che basta per intendersi!

Ah, ovvio, un pensiero anche all'alpinista-filosofo Silvio! Che le nostre quattro parole non ce le facciamo mancare mai in settimana. E con lui un pensiero pure a Franceso. Gli amici non si misurano tramite la frequenza con cui si sentono, ma dalle parole che dicono. Quindi, grazie. Anche per il tuo bel sito, nei giorni chiusi in ufficio una bella finestra sulle fantastiche montagne.

Chiudo qui la lista, con l'ultimo grazie, arrivato per ultimo in ordine cronologico ha scalato velocemente tutte le posizioni... Per cui, a Giulia, con tutto il cuore: Grazie! In una parola piccola si racchiude molto, e questo molto te lo devo tutto.

E ora, quel che sarà sarà, chiusa questa pagina, vedremo che verrà!

Saluti a tutti!